Antenna Design and Interface Dynamics for Cellular Handsets

A Major Qualifying Project

Submitted to the Faculty of Worcester Polytechnic Institute

in partial fulfillment of the requirements for the

Degree in Bachelor of Science

in

Electrical and Computer Engineering

By:

____

Matthew Crivello

____

Matthew Penrose

____

Tint Yadana Aung

Date: Month Day, Year

Sponsoring Organization:

Skyworks Solutions Inc.

20 Sylvan Road, Woburn, MA 01801

Approved:

____

Professor Reinhold Ludwig

____

Professor John McNeill

Abstract

This project involves the design and computational analysis of a Planar Inverted-F Antenna at a resonant frequency of 850 MHz in an effort to investigate and optimize its performance in the LG Nexus 5 D820 smartphone. A three-dimensional, full-wave computational model of the antenna was created with HFSS and variations of different physical parameters were conducted. The data from HFSS was exported into ADS for analog circuit modeling. The modeling predictions were successfully tested with a designed and constructed antenna.

Acknowledgements

We would like to thank Dr. David Whitefield and the Skyworks Inc. team for sponsoring this project. Specifically, we would like to thank Eric Austin for his guidance and his brilliant knowledge with the measurements taken in the Radio Frequency Lab at Skyworks Inc. We also would like to thank our projector advisor Professor Reinhold Ludwig and co-advisor Professor John McNeil for their expert advice and extraordinary support in the project and Professor Sergey Makarov and Dr. Gregory Noetscher for assisting us with their valuable HFSS expertise. Last but not least, thank you to Robert Boisse and Robert Brown for helping and guiding us throughout the project with their magnificent knowledge as electronic technicians.

Table of Contents

Table of Figures

Table of Tables

1. Introduction

Skyworks Solutions Inc. has sponsored a Major Qualifying Project (MQP) at Worcester Polytechnic Institute involving the simulation of antenna designs for cellular handset applications. The goal of this project is to provide Skyworks Solutions with a computational approach for understanding antenna designs using two prominent simulation programs: ANSYS' High Frequency Structural Simulator (HFSS) and Agilent Technology's Advanced Design System (ADS). Most modern cellular handsets utilize microstrip Planar Inverted-F Antennas (PIFAS) because of their efficiency in terms of cost, effective size, ease of fabrication, and gain at higher frequency bands. For these reasons, the project aimed at the analysis of this variety of antennas.

The MQP team designed a simplified PIFA model covering a similar frequency band as the low-band PIFA found in the LG Nexus 5 D820 model smartphone. A thorough parameter analysis was performed on the simplified PIFA using HFSS. This analysis demonstrated correlation of the geometry and material properties of the PIFA to its performance characteristics such as gain, return loss, and directionality. The results of these analyses are presented in the form of images, graphs, and tables found later in the report. Additionally, the results of the antenna optimization process in creating the simplified PIFA are included in the report.

To test the fidelity of the computational model, the MQP team fabricated a prototype design of the antenna system. Using a network analyzer, the electrical properties were verified against the computational model.

2. Background

Since the 1960’s, cellular phones have undergone an extensive technological revolution that has led to their prevalence in modern society. In colloquial speak, the most advanced iteration of the cellular phone is called the smartphone because these devices can perform a multitude of functions ranging from making basic phone calls to allowing users to access the internet. However, implementation of these functions requires a growing number of components, which in turn requires a reduction in the size of the multiple cellular antennas in each phone. The ever increasing component count has made it difficult to deploy conventional antennas. It is for this reason that many companies choose to utilize microstrip antennas in the design of their handsets. The currently preferred variety of these antennas is the Planar Inverted-F Antenna model, also known as the PIFA.

2.1. Microstrip Antennas

The microstrip antenna is a type of antenna that consists of a thin metal plane fabricated on a dielectric substrate, such as a printed circuit board (PCB), and is often physically aligned parallel to a ground plane. The form of microstrip antenna most often seen is the rectangular patch antenna, an example is shown in Figure 1. For this subclass of microstrip antenna, the metal plane consists of an electrically short transmission line (called the feed line), leading to a large rectangular metal trace with a typical length of about half the wavelength of the corresponding target resonant frequency.

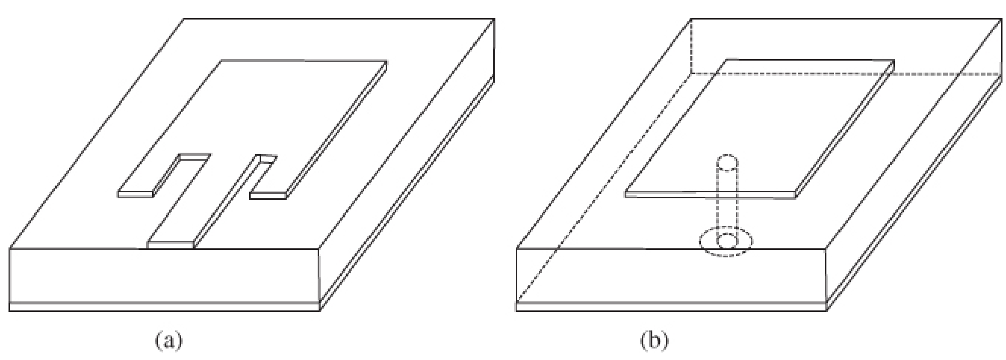

Figure 1. Simple rectangular patch antennas with a) inset and b) probe excitation. The radiating patches rest on layers of substrate parallel to the ground [1].

This layout leads to a radiation pattern that is directed towards the normal of the patch and polarized from the feed line to the opposite end of the radiator [1]. Radiating slots can be removed from the plane to alter the antenna gain, bandwidth and return loss, and different patches can be layered to provide operation at multiple frequencies.

Microstrip antennas are popular in mobile applications because they are fairly small, lightweight, rugged, and easy to mass produce. The original drawbacks with the designs, such as an insufficient bandwidth and single frequency operation, have largely been resolved. Different models of microstrip antennas have been developed, including, but not limited, to the Planar Inverted-F Antenna (PIFA) and the Folded Inverted Conformal Antenna (FICA). Each variation possesses its own distinctive properties in terms of gain, bandwidth, and size. This report will explore the characteristics of the PIFA.

2.2. Planar Inverted-F Antennas (PIFA)

PIFAs are one of the more popular varieties of microstrip antennas in today's market. This is due to the fact that they can be produced at lengths of a quarter wavelength as compared to the lengths of a half wavelength of the other microstrip antennas. Additionally, PIFAs are versatile in that they can be printed on the surface of a substrate or even inside of a phone's housing. PIFAs are named "Inverted-F Antennas" because their design resembles the letter F when drawn simplistically, as shown in Figure 2.

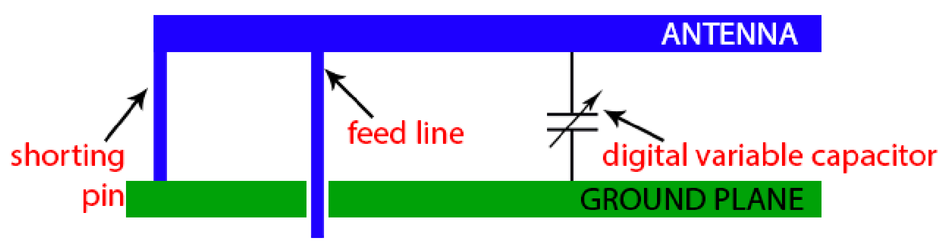

a)

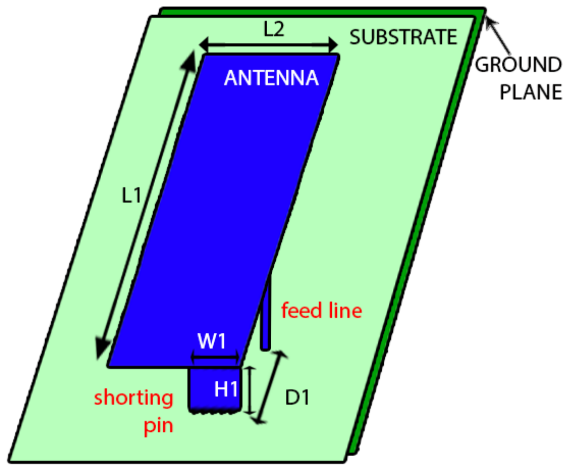

b)

Figure 2. Fundamental model of a simple PIFA design: a) side view, b) 3D view [2].

PIFAs are characterized by the use of a shorting pin as well as a so-called capacitive load tuner. The tuner is a tunable RF filter that allows the bandwidth of the antenna to be actively varied in applications involving the use of multiple frequency bands [3]. The device is able to accomplish these functions by varying the imaginary component of the antenna's impedance, allowing the resonance to be shifted based in the reactive components of the tuner. The shorting pin acts as a parallel inductance to the ground plane; it results in a wider effective bandwidth during operation, which can act as a reactive component in the antenna's impedance. The distance between the feed line and shorting pin is another major component in determining the impedance. The shorting pin is located just over a quarter wavelength from the "open" end of the PIFA. It is easiest to picture the operation of the PIFA by imagining a standard half-wavelength patch antenna with a shorting pin located at a point where the current distribution is null, as shown in Figure 3:

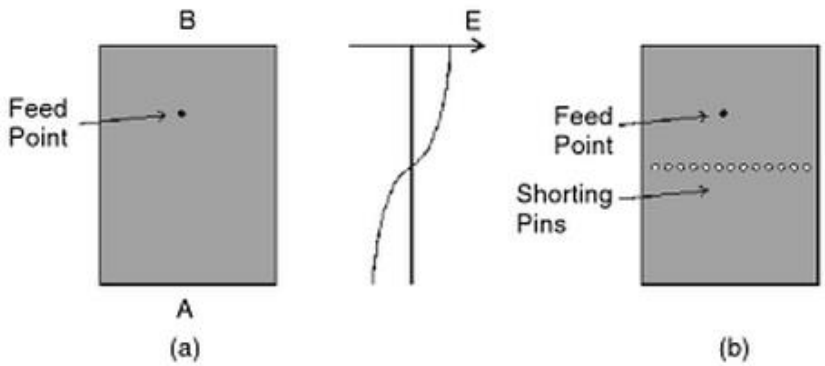

Figure 3. The diagram a) shows the structure of a typical half-wavelength patch antenna in relation to the electric field distribution along its length, while b) shows the distance at which a shorting plane or series of pins can be added to save room. The short must be added at a location where the current distribution is roughly zero [4].

The addition of the shorting pin makes the second half of the antenna opposite the feed essentially useless, allowing nearly a quarter-wavelength of the structure to be removed [4].

The tuning element in a PIFA allows for the implementation of multiple frequency bands, an ideal property of antennas in small-scale designs. Problems associated with PIFA designs are often related to poor bandwidth and gain, especially at low frequencies. However, tradeoffs can be made to improve one over the other. For example, including meandered lines in the layout structure of the PIFA can noticeably improve the bandwidth at the expense of reduced gain, as shown in Figure 5 [5].

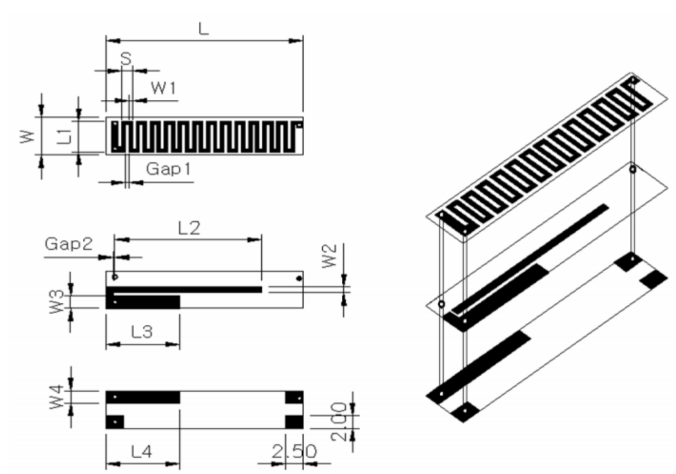

Figure 4. Structure of a meander-line PIFA proposed by Cho Inho, et al [6].

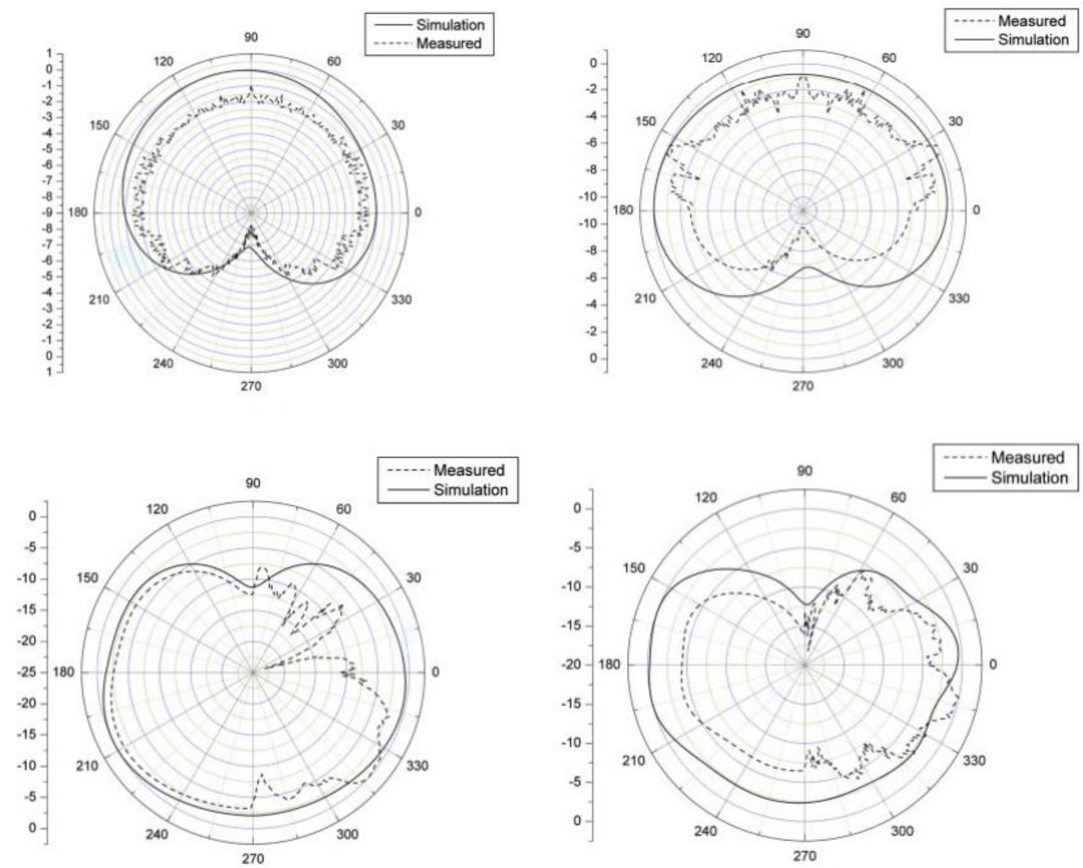

a) b)

Figure 5. Comparison of measured and simulated 2.2 GHz PIFA E-Plane (top row) and H-Plane (bottom row) radiation patterns (gain in dB) with a) one and b) two meandered lines [5].

PIFAs can be conveniently used to cover the ultra-high frequency range because the antenna dimensions are directly related to the wavelength of the resonant frequency. The length and width of the PIFA structure can be determined from:

$$L + W_1 - W_2 = \frac{\lambda_r}{4\sqrt{\varepsilon_r}} = \frac{c}{4f_r\sqrt{\varepsilon_r}} \qquad (1)$$

Parameters L and W_1 are the length and width of the conducting plate, W_2 is the width of the grounding pin or plane, λ is the wavelength of the resonant frequency, ε_r is the relative permittivity of the substrate the antenna is mounted on, c is the speed of light, and f_r is the resonant frequency [7, 8]. Selecting a substrate with a higher permittivity allows the length of the radiating component to be reduced;

unfortunately, this also reduces the gain and bandwidth of the antenna. The width of the microstrip feed line is related to the substrate permittivity through its relationship with the characteristic impedance:

$$Z_0 = \frac{377}{\sqrt{\varepsilon_r}}\frac{b}{a} \qquad (2)$$

Parameter *b* is defined as the distance between the feed line and the ground plane, and parameter *a* is defined as the width of the line [9]. If a different substrate with a greater permittivity were to be used, the width of the line would need to decrease to maintain the same characteristic impedance, Z_0.

The return loss of the antenna quantifies the power lost when delivered to the antenna, and thus a loss of power radiated. Return loss is caused by a mismatch of the antenna impedance to the characteristic line impedance. This parameter can be calculated by obtaining the reflection coefficient Γ, also known as the S_{11} scattering parameter. The return loss (RL) is a decibel value of the reflection coefficient, which represents the ratio of reflected versus incident voltage. Equations (3) and (4) show how these parameters are defined:

$$\Gamma = \frac{V_r}{V_i} = \frac{Z_L - Z_o}{Z_L + Z_o} \qquad (3)$$

$$RL_{dB} = -20 * log(|\Gamma|) \qquad (4)$$

V_r represents the reflected voltage wave, V_i represents the incident voltage wave, Z_L represents the impedance of the antenna, and Z_0 represents the characteristic impedance. It can be seen that matching the impedances will reduce the value of the reflection coefficient to zero. The degree of mismatch can also be referred to through the voltage standing wave ratio (*VSWR*) of the antenna, which represents the ratio of the maximum standing voltage wave amplitude to the minimum standing voltage wave amplitude: [7]:

$$VSWR = \frac{1+|\Gamma|}{1-|\Gamma|} \qquad (5)$$

The gain for a PIFA is maximized when the antenna is of resonant length, which amounts to the length of the radiating arm being a quarter of the wavelength (corresponding to the target resonant frequency). Since PIFAs can operate at both low and high frequencies, this means that the high-frequency models will be exceptionally small. The resonant lengths can vary depending on the design of the PIFA, which can include slits or folds in the main conductor. Adding slits allows the device to cover additional frequency bands and downshift the resonant frequencies while folds will upshift the resonant frequencies and reduce the necessary size of the radiating patch [10].

PIFA polarization is typically vertical and normal to the ground plane and occurs in the direction of the current in the feed line. In terms of radiation patterns, this results in a pattern that is considered omnidirectional in the plane parallel to the ground [11]. These are best determined using a computational software such as HFSS, but can also be measured from a fabricated model inside an anechoic chamber, a room completely covered with radiation absorbent material (RAM). Figure 6 explains in more detail how the patterns are understood in this system. Figure 7 shows the radiation patterns of a simple PIFA device in IEEE standard polar coordinates for antenna measurement systems [12]. In this scheme, it is important to note that θ denotes the angle moving clockwise away from the z axis and Φ is the angle moving counter-clockwise away from the x axis.

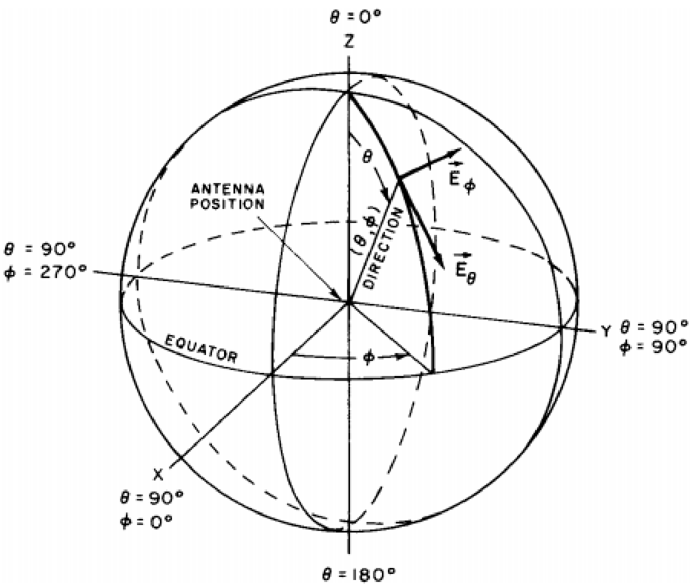

Figure 6. Spherical coordinates used for far-field antenna measurement systems [12]. Planes along the z-axis parallel to the XY plane are referred to as E_{Φ} planes while planes perpendicular to the XY-plane that rotate along the Z axis are called E_{Φ} planes.

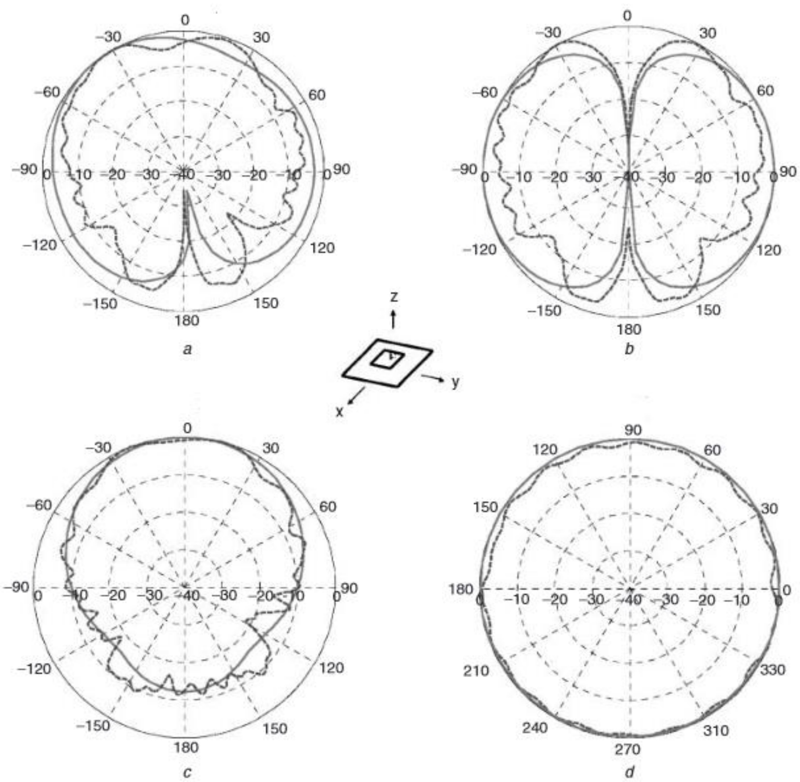

Figure 7. Simulated and measured normalized radiation patterns on the a) elevation E_{Φ} (Φ=0) Plane b) elevation E_{Φ} (Φ=90) Plane c) elevation E_{Φ} (Φ=90) Plane d) azimuth E_{Φ} (ϑ=90) plane for a simple rectangular PIFA operating at approximately 1.9 GHz. Simulated patterns are solid lines, measured patterns are dotted [13]. Since polarization is vertical, the E-plane is reflected in the vertical slices, or elevations.

It is important to discuss the ground plane in mobile PIFA designs. In most handsets, the ground plane takes up nearly the entire area of the device (usually a sheet of metal located behind and having the same dimensions as the LCD screen) and supports at least the main motherboard, the touch screen, and all antennas located in the phone. If the size or shape of the ground plane is changed, most if not all of the connected antennas will experience some change in signal strength. For PIFAs in particular, the antenna bandwidth and gain will both be reduced and the radiation patterns will fluctuate if the size of the plane is decreased. An example of these changes with size is shown in Figure 8. Placement of the shorting pin near one of the corners of the ground plane, preferably closer to the shorter edges, should provide improved gain and bandwidth [13]. The location of the ground plane between the antenna and the user's head is also important because it limits the radiation patterns generated in that direction, reducing the electromagnetic wave power absorption losses known as the Specific Absorption Rate [2, 11]. The E-plane, also known as the electric field, determines the polarization or orientation of the radiating wave. The H-plane is the magnetic field and is perpendicular to the E-plane. Since the ground plane is considered part of each antenna, radiation patterns are measured from the center of the ground plane on the E-plane (the XZ-plane) and the H-plane (the YZ-plane).

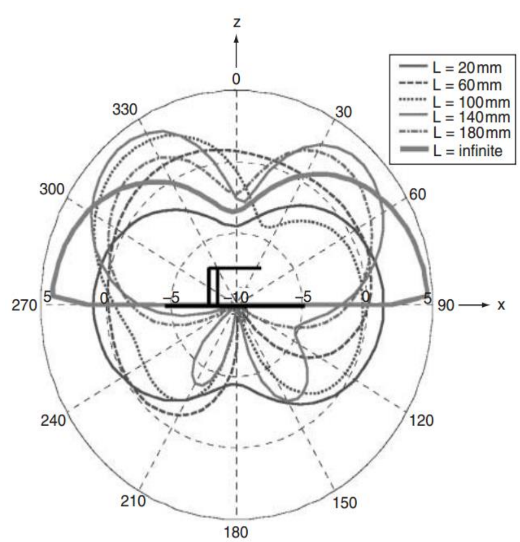

Figure 8. E-plane radiation patterns versus length of the ground plane[13].

Within the scope of this project, one widely-used real PIFA model is analyzed. Specifically, this is the main low band antenna of the Google/LG Nexus 5. Appendix 8.1 shows an image of the PIFA structure. For the North American D820 model, the frequency bands at which the antenna operates are the GSM 850 band, the WCDMA 850 band, LTE bands B5, B17, B26 and B41, and CDMA bands BC0 and BC10 [8]. To view which specific frequencies these bands cover, please refer to Appendix 8.2. Many of these frequencies overlap in the 850MHz range. GSM 850 is roughly equal to WCDMA 850 and LTE 5, and all of these frequencies are already covered by CDMA 0 and LTE 26. The two bands that seem to break this pattern of overlap are the LTE 17 and 41 bands. Overall, the antenna appears to be mainly resonant at a frequency range between 824 MHz and 894 MHz for all standards, but has additional resonances between 704 MHz and 746MHz (LTE B17) and between 2.496 GHz and 2.690 GHz (LTE B41) according to the LTE system specifications [14].

2.3. Tools to conduct performance analysis

The primary tool that was used in this project for modeling the antenna designs is called High Frequency Structure Simulator (HFSS). Originally released in 1989, HFSS has become the industry standard in high frequency electronic simulation. The program uses a numerical model known as the finite element method (FEM) whereby the solution domain is discretized into a large number of finite elements; the simulator accomplishes the discretization through adaptive mesh techniques. At the associated mesh nodes the program computes multiple parameters such as the electric and magnetic field components generated by the patch. HFSS will be used to model PIFA cell phone antennas using various practical substrates and an infinitely thin, perfectly conductive radiator. This causes the electric far field from the device to be formed in the normal of the plane. From the PIFA antenna simulations, the S_{11} parameter at various frequencies will be extracted for further implementation in the circuit simulator Advanced Design System (ADS). The amount of time taken to process a given simulation can increase substantially due to the complexity of the design as well as the frequency sweep range and resolution.

The structure in Figure 9, which includes 28 three dimensional elements (these make up the substrate, ground plane, and air boxes) and 5 two dimensional elements (these make up the patch, wave port, and feed line), was designed to operate at a frequency of 10GHz. This is an example HFSS model to show the capabilities of the program.

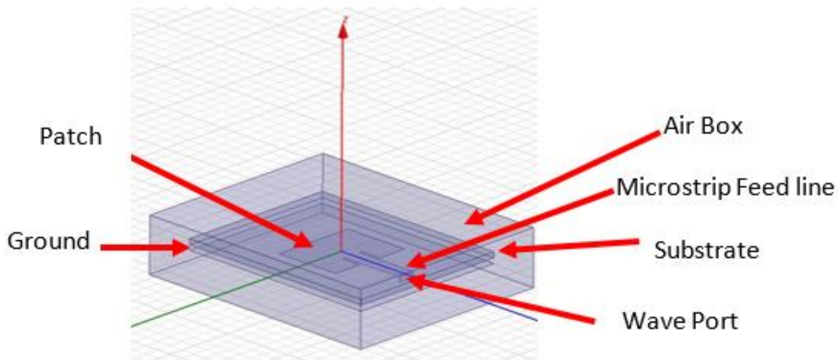

Figure 9. Simulated HFSS model of a 10GHz microstrip antenna 1.15 x 1.465 x 0.079 cm^3 in size with a substrate of ε_r = 2.2. The length of the patch is 1.19 cm, corresponding to 0.4 wavelengths. This is shorter than the half wavelength size predicted because the substrate is not air.

To analyze the patch antenna, a frequency sweep was performed from 8GHz to 12GHz at 400 steps of 0.01GHz increments. The solution was set to perform 20 passes of this sweep. The results of this frequency sweep can be seen as part of radiation patterns reported in of Figure 10.

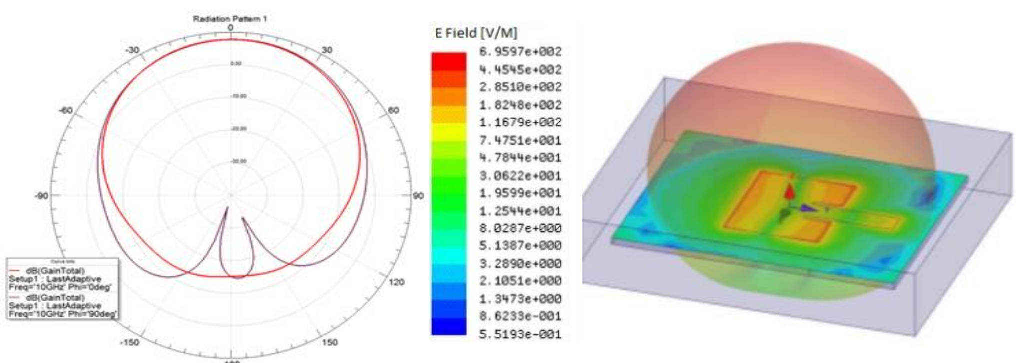

a) b)

Figure 10. The a) Radiation patterns of a 10GHz patch antenna in HFSS. -180^o corresponds to the center of the microstrip feed line b) 3D polar plot of the far-field radiation pattern and magnitude representation of the E Field.

More passes will lead to a more accurate result however, the computational time will increase. The simulation process took 19 minutes and 8 seconds to complete on a WPI remote server with the following specifications: 2 Quad-Core AMD Opteron 2.70 GHz processors and 24 GB of RAM.

Advanced Design System, or ADS, is a circuit modeling program widely used in industry for RF, microwave, and high speed digital applications. The wide market presence and relatively easy to use interface of the program makes ADS a prime choice for this project. The goal is to be able to take the relevant data from HFSS and import it into ADS for modeling with other circuit components such as antenna tuners. This will greatly improve the design process of cellular components since it allows the effects of changes to be more easily seen. Figure 11 shows an example ADS schematic. A simple matching network is implemented within this schematic consisting of a series capacitor and a shunt inductor. This matching network layout was chosen to mimic what is found in the Nexus 5. Included in this schematic is a resistor in shunt with the capacitor and a resistor in series with inductor. These elements, as well as the variable elements, are purely for tuning purposes and will be described in more detail in section 4.2. In input (on the left of the schematic) is part of the S-parameter sweep function found in ADS. The final component is the S1P antenna component found on the far right of the schematic. This component imports a touchstone file; it will be described in more detail in section 4.2.

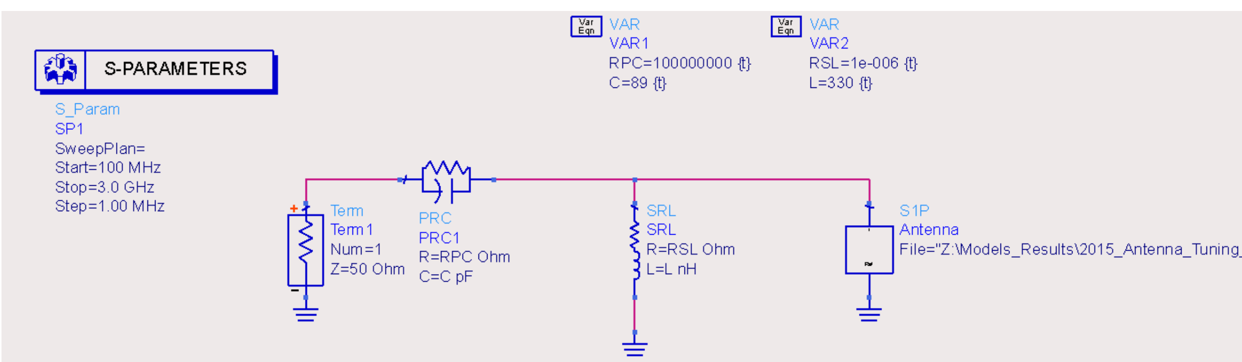

Figure 11: An example ADS schematic of a single port antenna attached to a matching network (parallel and series resistors are included for tuning purposes within ADS).

3. Methodology

3.1. Simulation and Analysis

The approach for this antenna project consists of three main stages: simulation and analysis, fabrication, and measurement. The simulation stage involved designing and modeling a PIFA within HFSS. To ensure that the PIFA is of practical relevance, the design attempts to emulate the properties of the Nexus 5 D820 main low-band antenna. It was decided that the final model be simplified, rather than an attempt to recreate the exact form of the Nexus antenna. This approach increases the ease with which the design can be evaluated and how to reduce meshing complexity to conserve resources within HFSS.

The simulation predictions are used to test the dependence of the antenna performance on a number of physical dimensions and electrical properties. A simplified model of the desired PIFA was fabricated using Altium and tested with a network analyzer. This was done to develop a comparison between expected values and those measured on a real device. The results of the simulations on the computational model were also exported into ADS for further testing with other electrical components, such as capacitive tuning devices and passive matching networks.

3.1.1. Initial Design

The initial HFSS design of the intended PIFA was simplified; it consisted of a substrate, one ground plane, a rectangular radiating patch, a rectangular shorting pin, a rectangular lumped port to feed the device, and a rectangular lumped capacitance. The dimensions of the ground plane and substrate were measured from the Nexus 5, assuming that the area of the LCD was equivalent to the area of the ground plane and that the vertical portion of substrate on the Nexus antenna represented the average thickness of substrate between the ground plane and the radiating patch. The substrate for this model was assumed to be FR-4 since it was the most readily available and relatively inexpensive material. The width of the patch was determined by measuring the width of the traces on the Nexus. The width of the feed-line, shorting pin and tuner were considered to be equal to that of the patch for this simulation. The length of the patch was determined by applying Equation (3) in light of the current dimensions, then determining the exact desired length through a parametric sweep of tune and feed positions, the antenna length, and the value of the tuning capacitor. A vacuum box was placed with boundaries at a minimum distance of λ/8 away from any radiating surface of the device, and then a perfectly matched air layer was generated using the PML wizard built in to HFSS.

An image of what the model looked like is shown in Figure 12. Since there was a time constraint early in the project's life cycle, the dimensions of this design were issued for fabrication and future models were based on the final Altium fabricated designs.

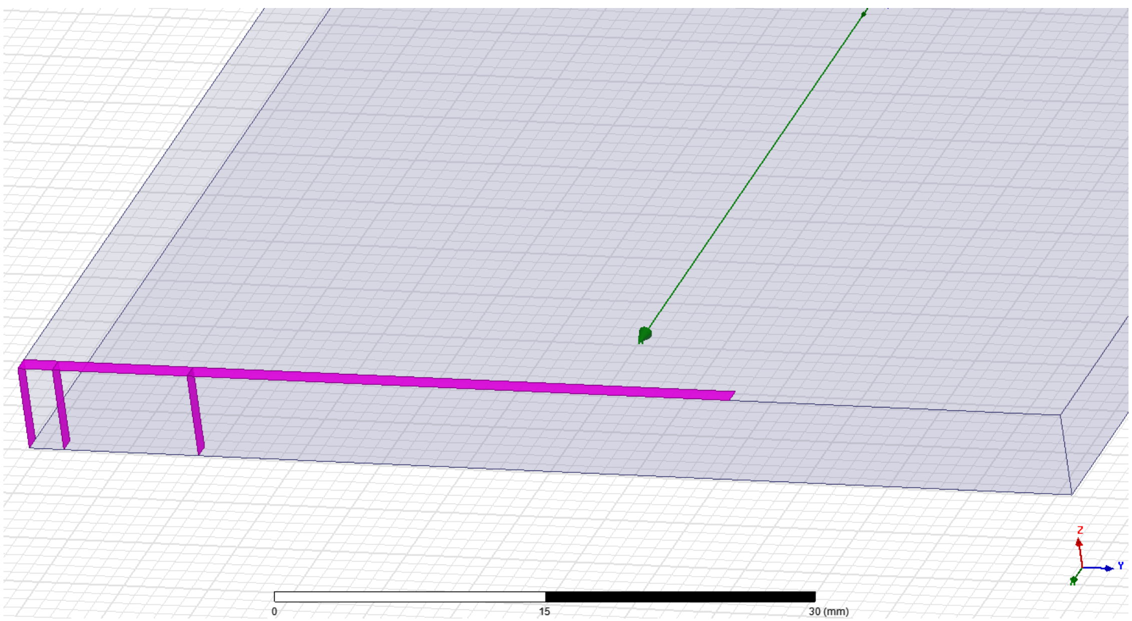

Figure 12. Close-up image of a simple PIFA design. It consists of a substrate, ground plane, radiating patch, shorting pin (the leftmost pin), a lumped feed port (the middle pin), and a tuning device (the rightmost pin).

3.1.2. Advanced Model

Once the simplified antenna was completed, efforts were undertaken to make the HFSS model as similar as possible to the submitted Altium design. This was done to generate results of the simulations that are as close to the real world model as possible. First, the substrate thickness of the model was changed to 4.8mm, since the final device was fabricated from of three 1.6mm layers. Next, the rectangular pins were replaced by three cylindrical vias, each with pads that would allow solid connections between layers. The radius of these pads was set to that of the vias with an additional length equivalent to ½ of the trace width, to ensure that the width of the patch was roughly equal along the entire length of the antenna. The via for the shorting pin extends directly to the ground plane, but that for the tuner and feed line extends to the top of the bottom layer, 2/3 of the way to the ground. This allowed small traces to be added, which permits port connections to be made and enabling the inclusion of a tuning device and a matching network for the antenna. An additional substrate was added to the antenna; this was used to simulate the area on which the components could be placed, and more traces were added to lead to the location of the SNP connector.

The model was also revised in such a way that the tuning capacitor was replaced by a second lumped port, which would allow the device to be exported as a 2-port network into ADS. This meant that the tuning sweep was now excluded from the results in HFSS, and would instead be performed alongside the matching network simulations in ADS. The intent was to capitalize on the strength of ADS, which allows the simulation of active networks alongside those of passive networks as compared to the entirely passive designs in HFSS. A short comparison of models using these components in ADS and in HFSS was performed to show the difference in how each program handles similar data points. To perform this, an additional HFSS model which incorporates the capacitive tuner was developed; it utilizes the nominal value found in ADS. Using this model, the reflection coefficient and gain of each device can be compared. The replacement is easily handled by redefining the second wave port as a lumped capacitance in HFSS.

3.1.3. Simulation Setup

The antenna model was designed to share as many properties as possible with the Nexus 5 low-band antenna. As mentioned earlier, the target device operates predominantly in a frequency band from 824 MHz to 894 MHz With this in mind, the resonant frequency of the final design was designed to be centered at 850 MHz.

HFSS includes a built-in parametric function which allows any number of design values to be varied across defined ranges. The program performs meshing operations and a frequency sweep for each possible permutation of the design, allowing the design with the most ideal characteristics to be identified from the matrix of simulations. A standard frequency range from 600 MHz to 1 GHz with a step size of 0.1 MHz was utilized in conjunction with the parametric analysis. This method of analysis substantially simplified the optimization process. However, there was a significant cost in terms of computational power. For the simulation of each individual parameter only a few simulations might be necessary. If this were performed, however, there would be a loss of optimization quality as a large number of permutations would be lost. Using the HFSS function, each sweep would stack exponentially. If six parameters were to be swept with ten steps each, the individual method would result in a total of 60 necessary simulations, but the array method would result in about 1,000,000 simulations, requiring about 16,667 times as much time to complete but acquiring 999,940 more data values for optimization.

To compensate for this, certain specified properties were excluded from the multivariable optimization analysis and given their own parametric sweeps. More specifically, the optimization sweep included the antenna length, tuning position and feed position, all three of which were considered variable in the terms of this project. Other values, which were considered fixed, were given separate 11 step simulations from 90% of the nominal value to 110% of the nominal value. These included antenna width, substrate thickness, via radius, and the position of the antenna along the ground plane. An 11x11 parameter sweep was performed for the area of the ground plane as well, to display how a change in ground size will affect the results.

3.2. Capstone Design Development

With the information gathered through many analysis iterations, the project team developed a simplified antenna design in Altium. With the help of Professor Sergey Makarov at WPI and Advanced Circuits, the fabrication of a simplified model of the Nexus 5 PIFA was completed. The performance of the fabricated model was aimed to reproduce the predictions of the computational one. This was done in an effort to display potential differences between a real and ideal antenna models, but additional strides were undertaken to make the analysis model match the structure of the physical model.

3.2.1. PCB Design in Altium

The physical design of the PIFA was conducted using the PCB design software Altium and fabricated at Advanced Circuits. The dimensions of the antenna and board were taken from the team's most recent HFSS model at the time. Once completed, the Gerber files from Altium were uploaded to the company for printing. The boards were ordered on January 22, 2015 and were received on February 4, 2015. The total fabrication and shipping process took about two weeks, as was expected. Once the boards were received, the construction of the PIFAs could commence which included assembly and component soldering by the team.

3.3. Measurements and Analysis of Prototype Antenna

With the completion of the simplified PIFA, the team made physical measurements of the electrical properties of the antenna. A network analyzer was used to measure the impedance of the device as well as the reflection coefficient of the device from 300 MHz to 3GHz. The reflection coefficient of the device was measured under multiple conditions with several network analyzers. These conditions were analyzed such that conclusions could be drawn concerning the sensitivity of the component to environmental influences.

Since we lacked the resources to accurately measure the radiation patterns, the requirements for which are discussed in IEEE Standard 149-1979 (R2008) and [12, 15], they will not be studied.

4. Results and Discussion

4.1. HFSS Simulations

The basic design of the antenna for this project was defined carefully, such that the model could adaptively adjust to changes in any given design parameter. An image of the local variables used in the project is shown in Figure 13.

Local Variables

Value Optimization Tuning Sensitivity Statistics

Name	Value	Unit	Evaluated Value	Type	Description
AirDistance	21.03	mm	21.03mm	Design	
FeedLength	ShortPosition+2*ViaRadius+TraceWidth+FeedPosition-.2mm		-27.82mm	Design	
FeedPosition	0.5	mm	0.5mm	Design	
GroundLength	109.58	mm	109.58mm	Design	
GroundWidth	61.64	mm	61.64mm	Design	
LengthToRadiator	0.001	mm	0.001mm	Design	
LumpedCap	0	pF	0pF	Design	
SecondLayerStretch	3	mm	3mm	Design	
ShortPosition	-GroundWidth/2+ViaRadius+TraceWidth/2		-29.92mm	Design	
ShortPositionMod	0	mm	0mm	Design	
SubstrateExtend	12	mm	12mm	Design	
SubstrateHang	0	mm	0mm	Design	
SubstrateHeight	4.8	mm	4.8mm	Design	
SubstrateLength	GroundLength+SubstrateHang		109.58mm	Design	
SubstrateWidth	61.64	mm	61.64mm	Design	
TestLength	51.7	mm	51.7mm	Design	
TestTunerLength	2	mm	2mm	Design	
TotalLength	51.7	mm	51.7mm	Design	
TracePosition	(GroundLength/2+SubstrateHang-ViaRadius)-ShortPositionMod		54.41mm	Design	
TraceWidth	1.04	mm	1.04mm	Design	
TunerCapacitance	0.1	pF	0.1pF	Design	
TunerLength	FeedLength+2*ViaRadius+TraceWidth+TunerPosition		-24.62mm	Design	
TunerPosition	1.4	mm	1.4mm	Design	
ViaRadius	0.38	mm	0.38mm	Design	

Figure 13. The local variables used for the project. All size and location measurements specified in this project are defined in terms of these variables.

Each specified location and size for the geometry are defined using some combination of these variables. As an example of how this was implemented, Figure 14 displays an image of the definitions for the position and size of the cylindrical tuning via.

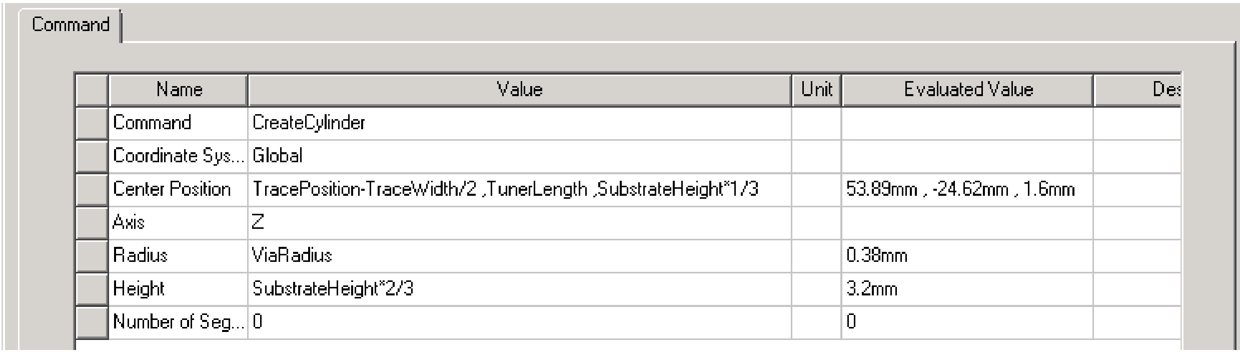

Command

	Name	Value	Unit	Evaluated Value	Des
	Command	CreateCylinder			
	Coordinate Sys...	Global			
	Center Position	TracePosition-TraceWidth/2 ,TunerLength ,SubstrateHeight*1/3		53.89mm , -24.62mm , 1.6mm	
	Axis	Z			
	Radius	ViaRadius		0.38mm	
	Height	SubstrateHeight*2/3		3.2mm	
	Number of Seg...	0		0	

Figure 14. The definitions for the size and position variables for the tuning via.

To achieve the desired resonant frequency, the initial length of the radiating arm of the PIFA was calculated using Equation (1). Assuming the electromagnetic waves travel at the speed of light, this resulted in a value of just under 40.3mm for an 850MHz antenna. The value was then optimized to be about 51.7mm through initial simulations, an increase of 28.3% from the expected value, as shown in Figure 15.

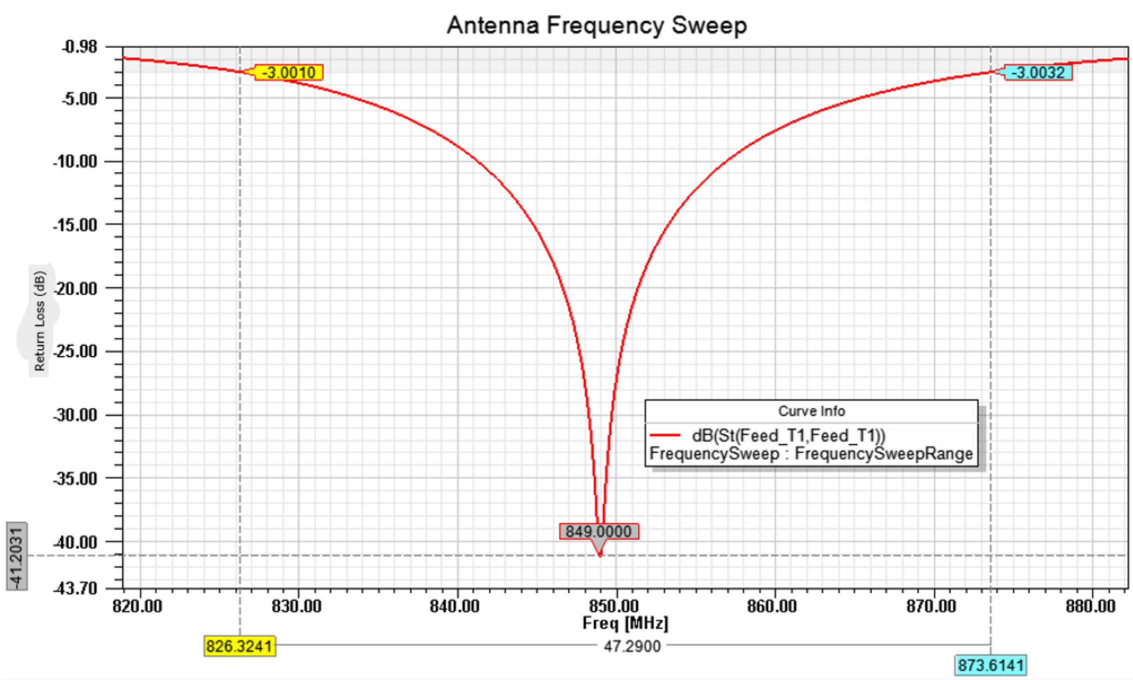

Figure 15. The optimal S_{11} results of the simplified antenna model. The design was chosen from 625 simulations obtained by performing a parametric sweep of the length of the antenna surface, the position of the feed line, the position of the tuning arm, and the value of the tuning capacitance.

The values of 51.7mm length, a 0.5mm feed position, and a 1.4 mm tuning position for this simulation were considered the nominal values for fabrication and future simulations. The capacitance value of 0.06pF was ignored in later simulations because tuning was performed within ADS rather than HFSS.

The original model and optimization sweep served mostly as a tool to aid the understanding of HFSS and antenna design and form the basis of more complex design operations. However, during later simulations and measurements from the fabricated antenna, it became clear that the simple model reflected the actual design very poorly. For this reason, the analysis of antenna parameters focuses primarily on the results found for the complex model.

The length of the microstrip line was included in the optimization process, with 10 steps from 48.0mm to 54.0mm measured as the distance between the shorting pin and the open end of the radiating patch. The width of the microstrip lines and the feed line were determined by measuring the width of the traces on the Nexus 5 D820 low-band antenna [8] with digital calipers, which yielded a value of 1.04mm. Since this width was considered set for the final design, it was excluded from the optimization sweep and an isolated parameter analysis was performed to demonstrate its effect on antenna bandwidth. Ten evenly spaced values from 0.88mm to 1.20mm were used for this sweep.

The position of the feed line plays a large role in determining the real component of the antenna impedance and, subsequently, the reflection coefficient and general radiation patterns of the antenna. The position of the feed was included in the optimization sweep, with values in 5 steps from 0.5mm to 2.0mm, measured as the distance between the feed and shorting pin. These values were generated from the basis set by the initial, simplified antenna parametric sweeps.

The position of the tuning arm and the nature of the tuning device are significant because they can be used to match the antenna's impedance to the coaxial feed-line. Matching the impedances changes the resonant frequency of the PIFA, which makes the tuner a crucial design component. It allows the antenna to perform properly at the desired frequency, which is vital in multiband applications. The position of the arm determines the voltage encountered by the tuner, which in this case was specified as an adjustable lumped capacitance. Since the tuner value was best tuned within the confines of ADS, which could simulate the matching network and tuning system simultaneously, only the tuner port position was analyzed as an optimization parameter in the HFSS optimization process. The position of the tuner, defined as the distance between the tuning arm and the feed pin, was varied with values in 5 equidistant steps from 0.1mm to 2.1mm. A short, separate parametric sweep was also performed on the value of the tuning capacitance as a passive component within HFSS, with 10 values ranging from 0 to 1pF. The results of this analysis are discussed further in section 4.5.3 Comparison of All Three Model Types. For the purposes of consistency, the tuning value was set to 0pF for all other analyses.

The results of the optimization parametric sweep, which included the total antenna length, the position of the feed-line, and the position of the tuning arm, are included in Figure 16. The purpose of the figure is to qualitatively show the range of resonances as a function of design parameter variations. Since there are so many results, it is impossible to display a legend containing labels for each line.

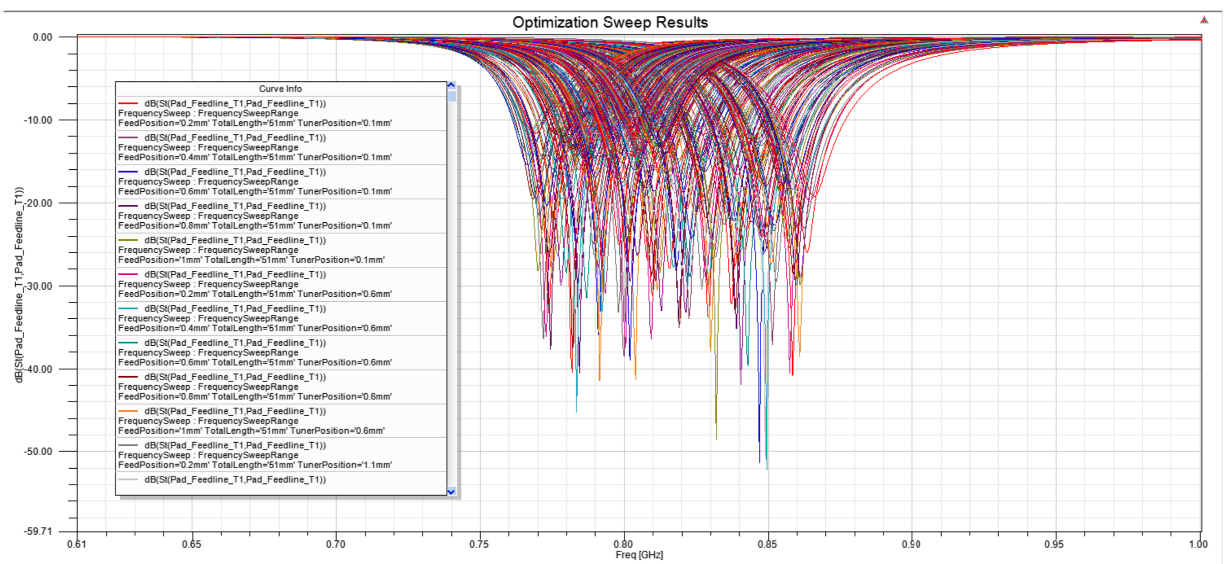

Figure 16. Optimization sweep results, zoomed in at resonances closest to 850MHz. The results of all 250 simulations are shown to provide a qualitative impression of the resonance spread as a function of critical design parameters.

From this collection of data, the most ideal version of the advanced model was determined to possess an antenna length of 48.67mm, a feed position of 1.625mm away from the shorting pin, and a tuner position of 1.1mm away from the feed-line. These values differed from the simple antenna model by 30.8% for the feed position, 6.23% for the antenna length, and 27.3% for the tuner position. It is worth noting that, while closer to the calculated value of 40.3mm, the antenna length is still 20.8% larger than expected. The S_{11} results for the selected values are shown in Figure 17. The frequency range for this result was expanded to show the full frequency range from 0 to 3GHz because, as discussed in Section 2.2, the Nexus 5 device has resonance at a frequency range from 2.496 GHz to 2.690 GHz as well as at the 850 MHz frequency bands.

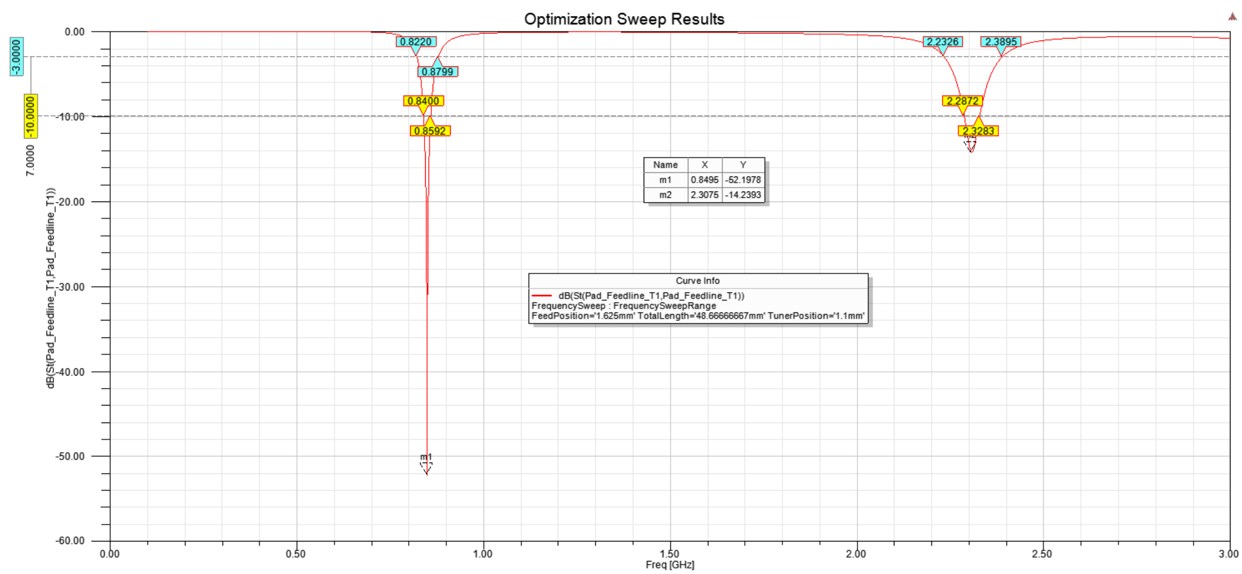

Figure 17. Image of the most "optimal" design, based on the results of sweeps on the relative feed position, antenna length, and tuner position. The bandwidths and resonances of both the 850MHz and 2.3MHz peaks are shown using markers.

For the remainder of testing the nominal values determined from the simple simulation will be used for the antenna length and tuner and feed positions, as those values were utilized for the fabrication of the physical antenna model.

The length and width of the ground plane directly affect the performance of a PIFA as well as the effectiveness of antenna tuning. The Nexus 5 utilizes a common ground plane on the back of the LCD screen for all of the antennas used in the phone, meaning any alteration made for the low-band antenna would affect those as well. Since changing these dimensions would be impractical, they were excluded from the general optimization analysis and were given an individual two-parameter sweep. The dimensions of the LCD were measured as the base values for the ground plane. The width and length of the ground plane were varied with a range from 55.476mm to 67.804mm (±10% of the measured width) and from 98.622mm to 120.538mm (±10% of the measured length), resulting in 10 equal steps for both and 100 necessary simulations. Each of these can be seen in the total sweep results shown in Figure 18, although for the sake of visibility Figure 19Figure 20 are also included. The latter figures show the S_{11} results for ground width and length as they are varied across fixed values of each other.

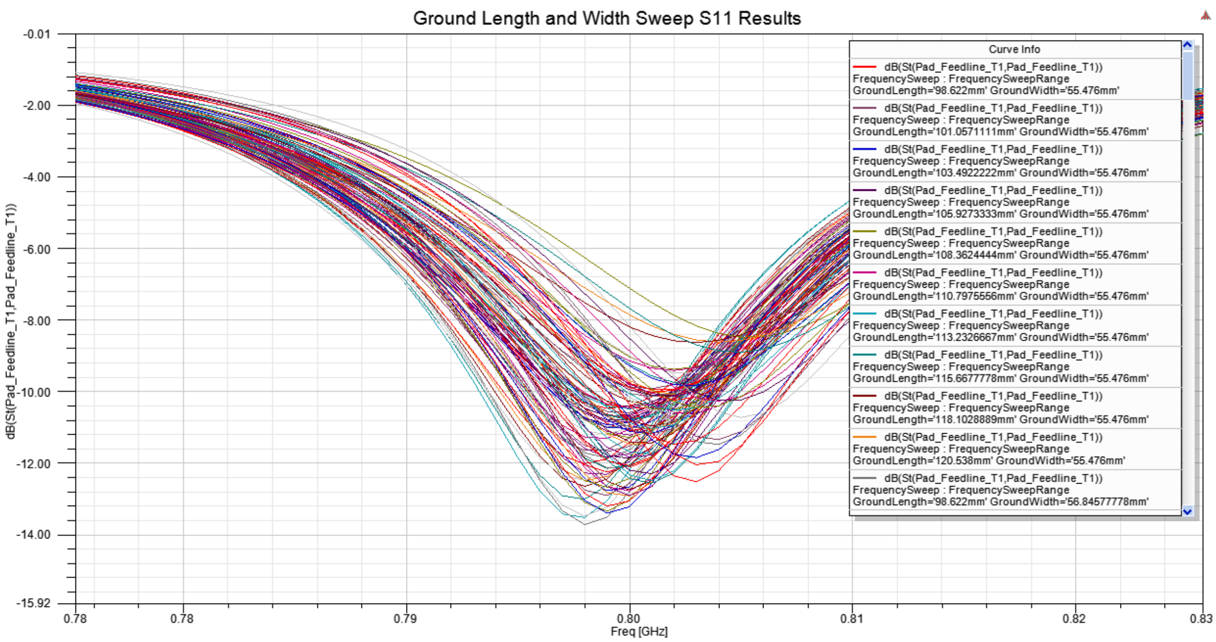

Figure 18. The combined S_{11} sweep results of the width and length of the ground plane.

To decipher the information in Figure 19Figure 20, the “Curve Info” legend proved very useful. As can be seen, each colored line corresponds to a different set of values shown in this table. Since the ground width is set to 60.955mm for the length sweep and the length is set to 108.362mm for the width sweep, the values for each are constant. However, the value for the parameter being swept varies from line to line. This can be used to track the shift of resonance as each is varied. It is notable that this analysis is much easier within HFSS, as moving the mouse pointer from one result to the next on the Curve Info field will highlight the corresponding traces.

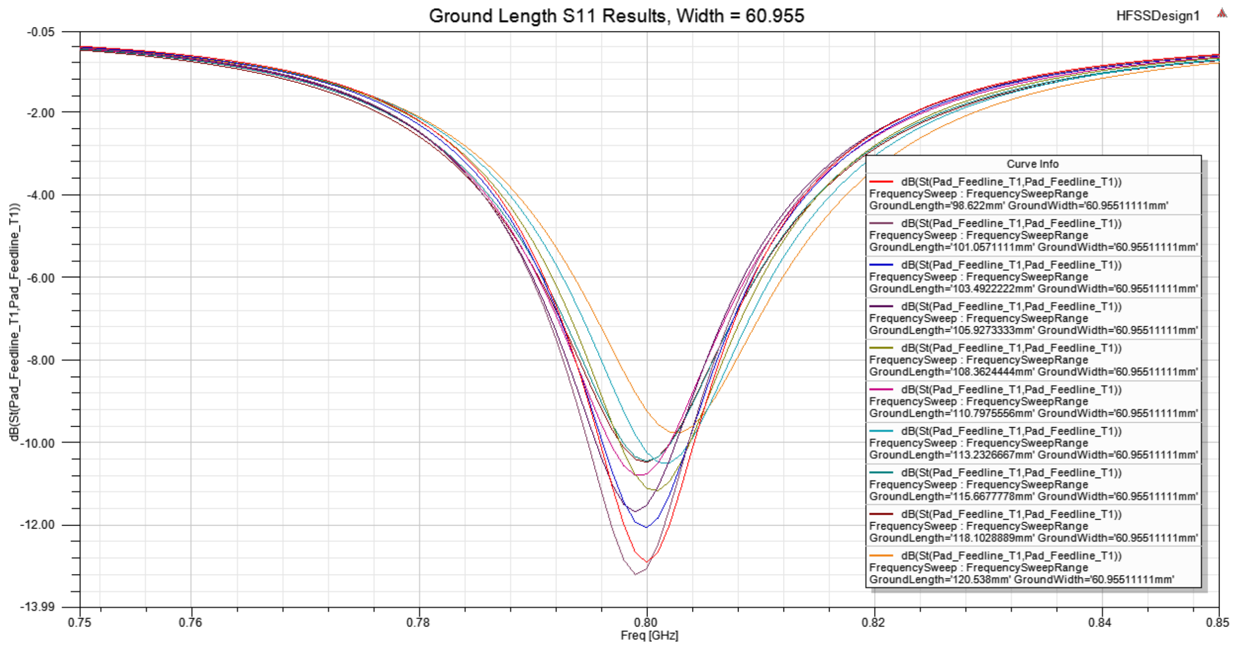

Figure 19. The S_{11} sweep results of the length of the ground plane along the X axis. As the length increases, the resonance simultaneously decreases in magnitude and increases in frequency. Theground width is set to 60.955mm.

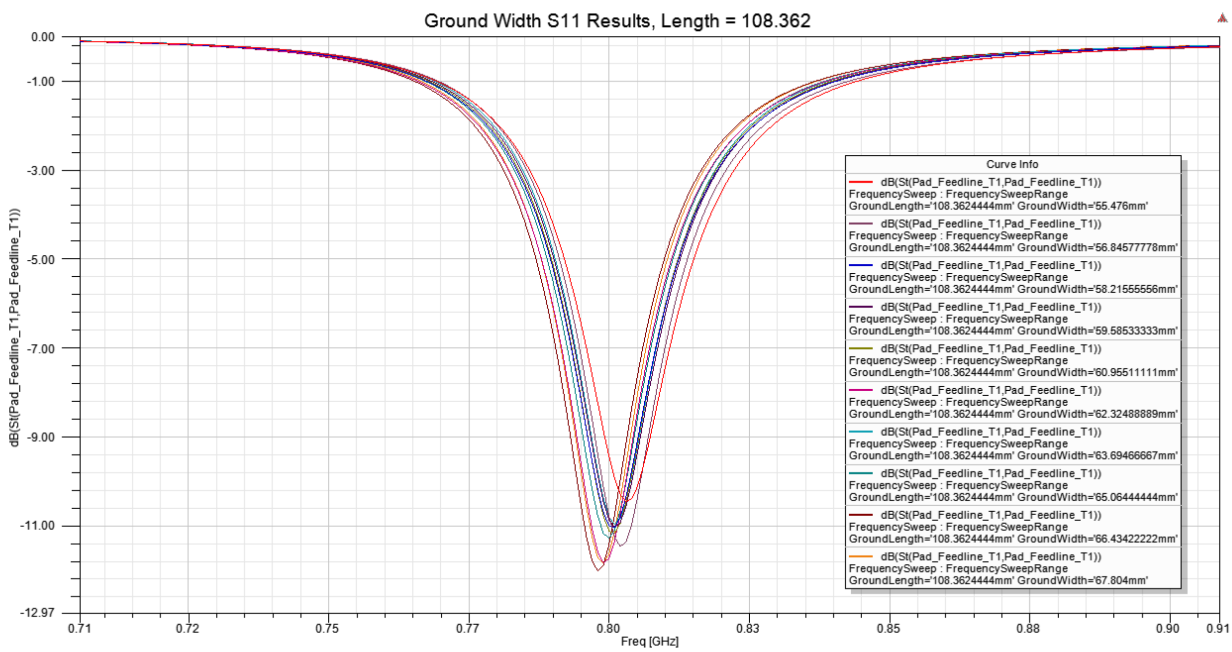

Figure 20. The S_{11} sweep results of the width of the ground plane along the Y axis. As the width increases, the resonance simultaneously increases in magnitude and decreases in frequency. The ground length is set to 108.362mm.

It is interesting to note that as the ground width is increased and the ground length is decreased, the resonance can generally be seen to downshift in frequency and increase in magnitude. There are some outliers from this behavior, however, as several times the changes might occur opposite how they are expected to. For example, both the 56.846mm and 62.325mm peaks both seem to have lower frequencies and higher magnitudes than their ground width "neighbors."

The substrate used by the PIFA has far reaching effects on the performance of the antenna. For this reason, it was important to quantify the changes in the antenna's radiation patterns as a function of the substrate's properties. Due to limitations in fabrication capabilities, and due to its general affordability, FR4 will be used for the construction of the final design. With this in mind, FR-4 (ε_r = 4.8) was used as a starting point in a separate parameter analysis of different substrates. For this sweep, the antenna behavior using substrates made of FR4, air, and four varieties of Rogers materials (RT/duroid 5870, RT/duroid 6010/6010LM, TMM 4, and TMM 6) were used. The Rogers substrates were used since they are known to be lossless and have a wide range of relative permittivity values. Figure 21 through Figure 26 include the S_{11} sweep results for the antenna with each examined substrate.

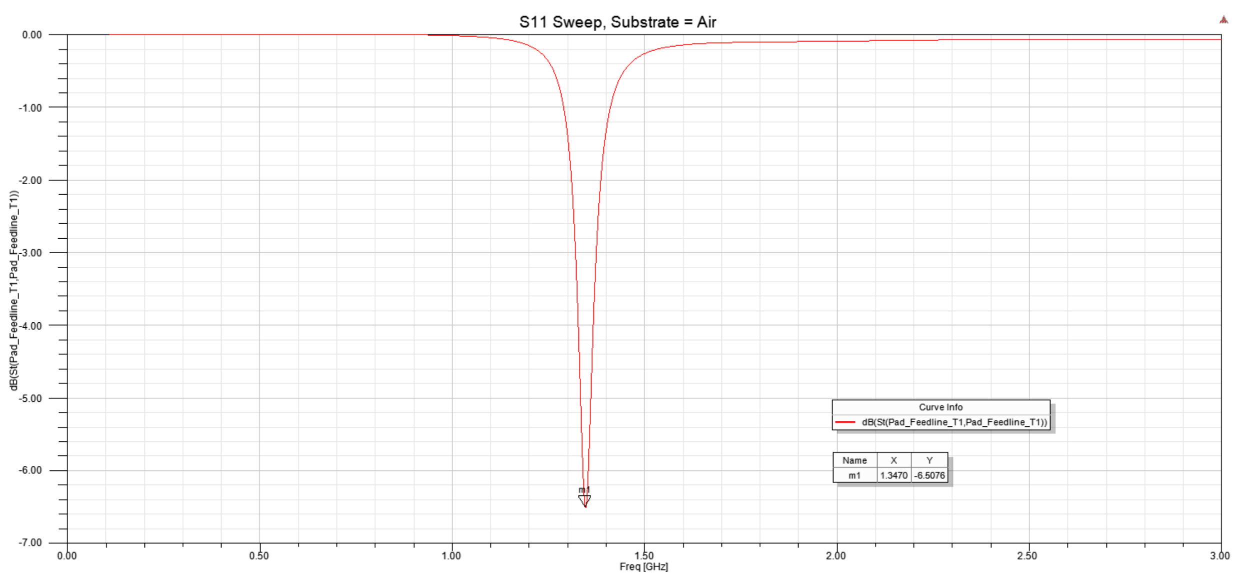

Figure 21. S_{11} results for the nominal antenna model using air (ε_r = 1.0006) as a substrate.

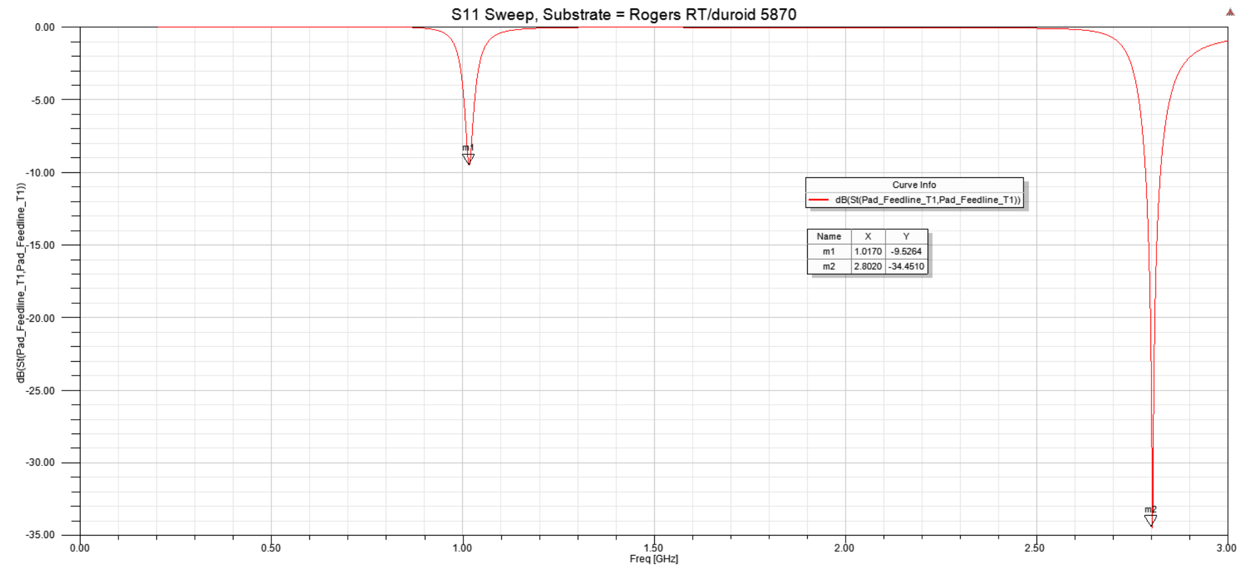

Figure 22. S_{11} results for the nominal antenna model using Rogers RT/duroid 5870 (ε_r = 2.33) as a substrate.

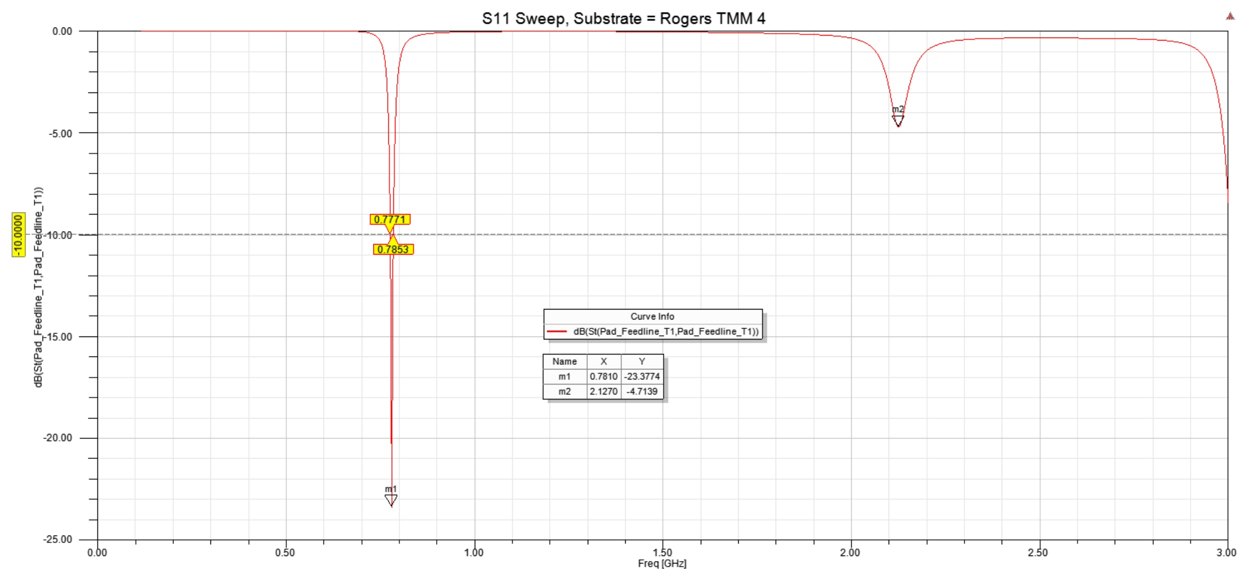

Figure 23. S_{11} results for the nominal antenna model using Rogers TM 4 (εr = 4.5) as a substrate.

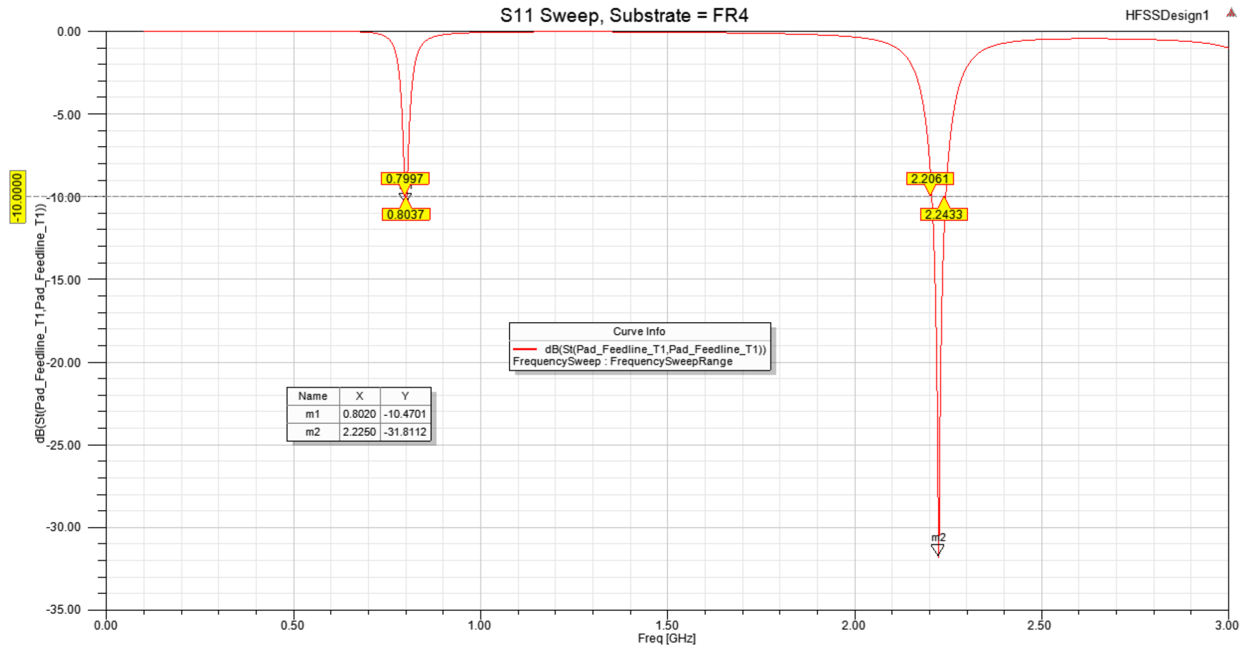

Figure 24. S_{11} results for the nominal antenna model using FR4 (ε_r = 4.8) as a substrate.

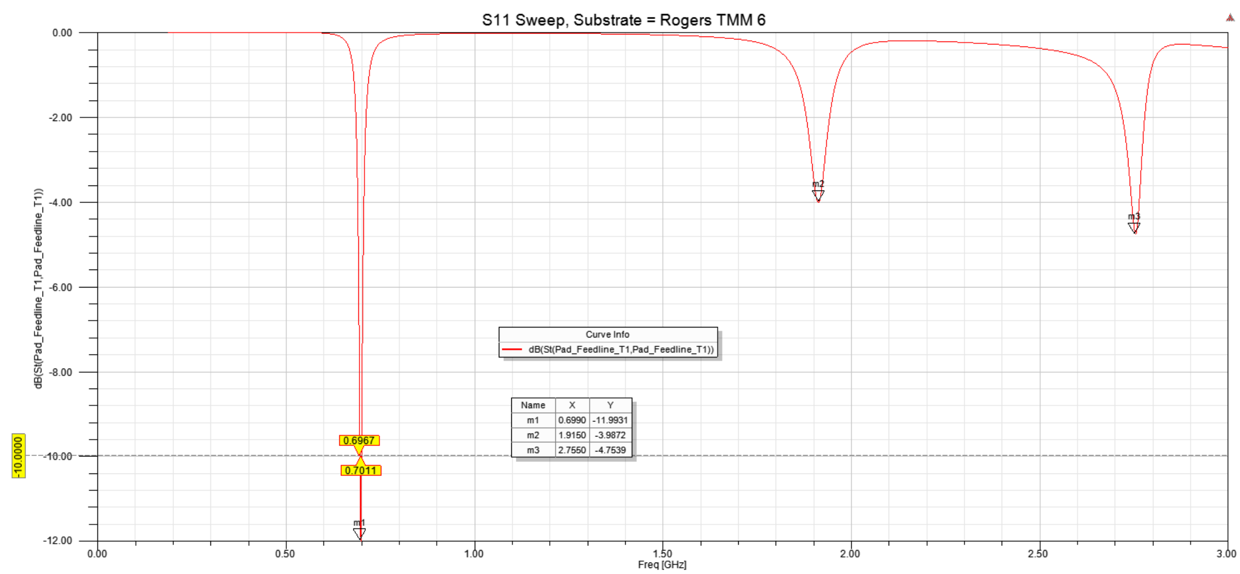

Figure 25. S_{11} results for the nominal antenna model using Rogers TM 6 (εr = 6) as a substrate.

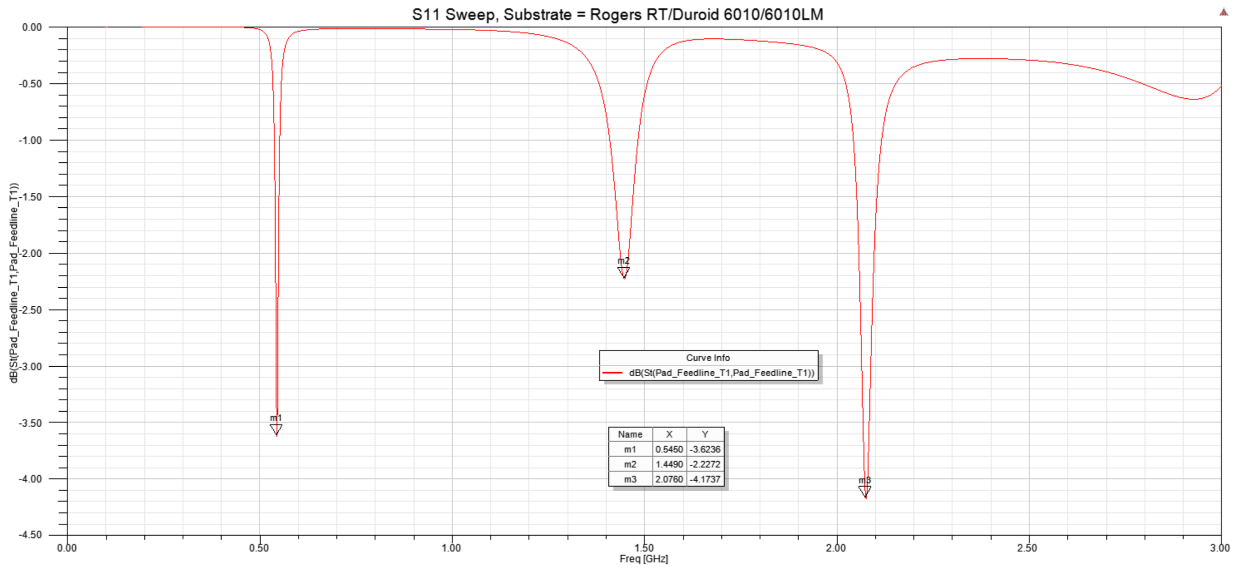

Figure 26. S_{11} results for the nominal antenna model using Rogers RT/duroid 6010 (ε_r = 10.2) as a substrate.

The results of these models show that the substrate has a very strong effect upon the behavior of the antenna. For example, it can be seen that, generally, the frequency of the resonance will decrease and the magnitude of the response increase as the relative permittivity of the substrate increases. However, Rogers TM 4 and RT/duroid 5870 both break the pattern for resonance magnitude, as TM4 has a much greater decibel peak than expected and the RT/duroid 5870 has a much smaller decibel peak than expected. Meanwhile, the frequency of resonance for either FR4 or TM 4 also breaks the pattern, as highlighted in Table 1.

Table 1. Comparison of S_{11} peak characteristics of the nominal antenna using various substrates. Outlying data points are highlighted.

Substrate	Relative Permittivity (ε_r)	Resonant Frequency (GHz)	Peak Resonance (dB)
Air	1.006	1.347	-6.51
Rogers RT/duroid 5870	2.33	1.017	-9.53
Rogers TM 4	4.5	0.781	-23.38
FR4	4.8	0.802	-10.47
Rogers TM 6	6	0.699	-11.99
Rogers RT/duroid 6010	10.2	0.545	-3.62

The distance separating the microstrip lines of the PIFA and the ground plane is vital to antenna performance. The thickness of the Nexus 5 substrate was used as a base value for this parameter. This value was measured to be about 5mm. Due to fabrication limitations the substrate thickness needed to be in multiples of 1.6mm, so a value of 4.8mm was assumed. Since this value in the Nexus 5 was assumed to be fixed, the measured thickness was used as a starting point of a parameter analysis apart from the optimization process. This sweep assumed that other substrate thicknesses could be used, and was performed in 10 steps from 4.32mm to 5.28mm. From the results, it can be seen that increasing the substrate generally leads to an increase in resonance magnitude and a downshift frequency. The results of the parameter sweep of substrate thickness are shown in Figure 27.

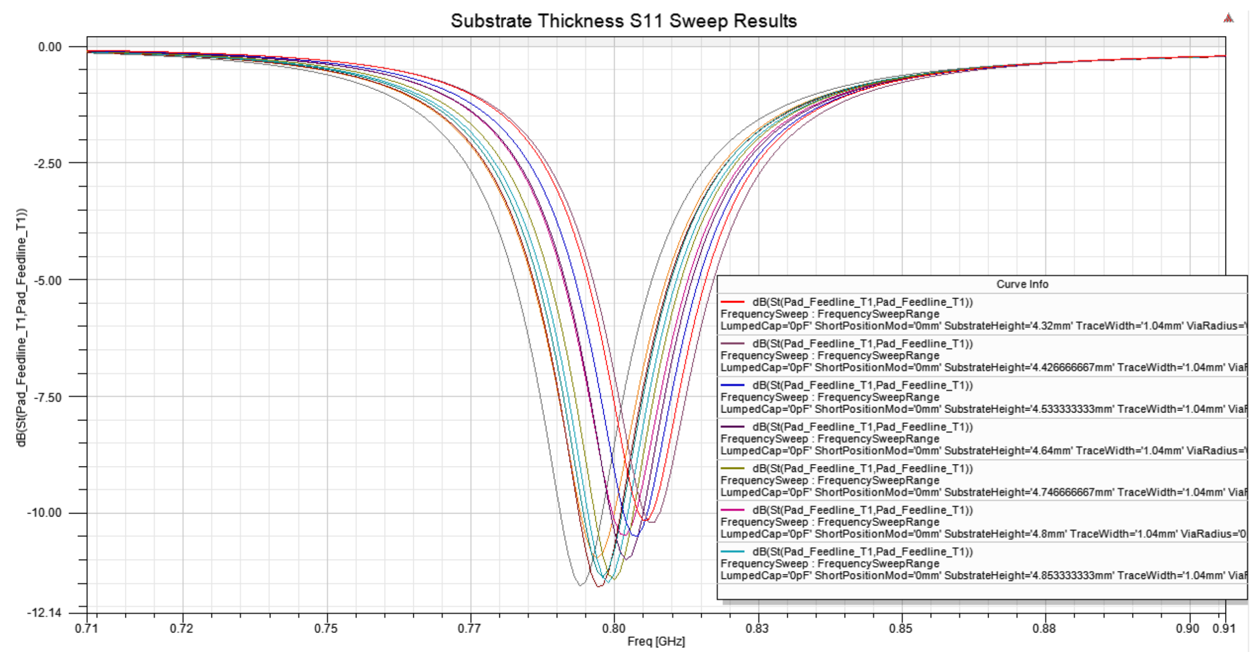

Figure 27. The S_{11} sweep results of the thickness of the substrate. As the thickness increases, the resonance simultaneously increases in magnitude and decreases in frequency.

It is possible that the relatively thick substrate or the relative permittivity of that substrate are responsible for the difference in length from that calculated. As discussed by Daniel Schaubert et al [16], the thickness of the substrate creates an inductive effect upon the antenna's impedance, which creates erratic results in terms of antenna behavior. This can possibly explain the fluctuations in the patterns noted in the substrate thickness sweep results. For the discussed experiment the unpredictable behavior began when the thickness of the substrate exceeded 0.02 wavelengths, which would be 3.22mm for the 850MHz antenna. This means that the behavior of the designed antenna, while attempting to mimic the

Nexus 5 device as closely as possible, may not be easily predictable. In this sense it is possible that the original measurement of the substrate thickness of the smartphone was incorrect, unless the actual substrate's relative permittivity is below 1.19 (although this seems unlikely).

The width and position of the shorting pin also play a role in the performance of PIFAs. The shorting pin was placed at the very end of the antenna, as that allows for the least amount of material and space to be used. The component was implemented as a multilayer via that stretches from the top layer of the substrate to the ground plane, so rather than a width in this case a radius was used. Due to design limitations this was a fixed value of 0.52mm. At points where the via contacted another surface, a pad that adds about 0.52mm, or roughly ½ of the line width, another pad was applied to the design. Because the value was fixed, a separate parametric sweep was performed for the via radius with 10 evenly spaced values from 0.342mm to 0.418mm, as seen in the Curve Info of Figure 28. The short position (effectively the position of the entire antenna) along the X axis was included in the optimization sweep, with 10 values ranging from 0mm to 10mm away from the nominal position as shown in Figure 29.

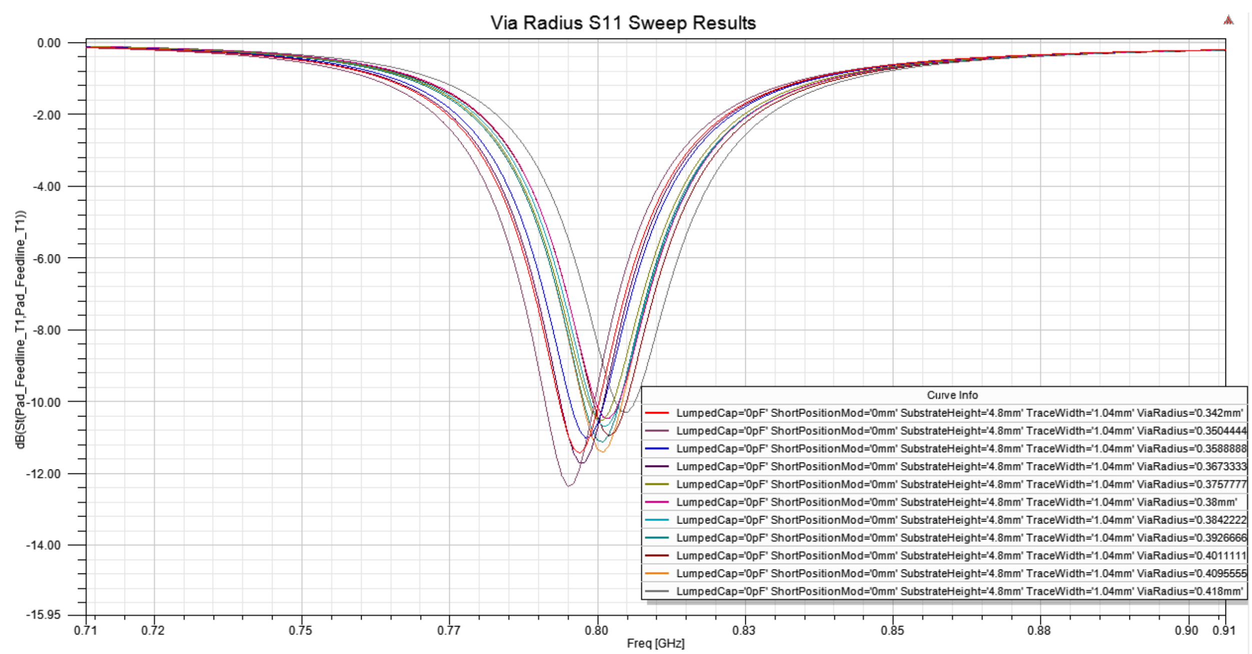

Figure 28. The S_{11} sweep results of the magnitude of the radius of the vias used for the shorting, feeding, and tuning pins.

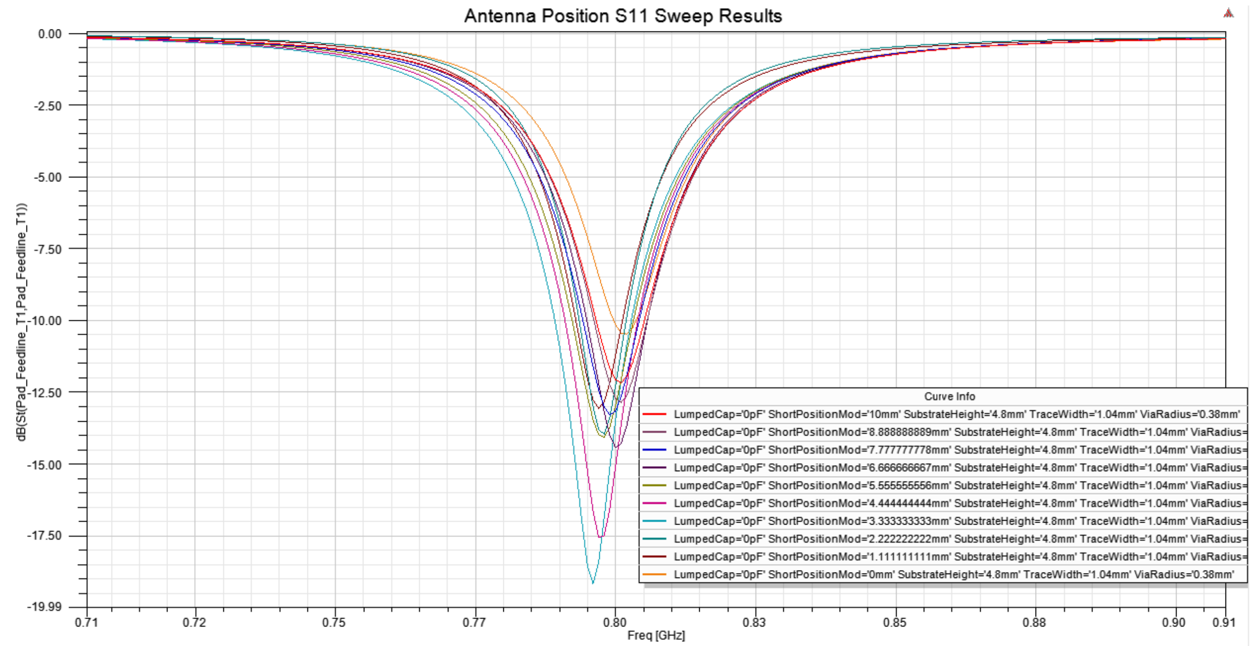

Figure 29. The S_{11} sweep results of the position of the antenna as a measurement of its distance along the X axis from the corner of the ground plane.

From the results shown in Figure 28, it would seem that decreasing the size of the vias tends to reduce the resonant frequency, but increase the magnitude of the decibel peak. In terms of antenna position in Figure 29, it should be noted that there is a change in pattern when the value of the position modifier exceeds 3mm, as at that point two previously disjointed portions of the ground plane connect. This ground overlap/connection can be seen in Figure 30. It is interesting to note that the largest magnitudes of response are both directly "after" the two ground surfaces are merged, and as the radiator and pins are shifted further along the ground plane the response tends to reverse. In short, there is an ideal position to achieve resonance on the device. This seems to support the idea that the antenna is most resonant the closer it is to the corner of the ground plane. It should be noted that the disjointed ground planes occurred due to difficulty modeling the coaxial connector used in the physical model, as ports within HFSS require both a reference and an output to determine current flow. Being able to model the exact coaxial connector would increase the accuracy of the simulations as compared to the physical device, as the traces for the connector could be defined more realistically.

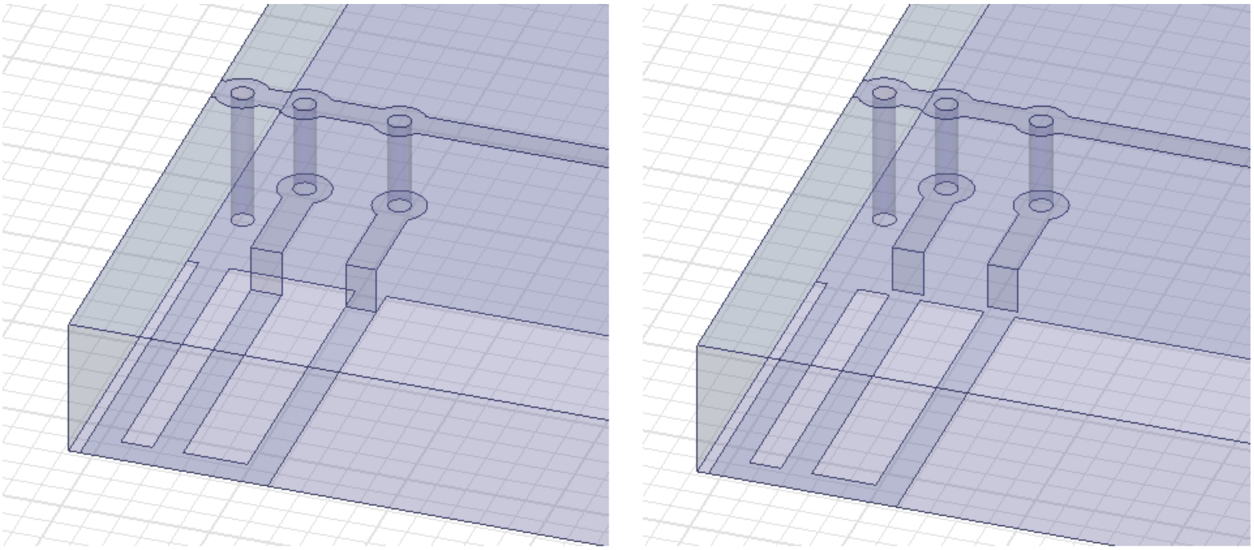

A) B)

Figure 30. Model of the antenna network when the antenna is shifted A) 2mm and B) 3.33mm. At 3mm, the two components of the ground plane overlap and combine.

The width of the antenna trace is important because it is a small component of the antenna's length. It is also noteworthy for being able to tweak the bandwidth of the antenna's operation. To analyze this parameter, which is considered to be a fixed value from the Nexus 5 device, a solitary parameter sweep was run across 10 values from 0.88mm to 1.2mm. The results are shown in Figure 31.

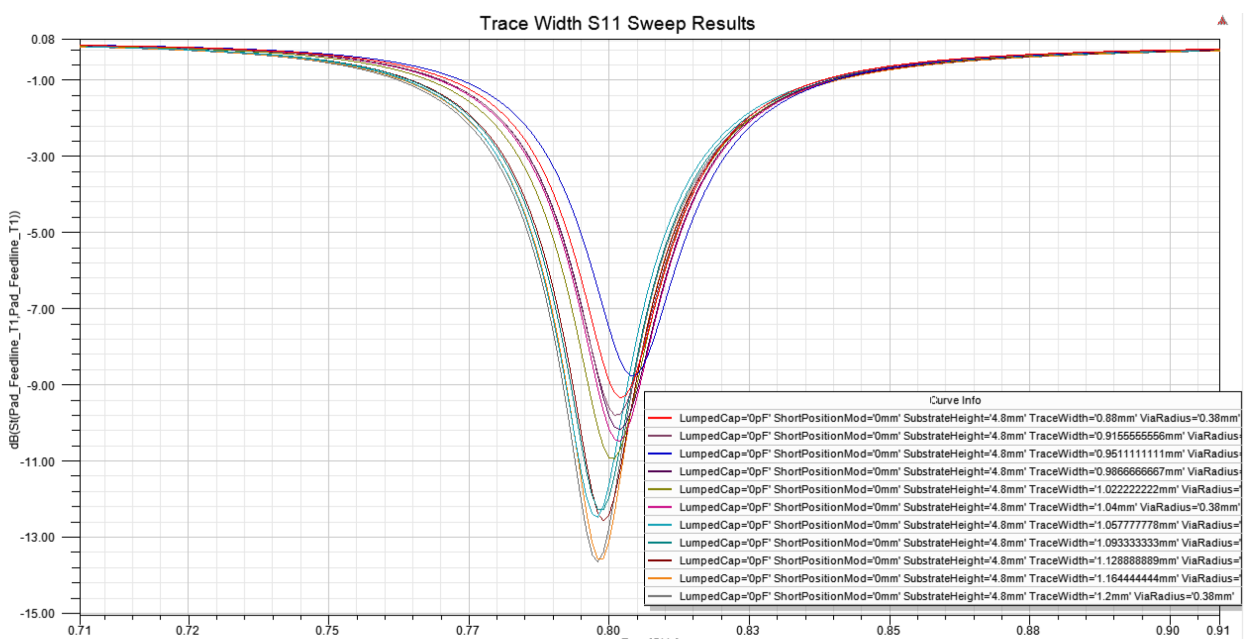

Figure 31. The S_{11} sweep results of the width of the microstrip lines.

The results of the trace width sweep show a trend of increasing magnitude and decreasing frequency of the S_{11} characteristic of the antenna as the width is increased. It can be noticed that the resonance shift indicates an increase in bandwidth, as the right sides of each slope seem to have similar characteristics, but the left side stretches outwards. From this, it would seem that the best strategy to increase the bandwidth at the resonant frequency would be to adjust the antenna to be resonant at a slightly higher frequency, then downshift it by increasing the radiator width.

4.2. ADS Model

The high frequency schematic modeling software Advanced Design System (ADS) is highly optimized for use in RF circuits. Taking advantage of the strength of this software, it was determined that ADS should be used for modeling the matching network of the device as well as varying the tuning capacitor. This was accomplished through the use of the one port and two port antenna components found in the component libraries of ADS as shown in Figure 32.

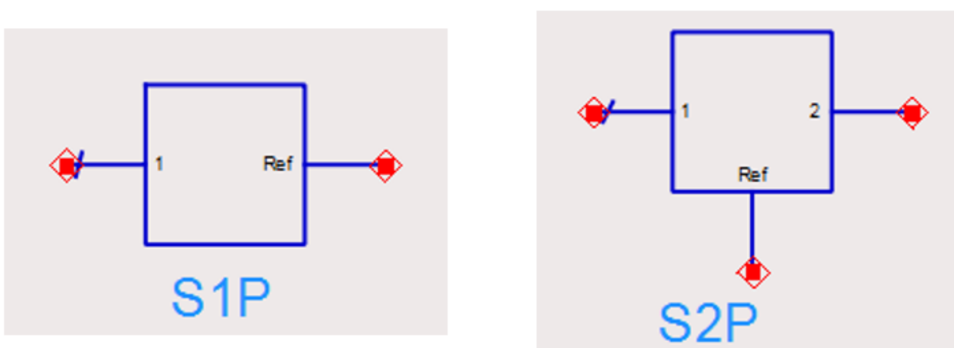

Figure 32. Examples of 1-port and 2-port, respectively, component models from ADS.

A touchstone file is an industry standard for network analyzers and circuit simulators [17]. The S_{11} parameters for a device, whether it is a simulated or a physical device, are recorded within the file. This allows the characteristics to be analyzed and displayed within other programs. The file format is .SnP where the *n* represents the number of ports in the measured system (i.e. a 1-port device would have an .S1P file, a 2-port device would have an .S2P file, etc.). The power of the touchstone file lies in the ability to transfer data from one environment to another. ADS is a powerful program for modeling circuit components and how they are interconnected. HFSS is a powerful program for modeling the characteristics of antennas. The touchstone file allows the characteristics of an antenna to be modeled within HFSS and then imported into ADS to be further analyzed with other components. This same method can be applied to a network analyzer. A frequency sweep performed for a physical device can be recorded into a touchstone file and then imported into ADS for further analysis. This makes comparisons between the computational and physical model possible in the same platform. Figure 33 gives an example of how a touchstone file imported into ADS represents the same data as seen in HFSS.

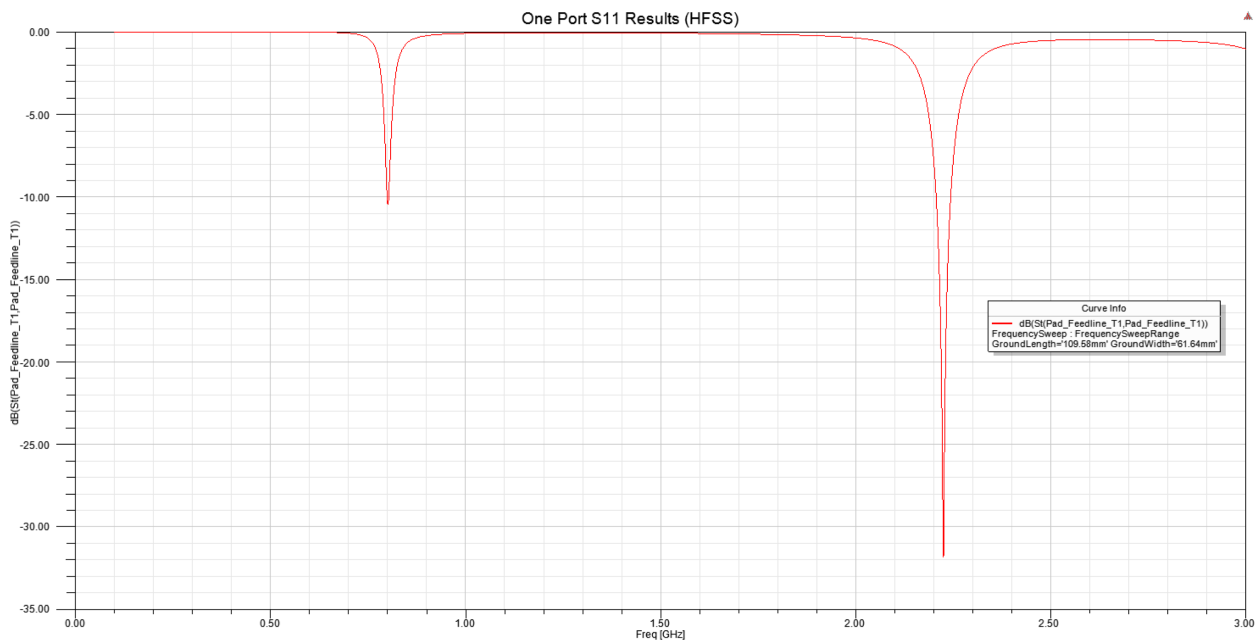

Figure 33. S_{11} parameter data for a 1-port antenna network in HFSS.

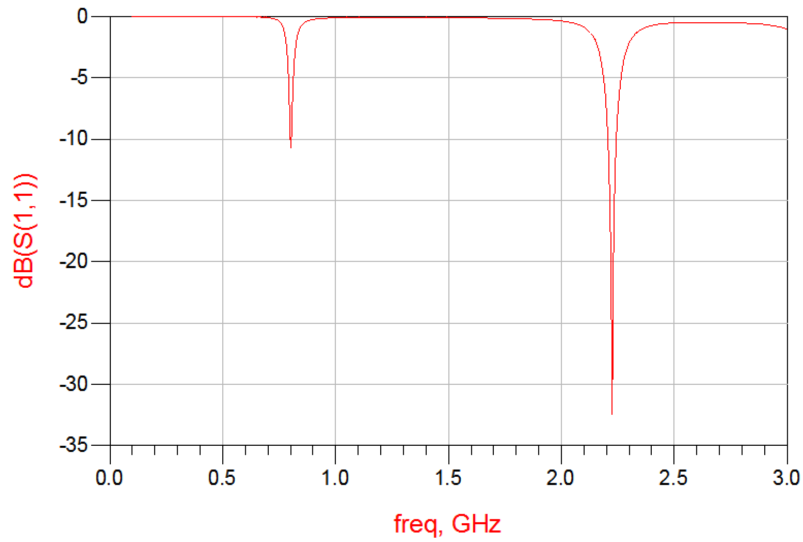

Figure 34. S_{11} parameter data from the HFSS Touchstone output modeled in ADS.

In the same manner as importing HFSS, importing a touchstone file from a network analyzer allows the modeling of the antenna characteristics within ADS. Figure 35 shows the S_{11} of the physical antenna on the network analyzer and in ADS.

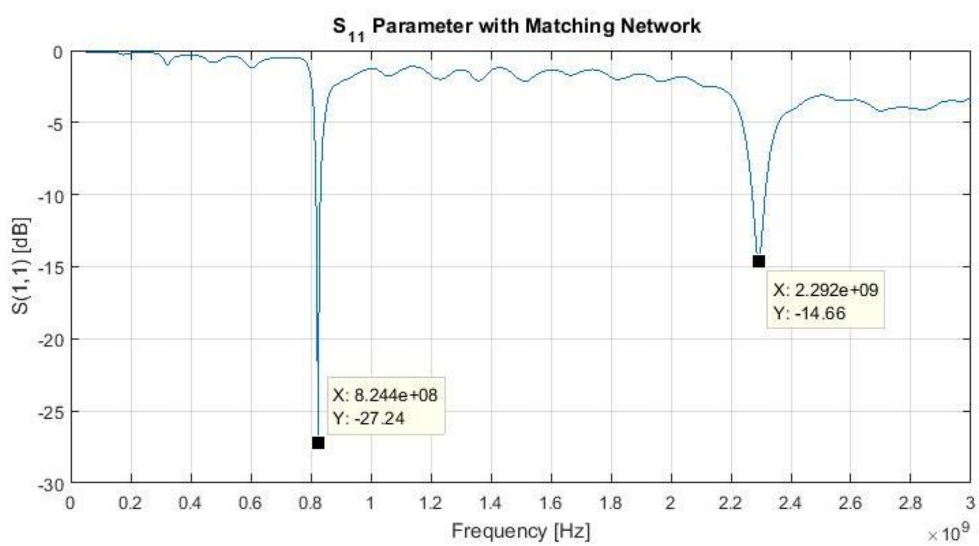

Figure 35. S_{11} data extracted from Antenna 1, plotted in Matlab.

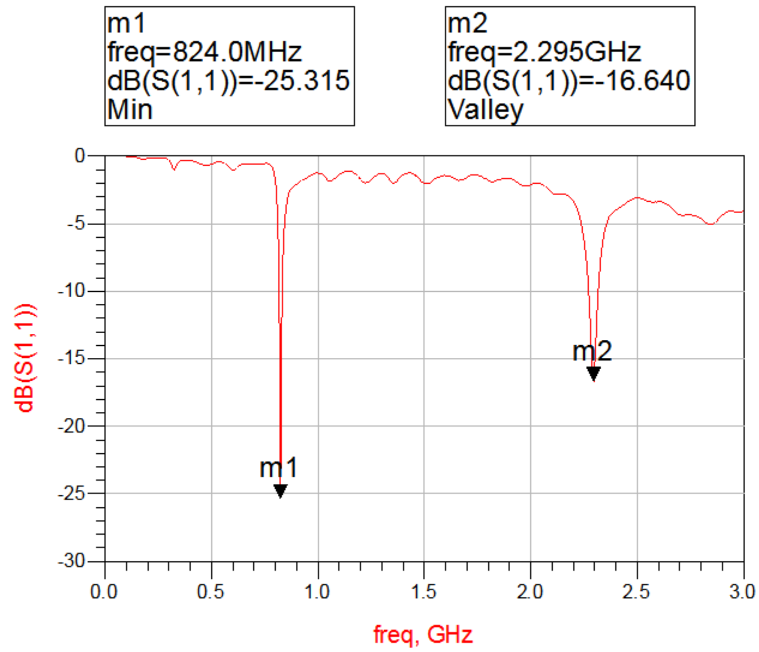

Figure 36. S_{11} data extracted from Antenna 1 and plotted in ADS.

The team created a two port antenna model within HFSS for the PIFA design. This allows for the connection of a tuning capacitor to the antenna. This plays to the strengths of both software with minimal discrepancy in results. Figure 36 and Figure 37 show the results of modeling the antenna with a 1pF tuning capacitor in ADS vs HFSS.

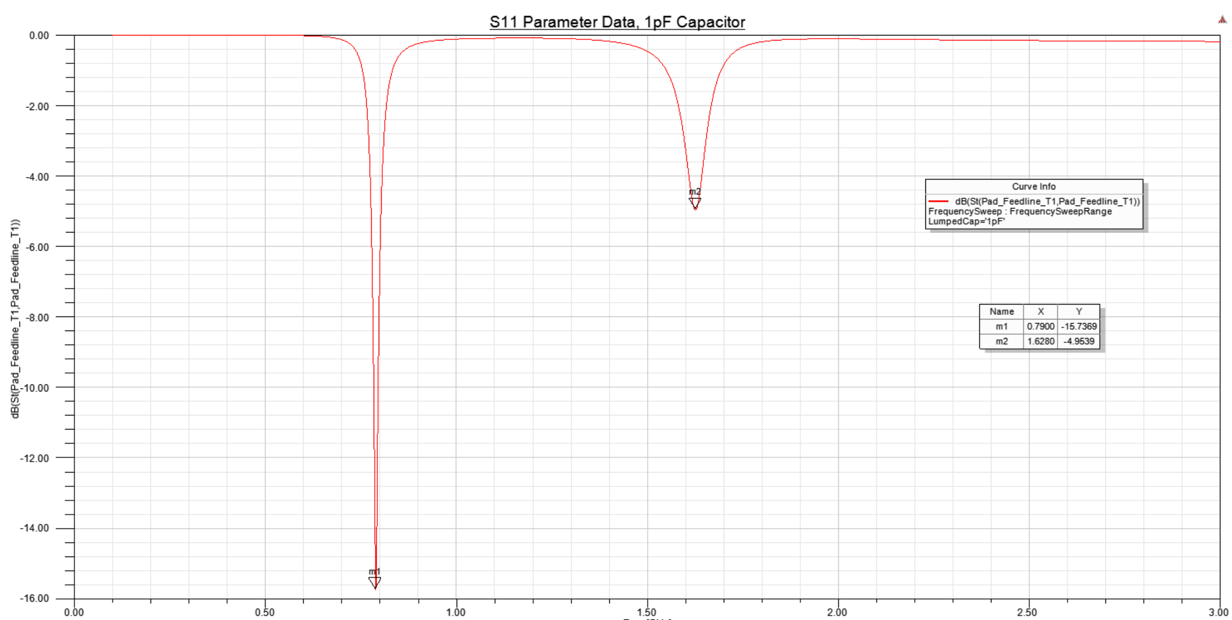

Figure 37. S_{11} parameter data with a 1pF tuning capacitance, in HFSS.

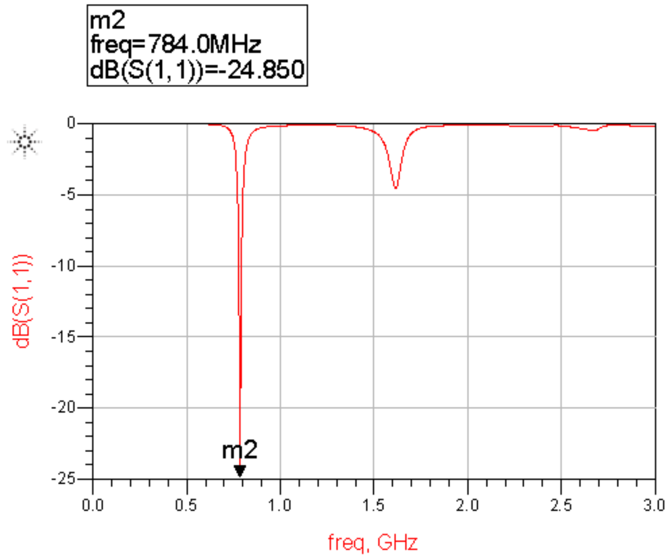

Figure 38. S_{11} parameter data with a 1pF tuning capacitance, in ADS.

As seen in Rigures 37 and 38, there is a difference between the results of the two programs. Since the difference is minimal, it is acceptable to use this method to present the behavior of the antenna under tuning conditions in order to ease the computational power required to run the HFSS simulations. The effects of varying a tuning capacitor within HFSS can take upwards of hours, whereas within ADS it takes seconds. While the results from HFSS are more accurate, the beneficial effects of reducing simulation time far outweigh the loss in precision.

The design of the circuit used in ADS, shown in Figure 39, was created with the tuning capabilities of ADS in mind. The resistor (RPC) in parallel with the capacitor (C) serves the purpose of being able to create a short by making the resistance extremely small. Essentially, this allows the capacitor to be removed in the tuning process without rerunning the simulation process. The resistor (RLS) in series with the inductor (L) serves a similar purpose. The value of the resistor can be increased to an extremely high number. This basically makes an open circuit thus removing the inductor from the circuit.

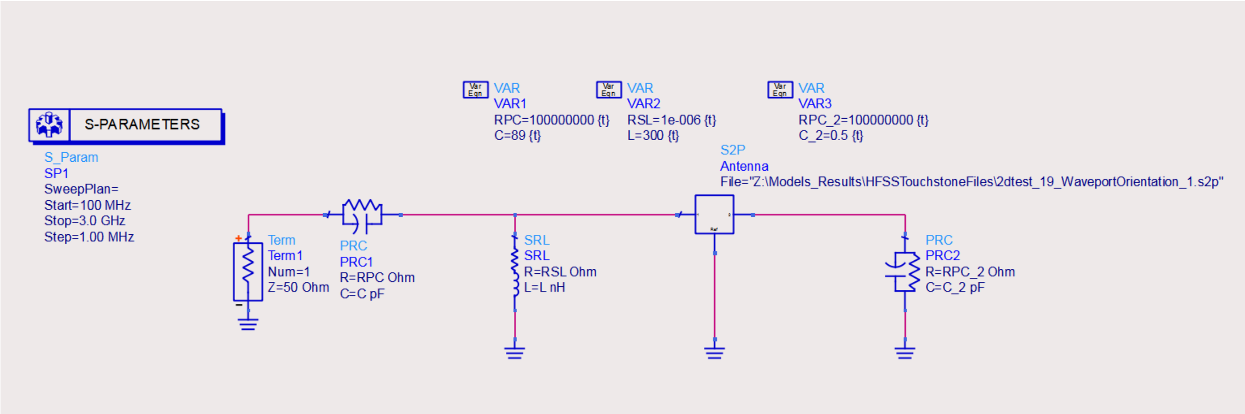

Figure 39. ADS 2-port system schematic.

The tuning capabilities of ADS allow the team to modify the values of different components and see the results of these modifications in real time. A direct result of this technique is the ability to easily determine the values of the capacitor and inductor for the matching network of the antenna. Figure 40 illustrates in the Smith Chart of what the process of creating the matching network using the tuning method entails. This tuning method was then applied to the tuning of the antenna within ADS. Figure 41 shows the effects of using the different capacitance values with the simulated antenna model from HFSS.

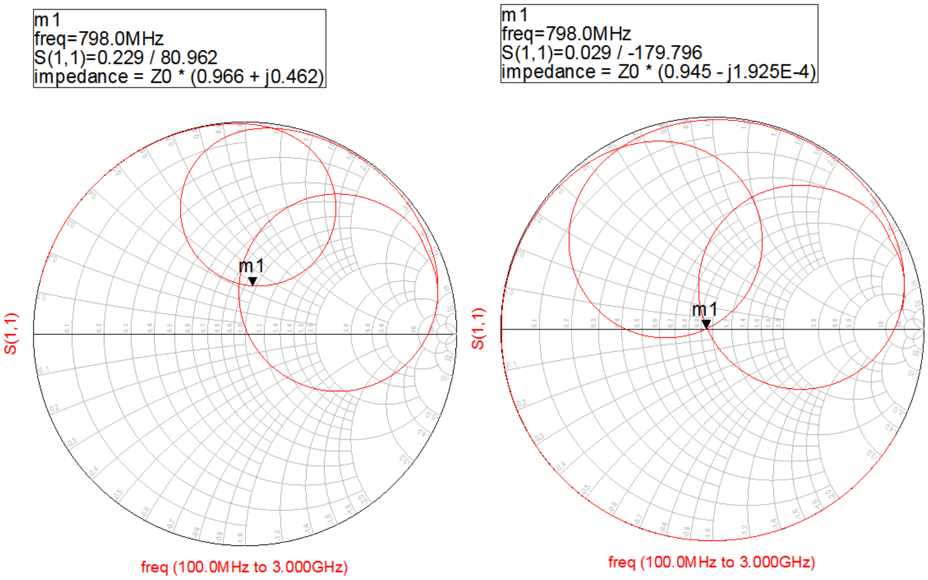

Figure 40. Smith Charts for the two port system in ADS before (left) and after (right) the matching circuit is applied.

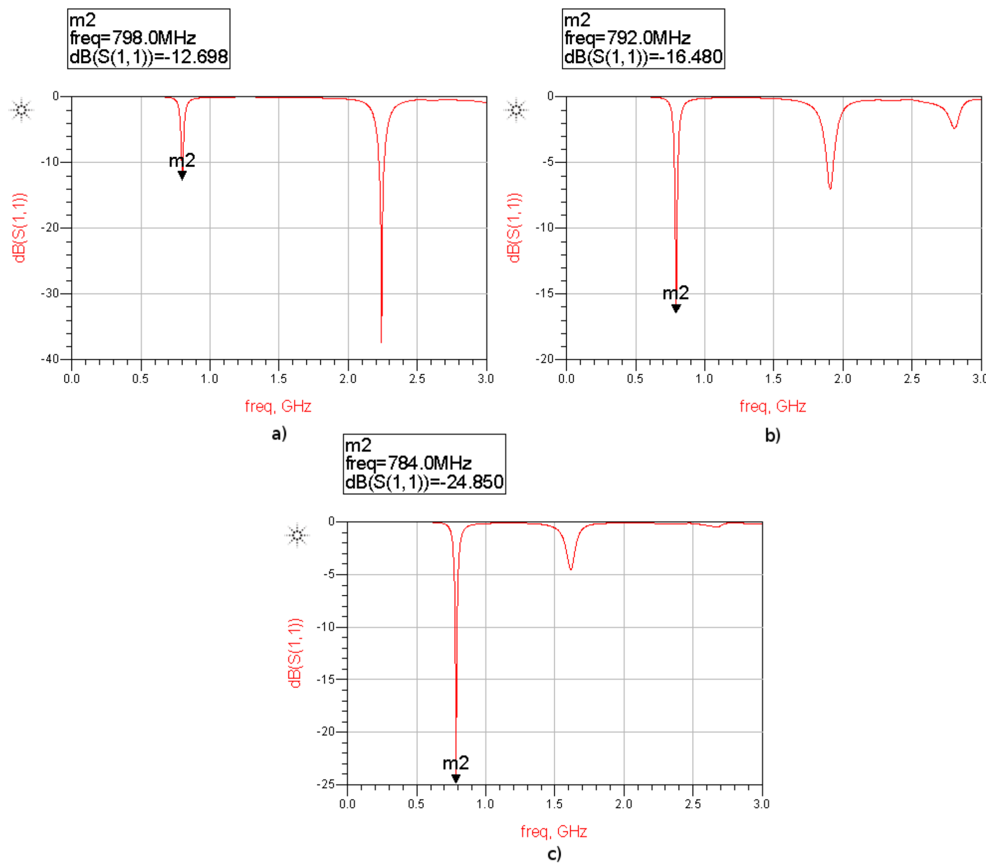

Figure 41. S_{11} parameter data for the matched 2-port network in ADS with a) 0pF b) 0.5pF and c) 1.0 pF tuning capacitors.

The increasing capacitance values show overall trend and effect on the S_{11} of the antenna. The resonant frequency moves 14.0 MHz and the magnitude of S_{11} at that resonant frequency decreased dramatically as the capacitance is increased. This shows the tradeoff of resonance versus reflection magnitude when tuning the antenna. The resonant frequency of may move to the desired frequency however, the optimal performance of the antenna will occur at its natural resonant frequency.

4.3. Physical Model

With the completion of the computational PIFA model, a 3D model for fabrication was created, see Figure 42. Altium was chosen for this task as it is a popular Printed Circuit Board (PCB) design software that can easily create acceptable files for printing through Advanced Circuits. Advanced Circuits was chosen as an outside company for board fabrication because of their high quality board construction and because of their offering of a student discount rate.

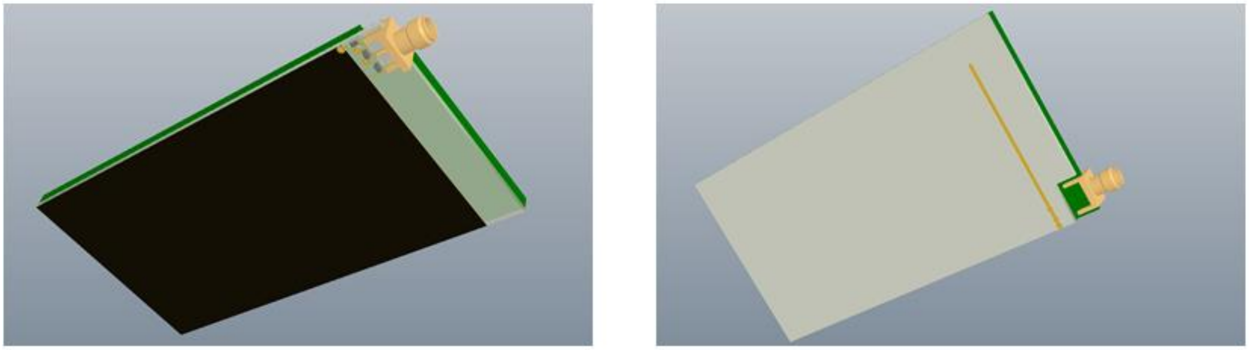

a) b)

Figure 42. The a) Bottom and b) top of the PIFA model designed in Altium.

4.3.1 Designing the Model in Altium

The PCBs were created using very specific dimensions obtained through the computational model. Important to the operation of the PIFA is the length of the radiating arm, the width of the microstrip line, the thickness of the substrate, the dimensions of the ground plane, and the positions of the shorting pin, feed point, and tuning point. The length of the radiating arm was found to be 51.7mm. The trace of the radiating arm is shown in Figure 43, and is measured from the left side of the shorting pin to the right side of the red antenna trace. This length was the optimum length of the radiating arm at the time of the creation of the physical model of the PIFA. Later it was determined that a slightly different arm length would result in a better resonant frequency of the antenna; this will be discussed in greater detail in Section 4.5.

Figure 43. Radiating arm of the antenna in Altium (the trace in red).

The width of the microstrip line and the dimensions of the ground plane were taken directly from the Nexus 5 as this is the model that this report is trying to emulate. The measurements were taken using digital calipers which introduce an uncertainty of about ±.02mm. This uncertainty is negligible for the purposes of this report. The width was found to be 1.04mm and the dimensions of the ground plane were determined to be 61.64mm by 109.58mm. These dimensions are displayed graphically in FiguresFigure 44Figure 45.

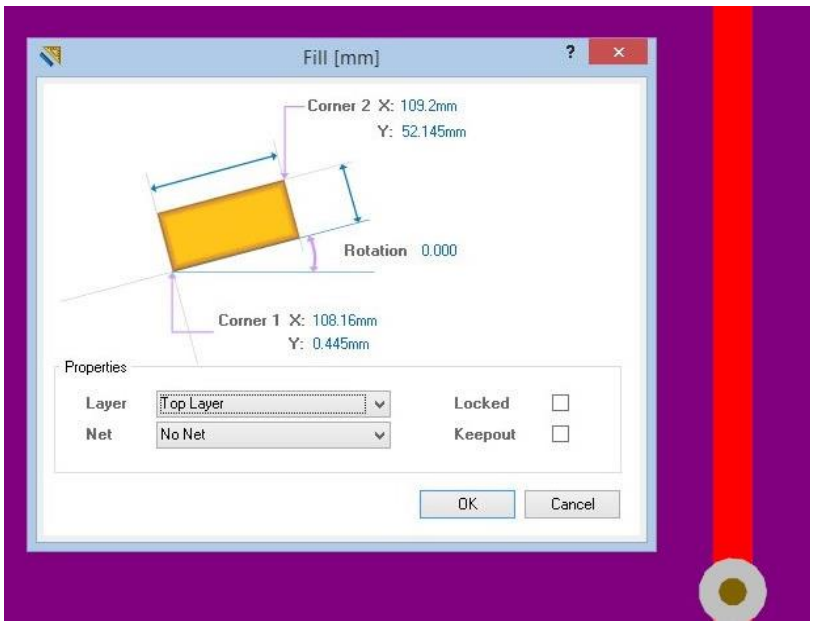

Figure 44. Width and length of the microstrip line given in X, Y coordinates.

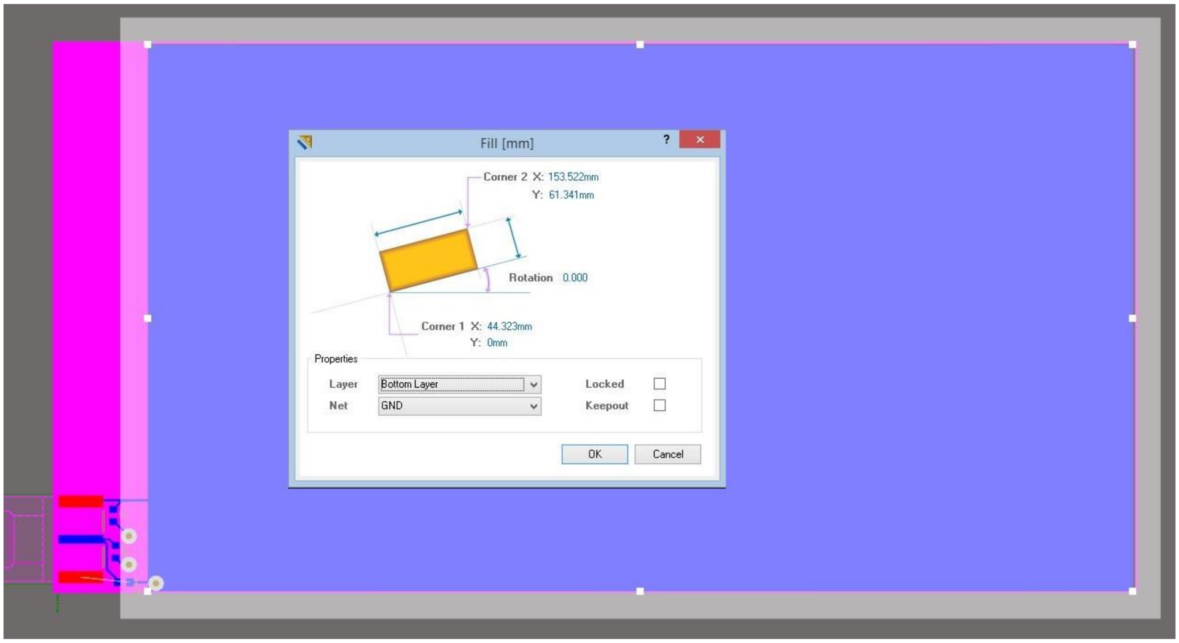

Figure 45. Dimensions of ground plane (blue square area) given in X, Y coordinates.

Like the length of the radiating arm, the positions of the shorting point, feed point, and tuning point were taken from the results of the HFSS computational model. The shorting pin was at the end of the radiating arm, the feed pin was 2.1mm from the end of the radiating arm, and the tuning pin was 5.3mm from the end of the radiating arm. The relative positions of these pins are shown in Figure 46.

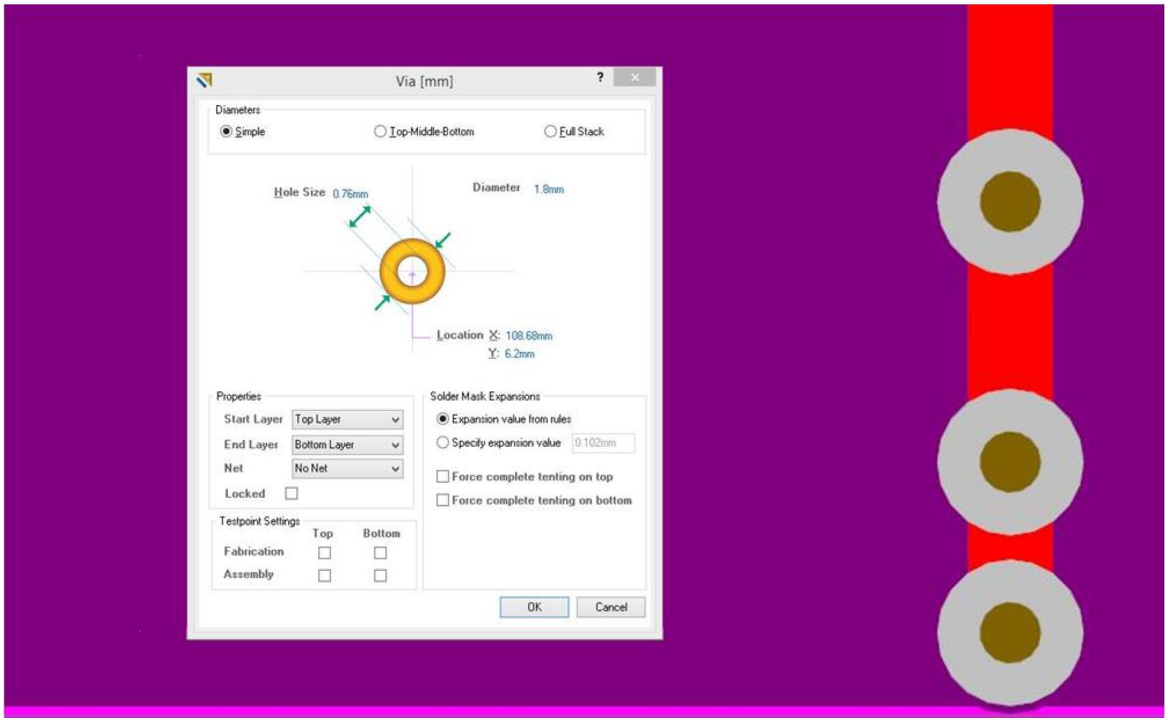

Figure 46. From bottom top: short, feed, and tuning point. The dimensions for the tuning point via are given. The other vias have identical dimensions except for the relative positions.

The thickness of the substrates posed the greatest challenge in creating the PCB. From the Nexus 5, the thickness of the substrate was determined to be 5.0mm. With the student rate, Advanced Circuits will only print boards of thickness 1.6mm. The solution to this problem was to layer boards in order to obtain a distance as close as possible of 4.8mm. With this in mind, three board layers were decided upon. The shorting pin, feed pin, and tuning pin will pass through each layer to reach ground plane and the respective components.

The top layer contains the radiating arm with vias for the shorting point, feed point, and tuning point. The computational model accounts for having vias in the radiating arm; this will remain consistent. The second layer will contain a via for the shorting pin and two pads extending from the position of the feed point and tuning point to about 3mm away ending in another via, as shown in Figure 47. This design property was done in order to keep the ground plane as undisturbed as possible with only the shorting pin breaking the plane. The shorting pin and feed pin will now extend into a substrate overhang.

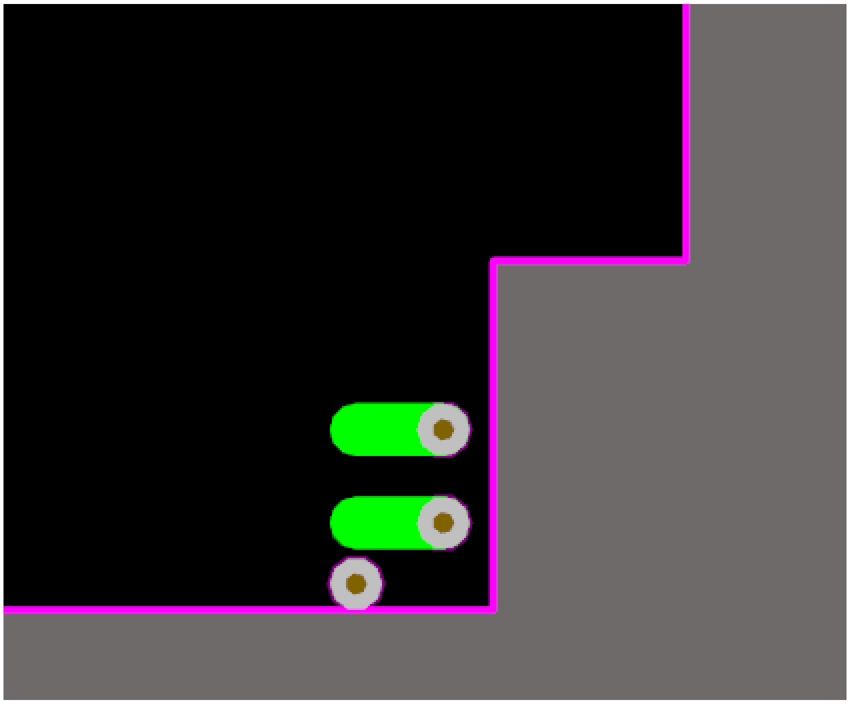

Figure 47. Middle layer with pads extending the connections for the tuning point and the feed point.

The bottom layer will contain the ground plane with the dimensions mentioned previously as well as via for the shorting pin to make contact. Pads for a matching network were placed in connecting the feed line to the SMA connector, as shown in Figure 48. The simple matching network consists of a series capacitor and a shunt inductor which is consistent with what is found on the Nexus 5. Another pad is placed in series with the tuning via and ground. This will provide a position for the tuning capacitor of the antenna. It is important to note that the position of the vias on each board must be placed properly so they line up from one layer to the next. The reasoning for this will become apparent in the following section where the assembly process will be reported in detail.

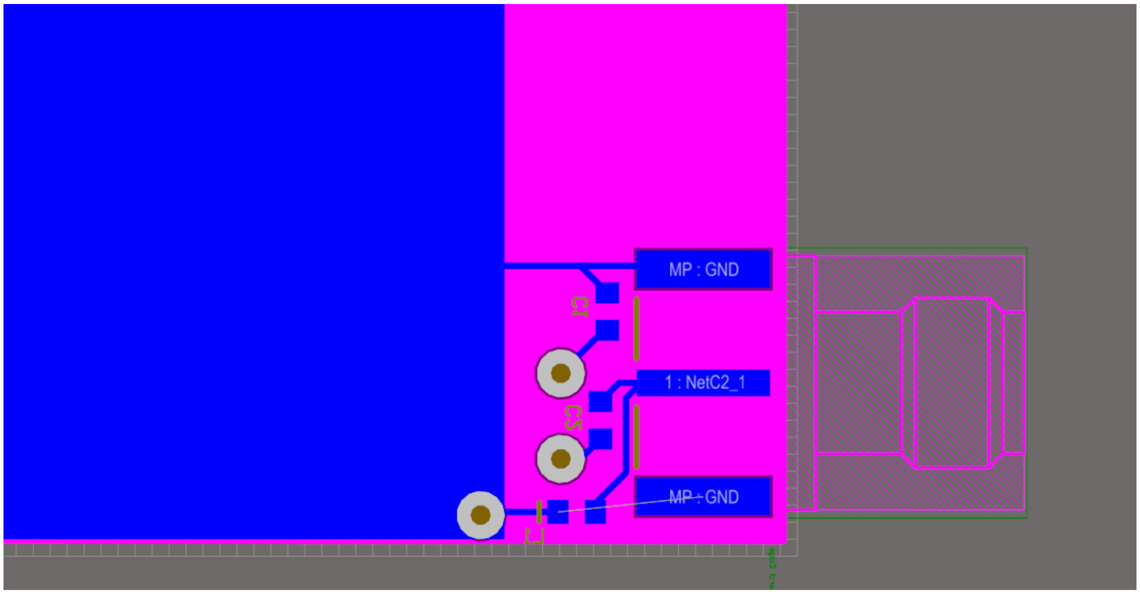

Figure 48. The matching network, tuning capacitor pad, and SMA connector pads (view of the underside of the bottom layer of the PIFA). The blue rectangle shows a portion of the ground plane with the shorting pin making a connection in the bottom right corner.

4.3.1 Assembling the Printed Circuit Board

After receiving the boards from Advanced Circuits, the assembly process could commence. Because of the student discount rate, the boards are not allowed to be perforated along the edges of the board. Each sheet contained the three layers of the board for one assembled PIFA. Three sheets were ordered so that if something happened to one of the boards, another could be used in its place. To solve the lack of perforation, each layer was cut from the sheet using a sheer press and sander to smooth out any rough edges. The original, unaltered boards are shown in Figure 49, while the sheared and sanded layers can be seen in Figure 50.

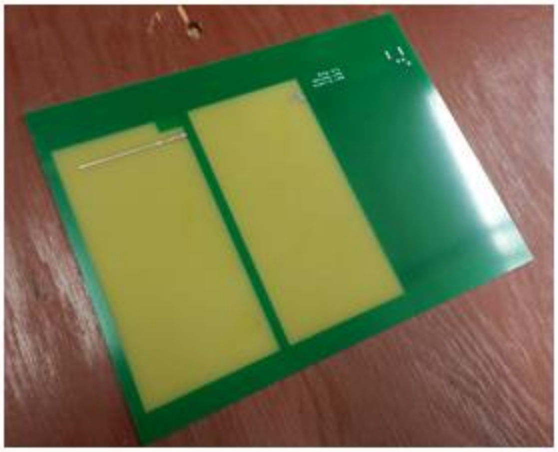
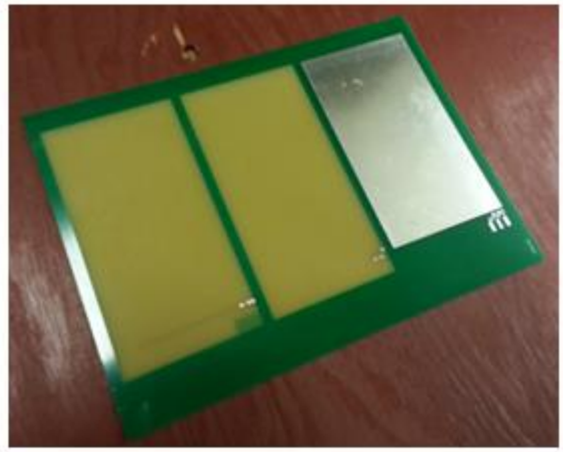

Figure 49. Top (left) and bottom (right) of the PCB sheets received from Advanced Circuits.

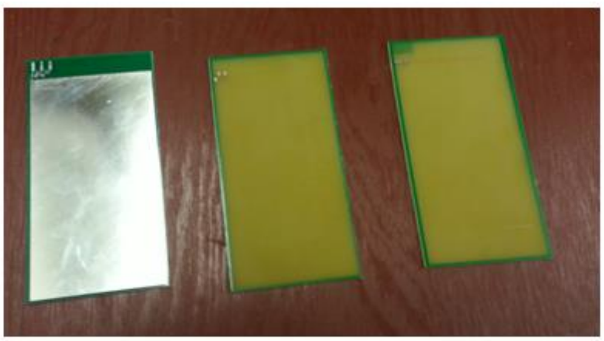
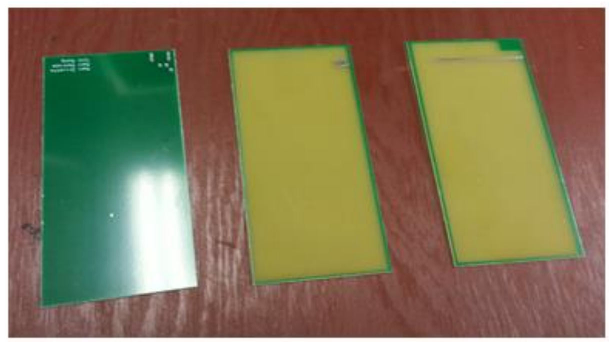

Figure 50. Top (left) and bottom (right) of the boards after they have been sheered from the sheet and the rough edges have been sanded.

Because of the layer nature of the boards, unconventional soldering techniques were utilized to make connections between each board. A small piece of 24 gauge wire was threaded through the vias creating the shorting pin passing through each layer of the board. Solder was used to make a solid connection between the wire and each via on each layer. This same technique was used to make the connections for the feed pin and tuning of the bottom layer to the middle layer. The wire could not be extended to the top layer because the feed and tuning vias for the top layer connect to pads on the middle layer. With this in mind, the pads on the middle layer were tinned with solder and then soldered to the top layer by melting solder through the vias of the top layer to the middle layer. This is very unconventional, however, with the use of enough solder, it can be accomplished to create a good connection. For this technique to be successful, it is imperative that the different vias and pads on each board layer line up perfectly.

With all of the connections made between the different layers of the device, the necessary testing components were added to the device. A standard edge mounted SMA connector was soldered to the board to interface with the coax lead from the network analyzer. A 0Ω resistor was placed in the series capacitor position of the matching network. The completed prototypes are visible in Figure 51. The resistor was used to create a short so initial measurements of the impedance of the antenna could be recorded. This measured impedance was used to calculate the values for the matching network to increase the power delivered to the device.

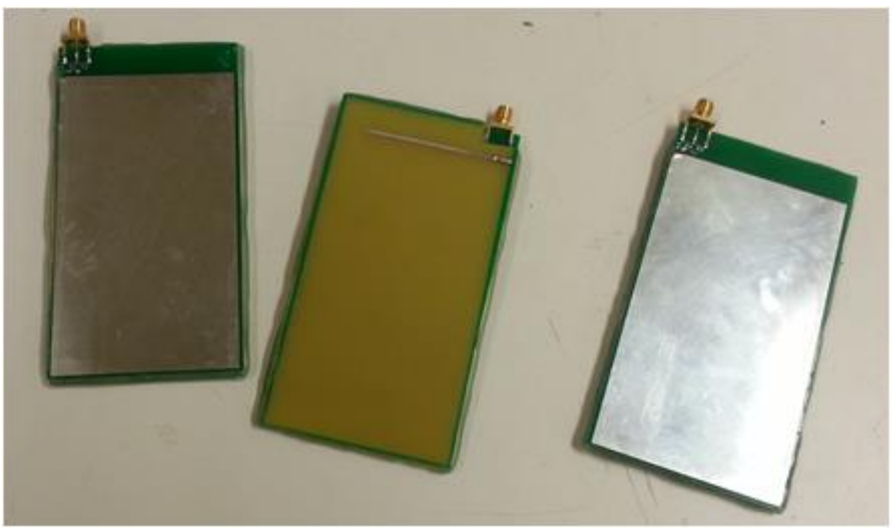

Figure 51. The assembled PIFA models with a SMA connector and a 0Ω resistor.

The final process in the construction of the device is keeping the three layers together. This posed another challenge as simply adding glue in between each layer would add another element to the substrate of the device. It was determined that a bead of glue along the edge of the device would be sufficient in creating a solid mechanical connection between the layers without adversely affecting the dielectric properties of the substrate. With this final step complete, the three devices were finally ready for testing with the network analyzer.

4.4. Measured Electrical Characteristics

This section focuses on reporting the results of the tests accomplished through the use of a network analyzer with varying tuning capacitance. The benefits of a matching network will also be presented here.

4.5.1 Preliminary Measurements of Antenna

Figure 52 shows the results of the S_{11} characteristics for the constructed PIFA. A frequency range of 0 to 2.5 GHz was used in order to observe a broad spectrum for the device. This sweep revealed two resonant frequencies: one at 825MHz and one at 2.295GHz. This follows the same trend as that of the Nexus 5. The PIFA was originally designed to naturally resonate (without a tuning capacitor) at 850MHz. There is a discrepancy of about 25MHz between the simulated model and the actual constructed model. This is most likely due to the layer method implemented in the construction of the PIFA. The layers of the device are not perfectly flat together allowing air in between the layers and thereby changing some of the characteristics of the device. There are other factors that could cause issues with the operation of the device, such as miscalculations in the lengths of different trace components. However, the layering method was determined to be the main cause of discrepancy in the resonant frequency. From Figure 52 it can be noted that S_{11} = -15.94dB at 825MHz. This is not ideal for a PIFA antenna, it is likely do to the mismatch between the network analyzer and the PIFA.

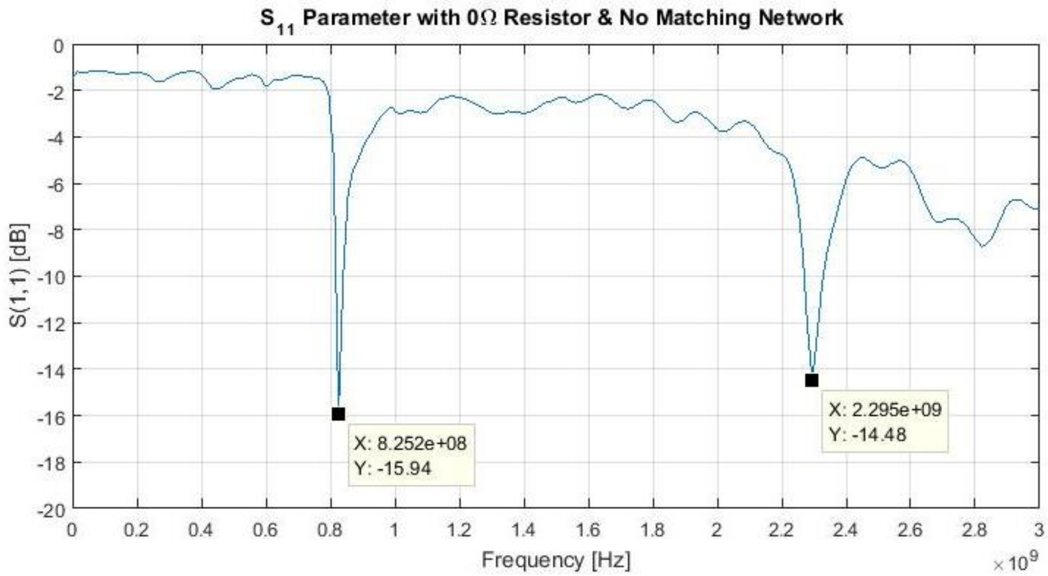

Figure 52. Reflection coefficient (S_{11}) for antenna 1 before the matching network was added.

Adding a matching network to the device allows more power to be transmitted to the antenna and less power to be reflected back to the source. This leads to an increase to the magnitude of the S_{11} parameter. Without the matching network, the S_{11} parameter value was -15.94 dB at 825 MHz, and with the matching network, the S_{11} parameter reaches -24.09 dB at 825 MHz, which is shown in Figure 53. This is a magnitude increase of 8.15 dB. It is important to note that these measurements were taken without the presence of a tuning capacitor. Once the tuning capacitor is included, the resonant frequency should shift, but the magnitude of the S_{11} should decrease. As a result, every increase in the magnitude of S_{11} is critical.

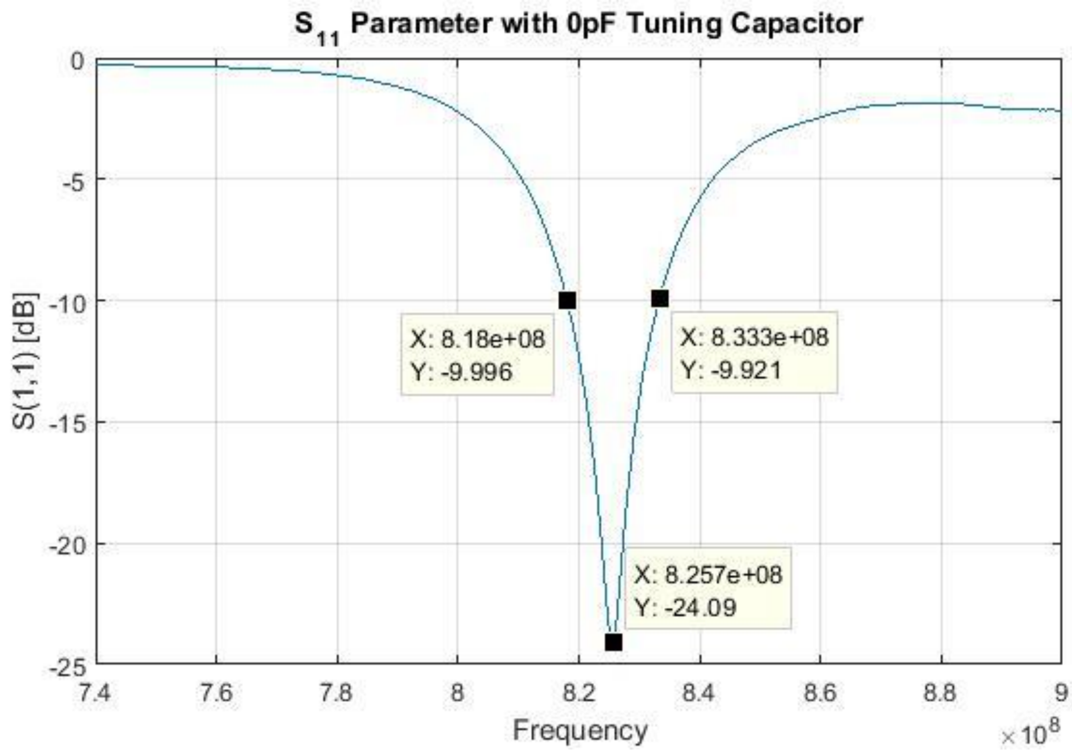

Figure 53. Reflection Coefficient (S_{11}) for Antenna 1, with matching network completed.

4.5.2 Tuned Measurements of Antenna

One of the major benefits of the PIFA is its ability to be tuned over a broad range of frequencies. This is achieved through the use of a variable tuning circuit attached to the tuning pin of the antenna. Because of the many complications of implementing a tuning circuit, different discrete capacitors were applied as tuners for the PIFA. It works in the same way as a variable tuning circuit; however, only one capacitance value can be measured at a time without having to change the component. Our method of tuning works for this project as the purpose is to see the different trends and verify the simulation results.

Figure 54 shows the results of using a 0.5 pF capacitor with the matched circuit. Using a network analyzer provided by WPI, a frequency sweep was performed between 740 MHz and 900 MHz. A small range was chosen for the purpose of focusing in on the desired resonant frequency and observing slight changes. It can be seen that the resonant frequency is shifted down by about 6 MHz from 825 MHz to about 819 MHz. This is consistent with what was expected. The magnitude of the S_{11} parameter increased about 1.8 dB from 24.09 dB to 25.91 dB.

Another important performance parameter that can be calculated is the bandwidth of the system. The bandwidth of a PIFA is determined over the range of frequencies at which the antenna will properly radiate. The cutoff for these frequencies is found when the magnitude of the S_{11} parameter drops about 10 dB before and after the resonant frequency. The cutoff frequency for the PIFA with a 0.5 pF capacitor is shown in Figure 54. The bandwidth is about 17.8 MHz. This is not a very good bandwidth for a PIFA, it will likely improve, however, by using a different type of substrate material. Later in the report, the different bandwidths will be compared alongside each other as well as compared to those of the computational models.

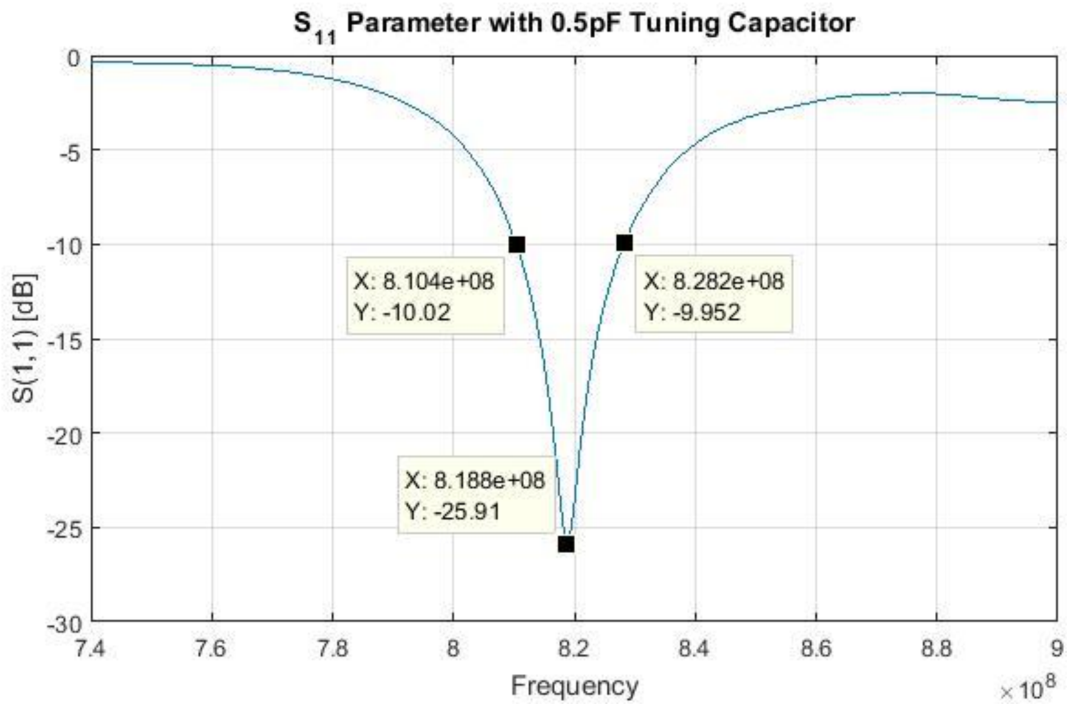

Figure 54. Reflection coefficient (S_{11}) of antenna 1 with a 0.5pF tuning capacitor.

As expected, adding a larger capacitor, here 1.0 pF, causes the resonant frequency to be shifted further down as shown in Figure 55. The resonant frequency shifted down by 16 MHz from 825 MHz to 809 MHz (compared to the resonant frequency of the PIFA without a tuning capacitor). Interestingly, the change in resonant frequency is not linear as a 0.5 pF capacitor shifts the resonant frequency by 6 MHz where as a 1.0 pF shifts the resonant frequency by 16 MHz. The antenna response follows more of an exponential trend than a linear trend for the shifting of the resonant frequency. The magnitude of the S_{11}

parameter decreased by 5.82 dB from 24.09 dB to 18.27 dB. This is unexpected, as this conflicts with the typical trend of trading off resonant frequency for resonance magnitude. The bandwidth of the antenna with a 1.0 pF capacitor is about 21.8 MHz where lower cutoff frequency being 799 MHz and the upper cutoff frequency being 821 MHz.

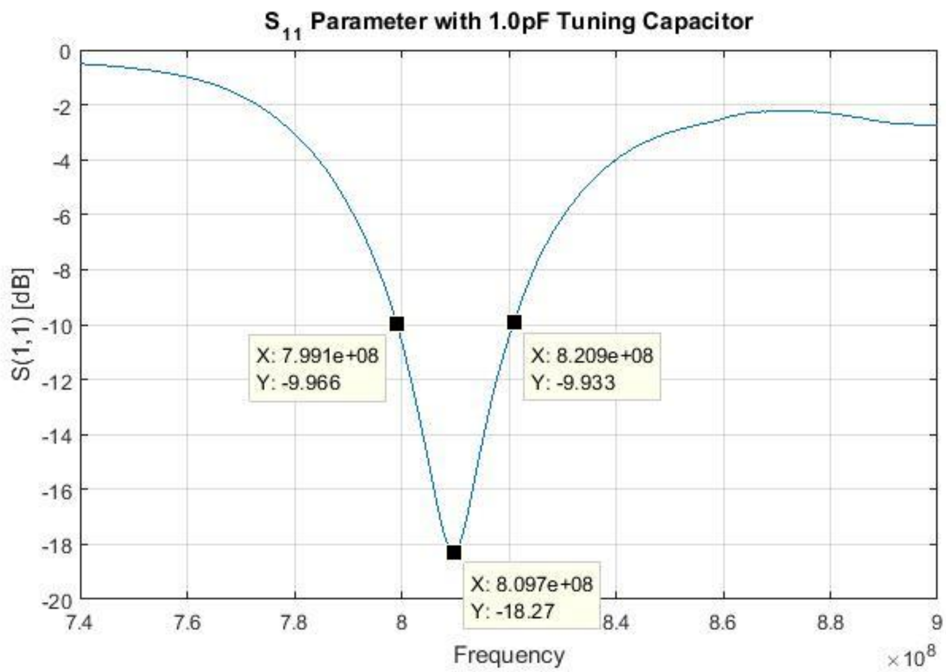

Figure 55. Reflection Coefficient (S_{11}) of Antenna 1 with a 1.0 pF tuning capacitor.

The physical model of the PIFA performed in the same way that a PIFA in theory should perform. The PIFA made by the team in this project did perform at optimal performance but there are many more design options to be considered in order to improve performance. The main issue with the performance of the physical model is the natural resonant frequency of the PIFA. The team originally intended for the antenna to have a natural resonant frequency of 850 MHz, but the actual physical model turned out to resonate at a frequency of about 825 MHz. This is about a 3% difference between what was designed and what was observed. It is most likely due to the layering method utilized by the team in the construction of the device. The overall characteristics of the PIFA do match up the computational models as will be discussed in more detail in the following section.

4.5.3 Comparison of All Three Model Types

With the measurements of the physical model completed, it is important to compare them to those of the computational models. The antenna was designed within HFSS as a two-port system with the tuning capacitor replaced with a lumped port. This allows the S_{11} parameters of the antenna to be exported into an .s2p touchstone file; it can then be simulated in ADS with different tuning capacitors. The different tuning capacitors can alternatively be modeled within HFSS itself. The results of these two methods as well as the results of the network analyzer measurements of the physical model can be seen in Table 2 below.

Table 2. A comparison of the antenna characteristics observed in the three different models.

	HFSS			ADS			Physical Model		
Tuning Capacitance (pf)	0	0.5	1	0	0.5	1	0	0.5	1
Peak S_{11} (dB)	-11.66	-13.75	-20.15	-12.70	-16.48	-24.85	-24.09	-25.91	-18.27
Resonant Frequency (MHz)	802.00	795.00	790.00	798.00	792.00	784.00	826.00	819.00	810.00
10 dB Bandwidth (MHz)	7.30	9.80	13.30	9.00	12.00	14.00	15.30	17.80	21.80
Fractional Bandwidth (%)	0.91	1.23	1.68	1.13	1.52	1.79	1.85	2.17	2.69
Quality Factor	109.86	81.12	59.40	88.67	66.00	56.00	53.99	46.01	37.16

As denoted in Table 2, the different methods of modeling the antenna return different results. This is surprising considering that antenna modeled within HFSS and ADS are structurally the same and only differ by the use of a 2-port model versus a 1-port model. However, the difference is understandable as HFSS assumes the feed port is perfectly matched to a 50 Ω source for each capacitance whereas ADS does not make this assumption. In ADS, the matching network keeps the calculated values used for the original natural resonant frequency. This is the same situation that might be found in a real word application as the matching network does not change with the applied tuning capacitance.

Figure 56 shows the different peak S_{11} magnitudes for the varying tuning capacitances applied to the three different antenna models:

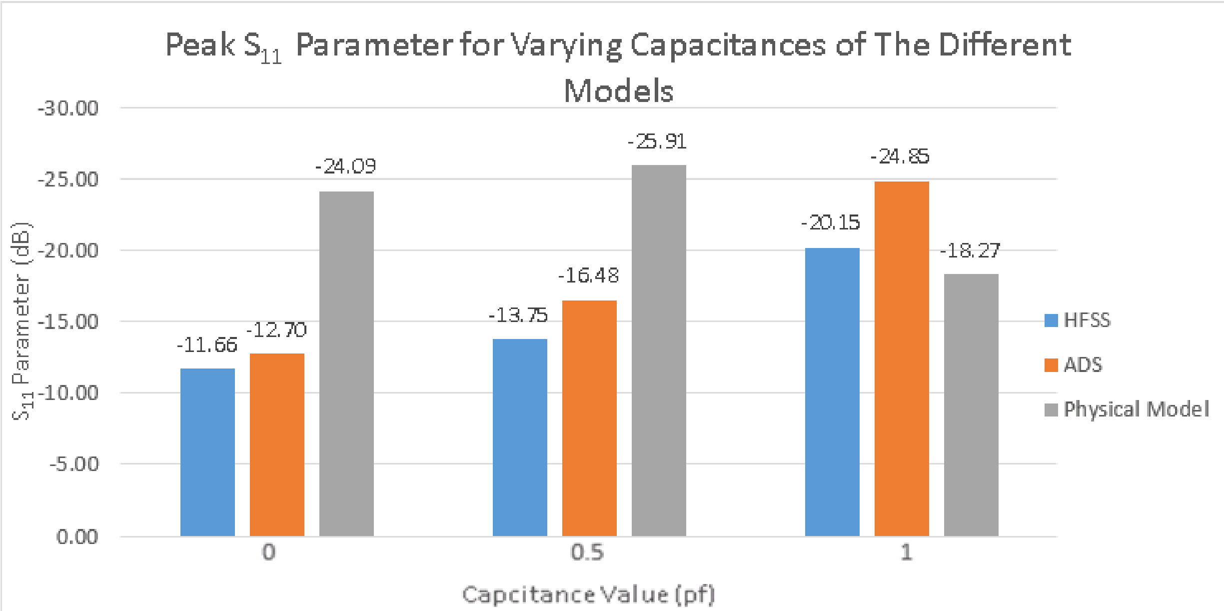

Figure 56. Peak S_{11} Parameter for Varying Capacitances of the Different Models.

As previously stated, the virtual models are very similar to each other but are slightly different from the physical model. It is important to observe the trend or change as a result of applying different tuning capacitances to the antenna. When a 0.5 pF capacitance was applied, the peak S_{11} magnitude of the HFSS increased by 2.09 dB from 11.66 dB to 13.75 dB, the peak S_{11} magnitude increased 3.78 dB from 12.7 dB to 16.48 dB, and the peak S_{11} magnitude increased 1.82 dB from 24.09 dB to 25.91 dB. When a 1.0 pF capacitance was applied, the peak S_{11} magnitude of HFSS increased by 6.4 dB from 13.75 dB to 20.15 dB, the peak S_{11} magnitude increased 8.37 dB from 16.48 dB to 24.85 dB, and the peak S_{11} magnitude decreased 7.64 dB from 25.91 dB to 18.27 dB. This property of the antenna is the sole property where the characteristics of the simulations did not match the characteristics observed in the physical model. Based on the results of the simulations, the peak S_{11} magnitude should increase when a 0.5 pF tuning capacitor is applied and then again when a 1.0 pF tuning capacitor is applied. The physical model exemplifies this trend for the 0.5 pF tuning capacitance, but it diverges from the simulations when a 1.0 pF tuning capacitance is used. The peak S_{11} magnitude decreases for 1.0 pF when the simulations say it should increase. This deviation from the simulated models is most likely due to the assembly method utilized by the team. Because of the layering technique, air is most likely present in-between the three layers causing changes in some of the measurement results.

Figure 57 displays the trend in the resonant frequencies of the PIFA as different tuning capacitance values are applied to the system:

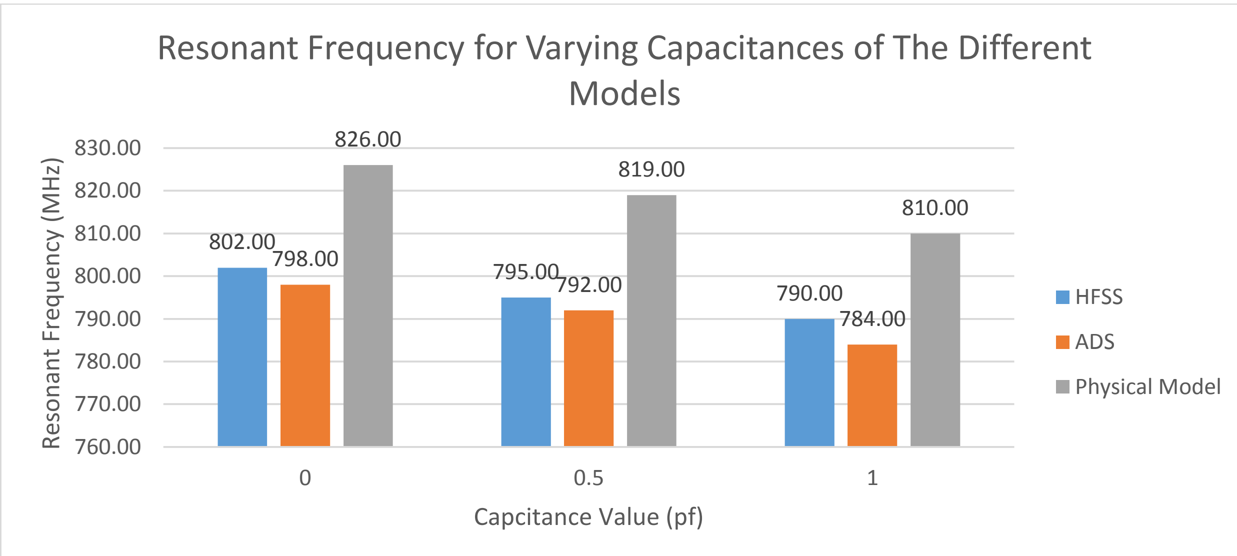

Figure 57. Resonant Frequency for Varying Capacitances of the Different Models.

As shown, the virtual models do not match exactly with the physical model nor do the computational models match each other exactly. This is due to the mismatch in the matching network as mentioned previously. The trend, however, does exemplify the validity of the computational model. As a 0.5 pF tuning capacitor is applied, the resonant frequency of the HFSS model decreases by 7 MHz from 802 MHz to 795 MHz, the ADS model decreases by 6 MHz from 798 MHz to 792 MHz, and the physical model decreases by 7 MHz from 826 MHz to 819 MHz A similar observation can be made when a 1.0 pF tuning capacitor is applied, the resonant frequency of the HFSS model decreases by 5 MHz from 795 MHz to 790 MHz, the ADS model decreases by 8 MHz from 792 MHz to 784 MHz, and the physical model decreases by 9 MHz from 819 MHz to 810 MHz. It can be concluded that adding a 0.5 pF tuning capacitor decreases the resonant frequency of the designed PIFA by about 6.67 MHz (an average of the three changes from the different models). This is a very good result as it documents that our computational models can be trusted in general, but does require some fine-tuning to adjust for the tolerances of the assembly process used in this project. Additionally, it can be concluded that adding a 1.0 pF tuning capacitor will further shift the resonant frequency down by about 7.33 MHz (an average of the three changes from the different models). The data would suggest that the HFSS model is better at modeling the effects of adding a tuning capacitor to a real world antenna for small capacitances but as the capacitance increases, the ADS model becomes more accurate at modeling the effects that would also be seen on the physical model.

The bandwidth of an antenna describes the range of frequencies over which the antenna will properly radiate. With this in mind, the bandwidth of the antenna with varying tuning capacitances applied was calculated and can be seen in Figure 58:

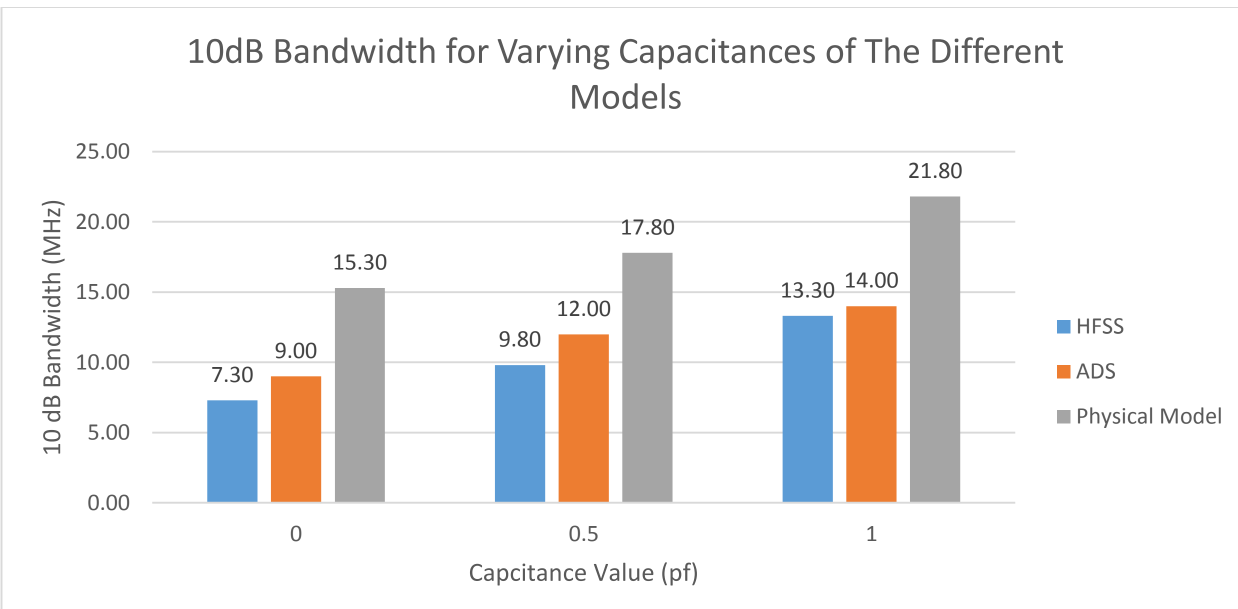

Figure 58. 10dB Bandwidth for Varying Capacitances of the Different Models.

The characteristics of the antenna can be seen to follow a trend of increased bandwidth as tuning capacitance is added. When adding a 0.5 pF tuning capacitance, the bandwidth of the HFSS model increased by 2.5 MHz from 7.3 MHz to 9.8 MHz, the bandwidth of the ADS model increased by 3 MHz from 9 MHz to 12 MHz, and the bandwidth of the physical model increased by 2.5 MHz from 15.3 MHz to 17.8 MHz. Similarly when adding a 1.0 pF tuning capacitance, the bandwidth of the HFSS model increased by 3.5 MHz from 9.8 MHz to 13.3 MHz, the bandwidth of the ADS model increased by 2 MHz from 12 MHz to 14 MHz, and the bandwidth of the physical model increased by 4 MHz from 17.8 MHz to 21.8 MHz. This shows a distinct correlation between bandwidth and the applied tuning capacitance. As higher tuning capacitances are applied, the bandwidth increases. This trend is seen across the three different models with the HFSS model most closely resembling the physical model. The changes observed in the bandwidth for the HFSS model were almost exactly the same as those seen in the physical model for both the 0.5 pF and 1.0 pF tuning capacitors. From the data of the three models it can be concluded that adding a 0.5 pF tuning capacitor to the PIFA will increase the bandwidth by 2.67 MHz (average), and that adding a 1.0 pF capacitor to the PIFA will increase the bandwidth by 3.17 MHz (average).

Derived from the antenna bandwidth, the fractional bandwidth and quality factor for the antenna as different tuning capacitors are applied can be seen in Figure 59 and Figure 60, respectively. Because of their dependence on the bandwidth of the antenna, both figures reflect the dependence of the fractional bandwidth and quality factor of the antenna on the tuning capacitance applied to the antenna. The quality factors seen in Figure 60 for the different tuning capacitances are relatively low for an antenna. This is to be expected based on our first attempt of fabricating an antenna. By using a substrate with a lower dielectric constant or by decreasing the thickness of the substrate, the quality factor can be increased but this will decrease the bandwidth of the antenna [18].

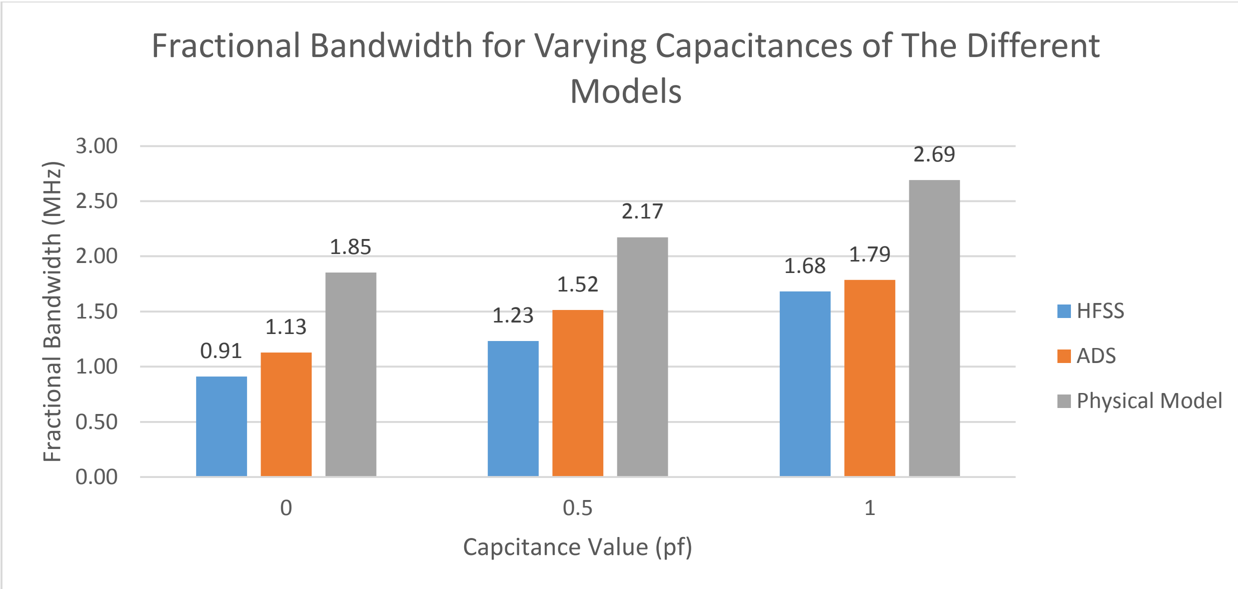

Figure 59. Fractional Bandwidth for Varying Capacitances of the Different Models.

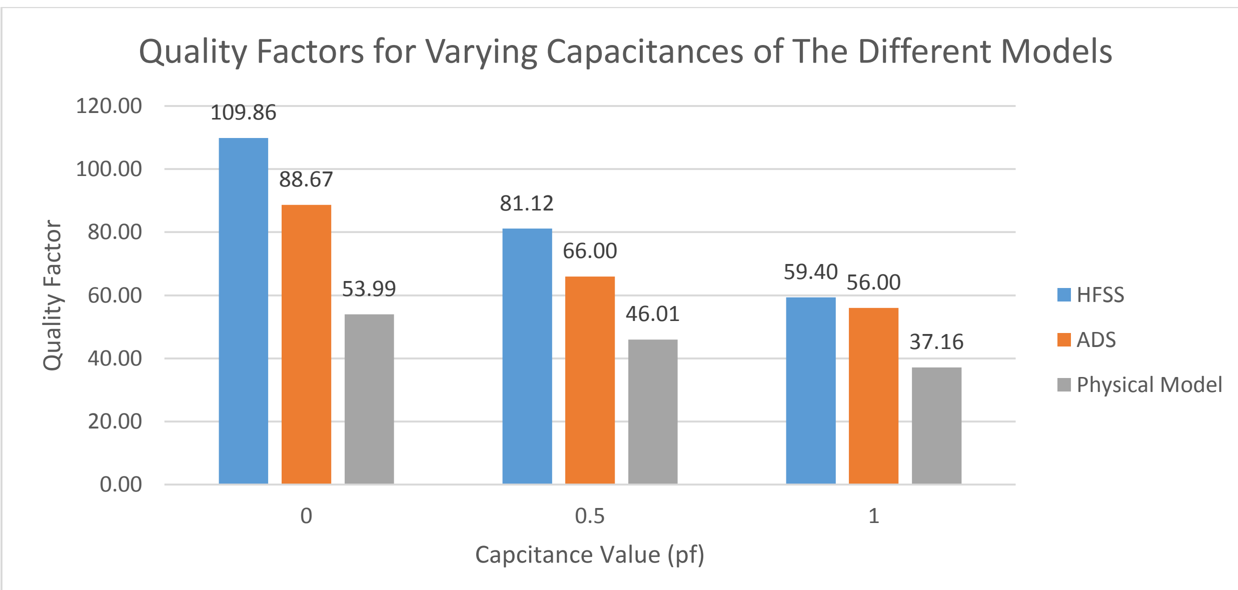

Figure 60. Quality Factors for Varying Capacitances of the Different Models.

4.5. HFSS Characteristic Analysis

Two computational PIFA models were produced during the course of this project, both of which have similar structures. The first model was developed to mimic the form and characteristics of the fabricated antenna model, the properties of which were optimized using an elementary model. The second design is the same antenna, but the length of the antenna and positions of the antenna feed line and tuner were optimized. Further details towards the development of these models are discussed in Section 4.1, HFSS Simulations.

Both models consist of 54,293 meshed tetrahedral elements, which comprise the substrate, vacuum surrounding the substrate, and the perfectly matched air layer surrounding the device. These mesh elements increase the time necessary to complete each iteration of the simulation.

The two designs can be compared through an analysis of several key characteristics. First, this section will seek to observe the difference between the surface current densities across all conductive surfaces of the antennas. Afterwards, the reflection coefficient characteristics (in dB) and the radiation patterns (the real component of the electric field, E) of both devices will be contrasted.

Surface current densities are an important characteristic to observe because they can be used to predict the voltage at different points along the antenna's conductor structure. This can be helpful in determining the location of the tuning arm on an antenna. Figure 61 and Figure 62 show the current densities for the "real" and optimized antenna models. As can be seen, both antennas have very low current distributions in the ground plane and in the tuning arm (as should be expected, since the tuner value is negligible for these simulations). However, there is a clear difference in the current densities of the feed line and in the radiating patch of both. In the optimized model, very little current flows through the feed and ground near the antenna, whereas in the real model most current is in the area directly adjacent to the lumped port. It is desired that the majority of the radiation be in the radiating patch, as the current there determines the strength of the signal received or transceiver. As is also noticeable, the optimized model takes full advantage of the length of the antenna, whereas the fabricated model neglects the portion of the line between the feed and the shorting pin.

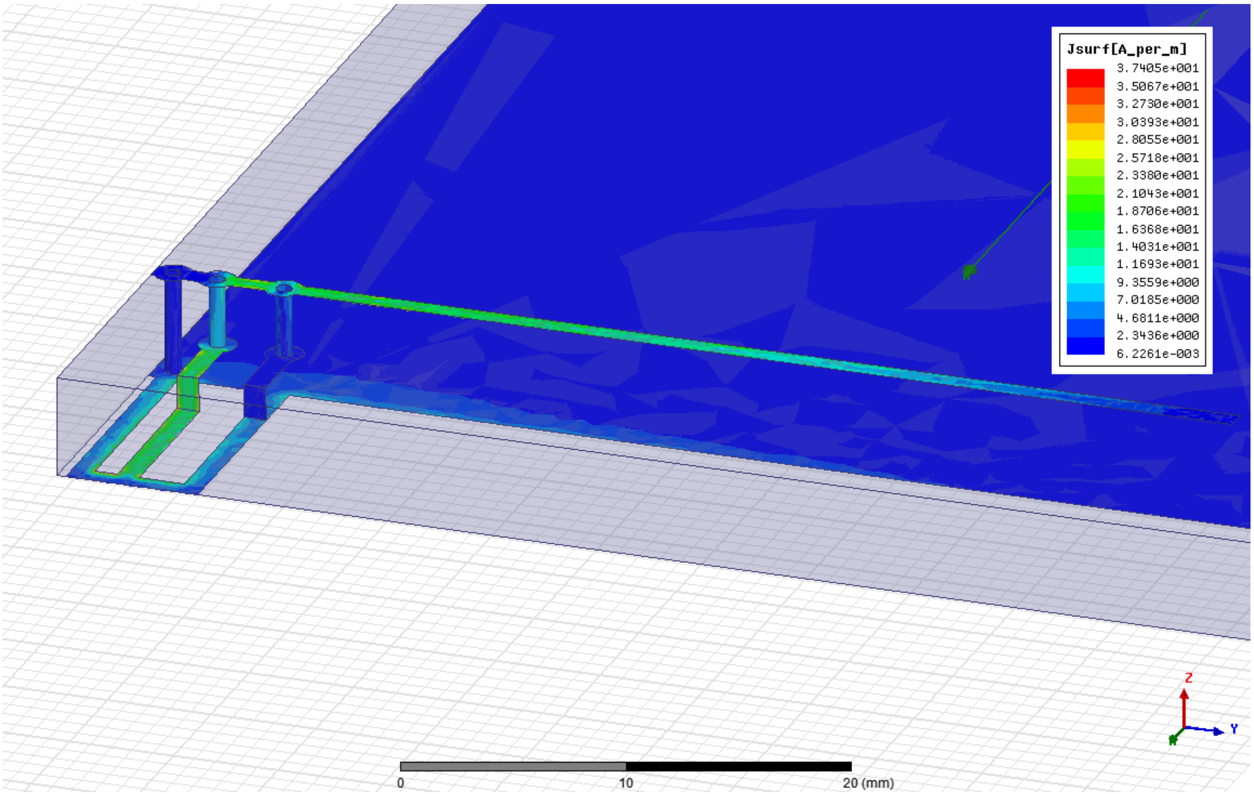

Figure 61. Surface current density in A/m across all conductive surfaces for the antenna modeled after the Altium design at 0 phase. Due to the radial feed, the current density is fairly constant across the width of the channel.

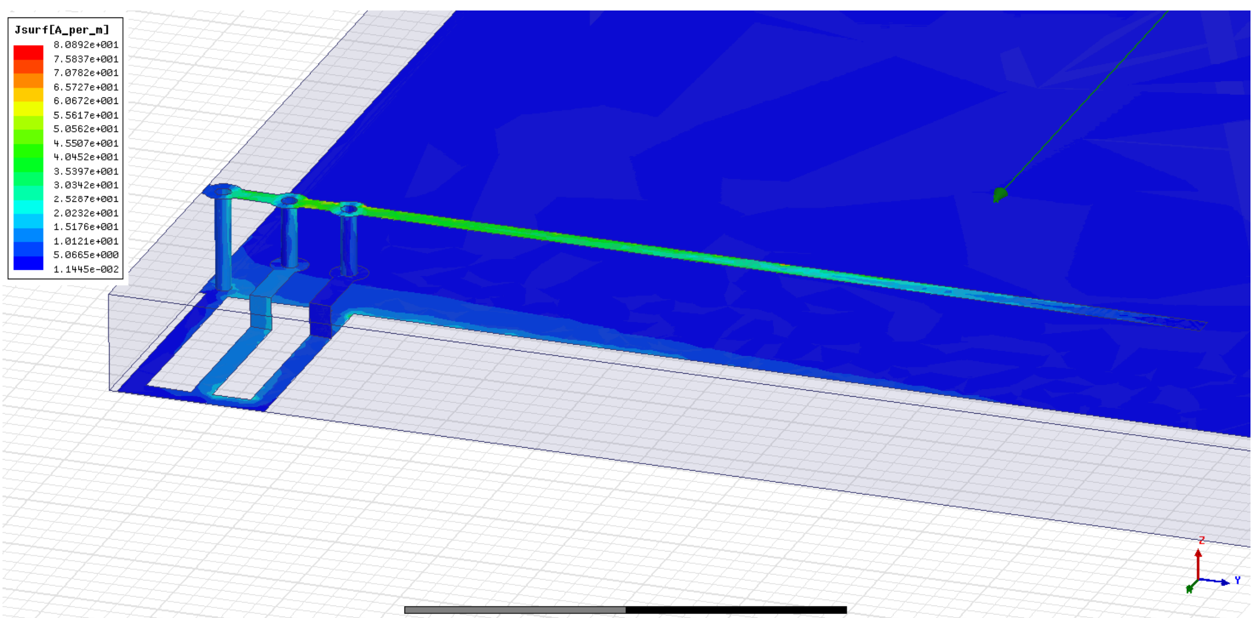

Figure 62. Surface current density in A/m across all conductive surfaces for the optimized antenna at 0 phase.

The reflection coefficient monitors the power lost at the input of an antenna, which is generally a function of how matched the impedance of the antenna is to its source at a given frequency. This behavior was used to select the best model during the optimization process, as it is a good measure to estimate the power radiated by the antenna and to judge the effectiveness at targeting the desired resonance. The S_{11} plots for both antennas are shown in Figure 63 and Figure 64. A comparison between the two antenna model characteristics is included in Table 3.

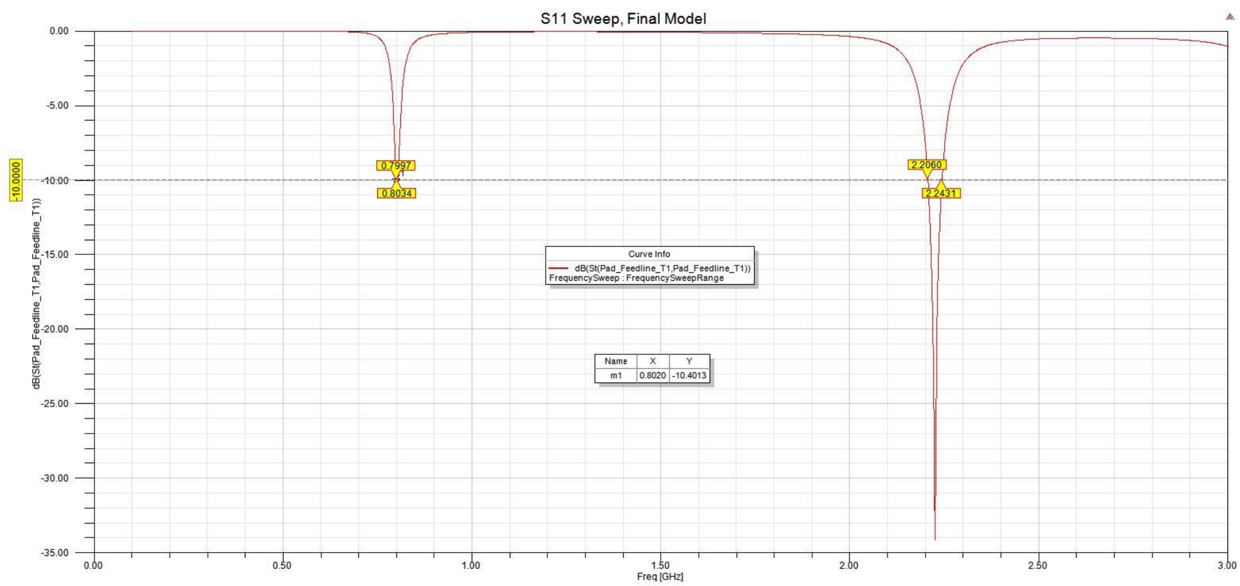

Figure 63. S_{11} (reflection coefficient) measurements for the original complex model.

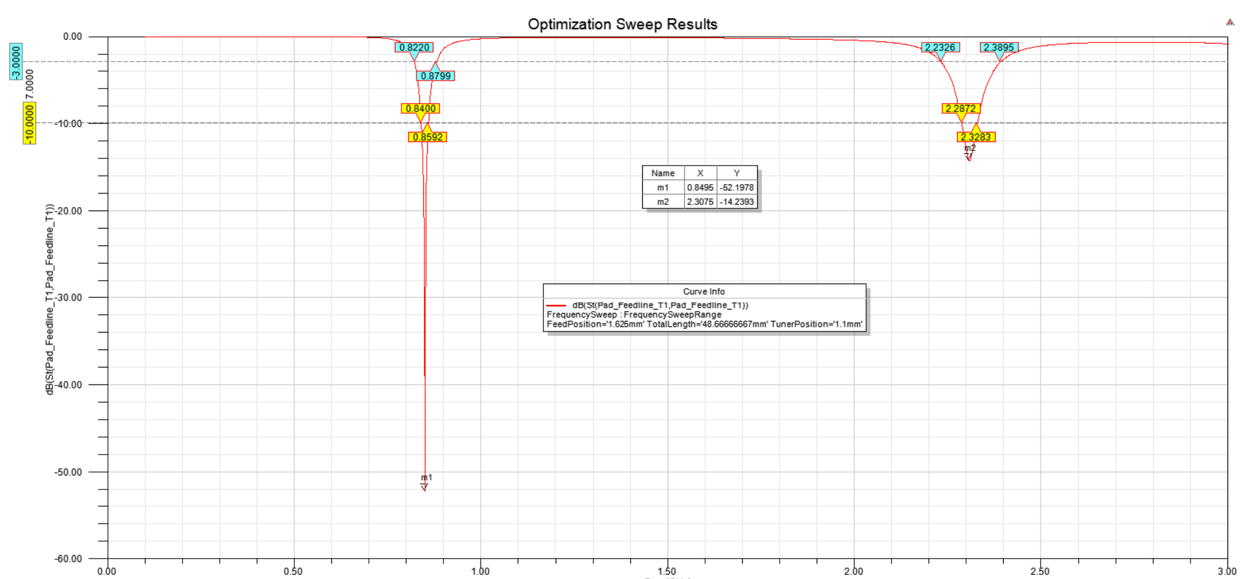

Figure 64. S_{11} (reflection coefficient) measurements for the optimized complex model.

Table 3. Comparison of the original vs. the optimized complex PIFA models.

Parameter	Original Complex Model	Optimized Complex Model
Peak S_{11} near 850MHz (dB)	-10.40	-52.20
Resonant Frequency (MHz)	802.0	849.6
10 dB Bandwidth (MHz)	7.30	19.2
Fractional Bandwidth (%)	0.91	2.25
Quality Factor	109.86	44.25

As can be seen in Table 3, the optimized model is shown to perform better in terms of resonance and bandwidth when compared to the Altium designs.

The radiation patterns are a key characteristic in displaying the performance of the antenna in different spatial directions, as described in Figure 6. Since there are a large number of possible results, eight two-dimensional radiation patterns for each antenna are included in Appendix 7.3. The three dimensional models, transparently overlaid on the antenna models, are shown in Figure 65 and Figure 66.

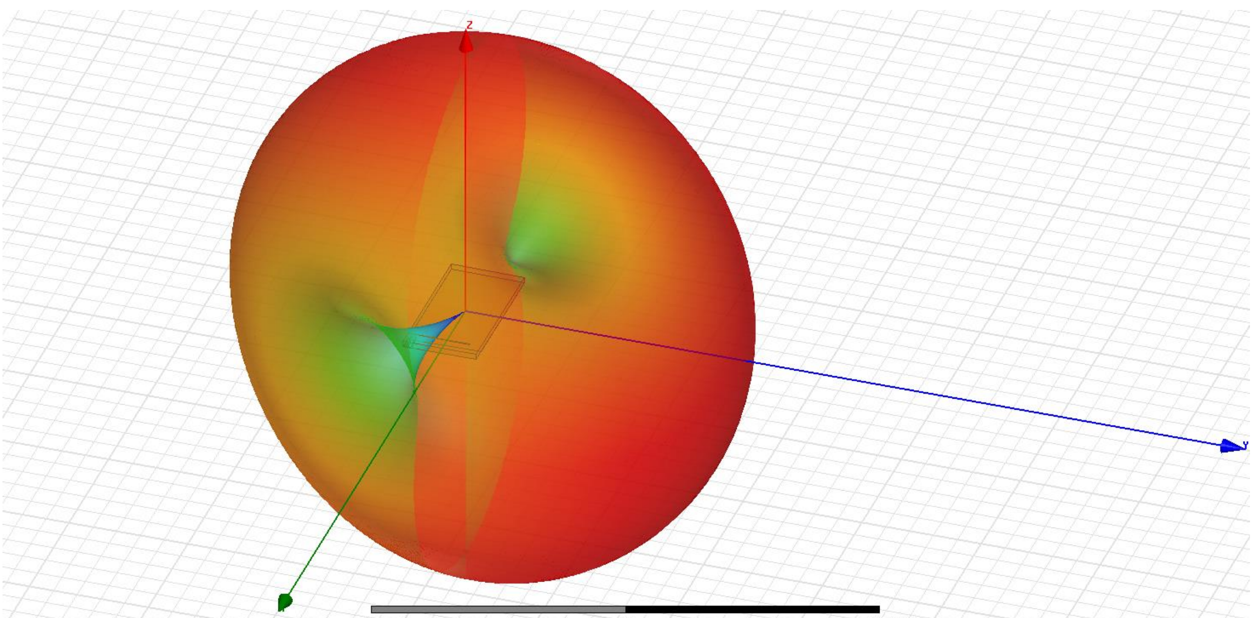

Figure 65. Three-dimensional far-field radiation pattern for the real, non-optimized antenna model overlaid on the antenna model.

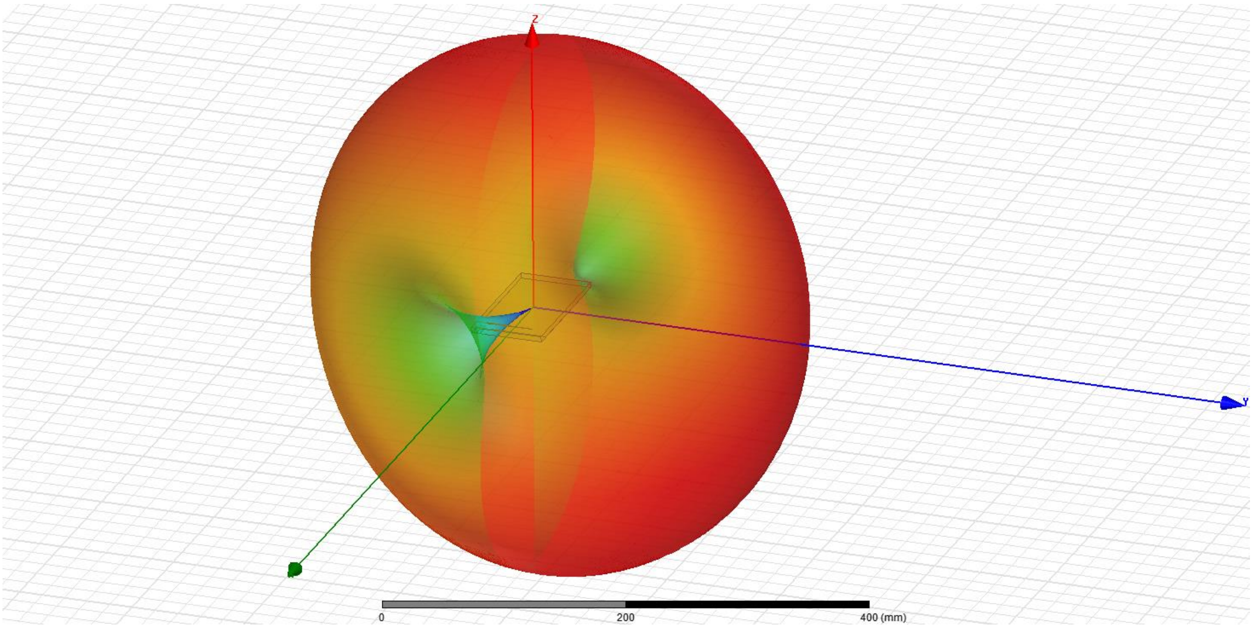

Figure 66. Three-dimensional far-field radiation patterns for the optimized antenna model overlaid on the antenna model.

It should be noted that while the optimized antenna outperforms the original complex antenna in terms of resonance and current density, the antenna's radiation patterns are almost uniformly 10dB lower in magnitude. Additionally, both models have misshaped patterns from those expected: a PIFA should have radiation patterns resembling a doughnut in line with the patch. While the doughnut shape is noticeable, it is aligned at an angle from the X axis. This may be due to the antenna's location on the corner of the antenna, since the area with the lowest decibel values is directed towards the shorting pin.

5. Conclusions

The goals of the project were to develop a computational approach capable of simulating antenna designs for cellular handsets using HFSS and ADS. An additional goal was the construction of a simplified PIFA system in an effort to replicate low-band antenna of the North American Nexus 5 smartphone; specifically, the antenna design targeted a resonance at the GSM 850 frequency band. The developed HFSS three-dimensional computational model was successfully tested against h both the ADS software package and a PCB fabricated simplified antenna. Each method yielded slightly different, but consistent results.

Once confidence in the computational approach was established, a series of parametric sweeps was conducted to arrive at the dimensions of the optimal antenna design. From the results of this optimized antenna model, it was determined that the resonant frequency, quality factor, and E-field radiation patterns can all be improved through detailed design parameter variations. Our optimized design covered much of the GSM 850 band, and the model predictions have yielded useful device data for this particular range of frequencies.

Additional parametric sweeps were performed on various dimensions of the final model to determine how each affected the overall performance of the final PIFA design. These studies can provide important insight into which parameters may become limiting factors in a commissioned cellular antenna and what measures can be taken to alter or compensate for them. The resulting model predictions are also useful in generating a more intuitive understanding of how the form of the antenna affects its functionality.

6. Recommendations and Future Research

While this project achieved its goals, there is considerable room for improvement and further research. For example, one of the possible reasons there was a difference between the physical and computational models is that there may have been a difference in the relative permittivity of the substrate and/or a small change in thickness of the substrate during fabrication. It is likely that there may be an air gap and potentially hot glue between each of the three layers that comprise the final model. To avoid this problem in the future, it is recommended that the antenna be built as a single layer board. Additionally, it is recommended that other substrates than FR4 are to be explored. This is because FR4 is considered a very lossy substrate compared to others, such as the Rogers substrates (which we analyzed in Section 4.1). Changing the relative permittivity may also permit the bandwidth of the antenna to be improved.

Additional experiments should be performed using various wide and multiband antenna techniques, including meandering, slotting, and folding. Using these techniques, it is possible that the antenna can be designed to be even further condensed into the corner of the substrate; portions of it may even be printed along the edge of the substrate as it is on the Nexus 5 antenna. Slotting should also allow multiple resonances to be used on the same device, and minor adjustments to this may allow multiple resonances in the 850MHz band to exist.

In terms of simulation techniques, it should be noted that, due to the necessary computational time required, the HFSS simulations were set to 12 adaptive passes at a 10^{-9} Δs value for convergence. This implies that the antenna model would attempt to converge to under 10^{-7}% error in the value of the antenna's S parameters only after 12 frequency passes are performed. Unfortunately, many of the simulations performed did not meet this stringent convergence criterion, which meant the results were open to a certain, difficult to quantify error magnitude. Unfortunately, increasing the number of passes would significantly increase the required computational time, even on the most powerful server platform.

However, carrying out these extensive computational efforts may remove some of the outliers observed in the analyses of the HFSS parameter sweeps.

7. Appendix

7.1. Antenna Structure of Nexus 5

Like most smartphones, the LG Nexus 5 has six PIFAs; the Global Positioning System (GPS), the Diversity Receiver (DRx), the Wireless Local Area Network (WLAN) or referred to as Wi-Fi, the Main Low Band Antenna, the Main High/Mid Band Antenna and the Near Field Communication (NFC).

Figure 67. The structure of the Nexus 5 handset from Skyworks Solutions, showing the locations of all of its PIFA devices. X-ray images are also shown that reveal the trace patterns of the antennas.

7.2. Standard Frequency Bands

In this section we report on the various frequency bands handsets used around the world. There are many different standards of bandwidths that develop along with the generations of antenna technology, many of which overlap. CDMA, WCDMA and GSM reflect 3G standards and LTE reflects 4G standards [19].

7.2.1. CDMA/IS-2000 Band Classes [20]

Subfield (see [9])	**Subfield Description**
BAND_CLASS_0	800 MHz cellular band
BAND_CLASS_1	1.8 to 2.0 GHz PCS band
BAND_CLASS_2	872 to 960 MHz TACS band
BAND_CLASS_3	832 to 925 MHz JTACS band
BAND_CLASS_4	1.75 to 1.87 GHz Korean PCS band
BAND_CLASS_5	450 MHz NMT band
BAND_CLASS_6	2 GHz IMT-2000 band
BAND_CLASS_7	Upper 700 MHz band
BAND_CLASS_8	1800 MHz band
BAND_CLASS_9	900 MHz band
BAND_CLASS_10	Secondary 800 MHz band
BAND_CLASS_11	400 MHz European PAMR band
BAND_CLASS_12	800 MHz PAMR band
BAND_CLASS_13	2.5 GHz IMT-2000 Extension Band
BAND_CLASS_14	US PCS 1.9GHz Band
BAND_CLASS_15	AWS Band
BAND_CLASS_16	US 2.5GHz Band
BAND_CLASS_17	US 2.5GHz Forward Link Only Band
BAND_CLASS_18	700 MHz Public Safety Band
BAND_CLASS_19	Lower 700 MHz Band
BAND_CLASS_20	L-Band
BAND_CLASS_21	S-Band
BAND_CLASS_31	Wildcard Band Class

Figure 68. CDMA Standard Band Classes.

System Designator	Band Subclass	Transmit Frequency Band (MHz)	
		Access Terminal	Access Network
A	0	824.025–835.005 844.995–846.495	869.025–880.005 889.995–891.495
	1	824.025–835.005 844.995–848.985	869.025–880.005 889.995–893.985
	2	824.025-829.995	869.025-874.995
	3	815.025-829.995	860.025-874.995
B	0	835.005–844.995 846.495–848.985	880.005–889.995 891.495–893.985
	1	835.005–844.995	880.005–889.995

Figure 69. CDMA Band Class 0 Specifications.

System Designator	Band Subclass	Transmit Frequency Band (MHz)	
		Access Terminal	Access Network
A	0	806.000–810.975	851.000–855.975
B	1	811.000–815.975	856.000–860.975
C	2	816.000–820.975	861.000–865.975
D	3	821.000–823.975	866.000–868.975
E	4	896.000–900.975	935.000–939.975

Figure 70. CDMA Band Class 10 Specifications.

7.2.2. LTE/EUTRA Frequency Bands [14]

E-UTRA Operating Band	Uplink (UL) operating band BS receive UE transmit			Downlink (DL) operating band BS transmit UE receive			Duplex Mode
	F_{UL_low}	–	F_{UL_high}	F_{DL_low}	–	F_{DL_high}	
1	1920 MHz	–	1980 MHz	2110 MHz	–	2170 MHz	FDD
2	1850 MHz	–	1910 MHz	1930 MHz	–	1990 MHz	FDD
3	1710 MHz	–	1785 MHz	1805 MHz	–	1880 MHz	FDD
4	1710 MHz	–	1755 MHz	2110 MHz	–	2155 MHz	FDD
5	824 MHz	–	849 MHz	869 MHz	–	894MHz	FDD
6[1]	830 MHz	–	840 MHz	875 MHz	–	885 MHz	FDD
7	2500 MHz	–	2570 MHz	2620 MHz	–	2690 MHz	FDD
8	880 MHz	–	915 MHz	925 MHz	–	960 MHz	FDD
9	1749.9 MHz	–	1784.9 MHz	1844.9 MHz	–	1879.9 MHz	FDD
10	1710 MHz	–	1770 MHz	2110 MHz	–	2170 MHz	FDD
11	1427.9 MHz	–	1447.9 MHz	1475.9 MHz	–	1495.9 MHz	FDD
12	699 MHz	–	716 MHz	729 MHz	–	746 MHz	FDD
13	777 MHz	–	787 MHz	746 MHz	–	756 MHz	FDD
14	788 MHz	–	798 MHz	758 MHz	–	768 MHz	FDD
15	Reserved			Reserved			FDD
16	Reserved			Reserved			FDD
17	704 MHz	–	716 MHz	734 MHz	–	746 MHz	FDD
18	815 MHz	–	830 MHz	860 MHz	–	875 MHz	FDD
19	830 MHz	–	845 MHz	875 MHz	–	890 MHz	FDD
20	832 MHz	–	862 MHz	791 MHz	–	821 MHz	FDD
21	1447.9 MHz	–	1462.9 MHz	1495.9 MHz	–	1510.9 MHz	FDD
22	3410 MHz	–	3490 MHz	3510 MHz	–	3590 MHz	FDD
23	2000 MHz	–	2020 MHz	2180 MHz	–	2200 MHz	FDD
24	1626.5 MHz	–	1660.5 MHz	1525 MHz	–	1559 MHz	FDD
25	1850 MHz	–	1915 MHz	1930 MHz	–	1995 MHz	FDD
26	814 MHz	–	849 MHz	859 MHz	–	894 MHz	FDD
27	807 MHz	–	824 MHz	852 MHz	–	869 MHz	FDD
28	703 MHz	–	748 MHz	758 MHz	–	803 MHz	FDD
29	N/A			717 MHz	–	728 MHz	FDD[2]
...							
33	1900 MHz	–	1920 MHz	1900 MHz	–	1920 MHz	TDD
34	2010 MHz	–	2025 MHz	2010 MHz	–	2025 MHz	TDD
35	1850 MHz	–	1910 MHz	1850 MHz	–	1910 MHz	TDD
36	1930 MHz	–	1990 MHz	1930 MHz	–	1990 MHz	TDD
37	1910 MHz	–	1930 MHz	1910 MHz	–	1930 MHz	TDD
38	2570 MHz	–	2620 MHz	2570 MHz	–	2620 MHz	TDD
39	1880 MHz	–	1920 MHz	1880 MHz	–	1920 MHz	TDD
40	2300 MHz	–	2400 MHz	2300 MHz	–	2400 MHz	TDD
41	2496 MHz		2690 MHz	2496 MHz		2690 MHz	TDD
42	3400 MHz	–	3600 MHz	3400 MHz	–	3600 MHz	TDD
43	3600 MHz	–	3800 MHz	3600 MHz	–	3800 MHz	TDD
44	703 MHz	–	803 MHz	703 MHz	–	803 MHz	TDD

NOTE 1: Band 6 is not applicable
NOTE 2: Restricted to E-UTRA operation when carrier aggregation is configured. The downlink operating band is paired with the uplink operating band (external) of the carrier aggregation configuration that is supporting the configured Pcell.

Figure 71. LTE standard frequency band specifications.

7.2.3. WCDMA/UMTS/UTRA FDD Frequency Bands [21]

Operating Band	UL Frequencies UE transmit, Node B receive	DL frequencies UE receive, Node B transmit
I	1920 - 1980 MHz	2110 -2170 MHz
II	1850 -1910 MHz	1930 -1990 MHz
III	1710-1785 MHz	1805-1880 MHz
IV	1710-1755 MHz	2110-2155 MHz
V	824 - 849 MHz	869-894 MHz
VI	830-840 MHz	875-885 MHz
VII	2500-2570 MHz	2620-2690 MHz
VIII	880 - 915 MHz	925 - 960 MHz
IX	1749.9-1784.9 MHz	1844.9-1879.9 MHz
X	1710-1770 MHz	2110-2170 MHz
XI	1427.9 - 1447.9 MHz	1475.9 - 1495.9 MHz
XII	699 – 716 MHz	729 – 746 MHz
XIII	777 - 787 MHz	746 - 756 MHz
XIV	788 – 798 MHz	758 – 768 MHz
XV	Reserved	Reserved
XVI	Reserved	Reserved
XVII	Reserved	Reserved
XVIII	Reserved	Reserved
XIX	830 – 845MHz	875 – 890 MHz
XX	832 – 862 MHz	791 – 821 MHz
XXI	1447.9 – 1462.9 MHz	1495.9 – 1510.9 MHz
XXII	3410 – 3490 MHz	3510 – 3590 MHz
XXV	1850 – 1915 MHz	1930 – 1995 MHz
XXVI	814 – 849 MHz	859 – 894 MHz
XXXII[1]	N/A	1452 – 1496 MHz
NOTE 1: Restricted to UTRA operation when dual band is configured (e.g., DB-DC-HSDPA or dual band 4C-HSDPA). The down link frequenc(ies) of this band are paired with the uplink frequenc(ies) of the other FDD band (external) of the dual band configuration.		

Figure 72. WCDMA/UMTS standard frequency band specifications.

7.2.4. GSM Frequency Bands [22]

Table 4. GSM standard frequency band specifications.

Operating Band	Uplink Frequencies (MHz)	Downlink Frequencies (MHz)
T-GSM 380	380.2-389.8	390.2-399.8
T-GSM 410	410.2-419.8	420.2-429.8
GSM 450	450.4-457.6	460.4-467.6
GSM 480	478.8-486	488.8-496
GSM 710	698-716	728-746
GSM 750	747-763	777-793
GSM 810	806-821	851-866
GSM 850	824-849	869-894
P-GSM 900	890-915	935-960
E-GSM 900	880-915	925-960
R-GSM 900	876-915	921-960
Void	Void	Void
DCS 1800	1710-1785	1805-1880
PCS 1800	1850-1910	1930-1990
ER-GSM 900	873-915	918-960

7.3. Antenna Radiation Patterns

This section includes additional images of the radiation patterns of the original and complex optimized antenna models as a function of Φ and θ.

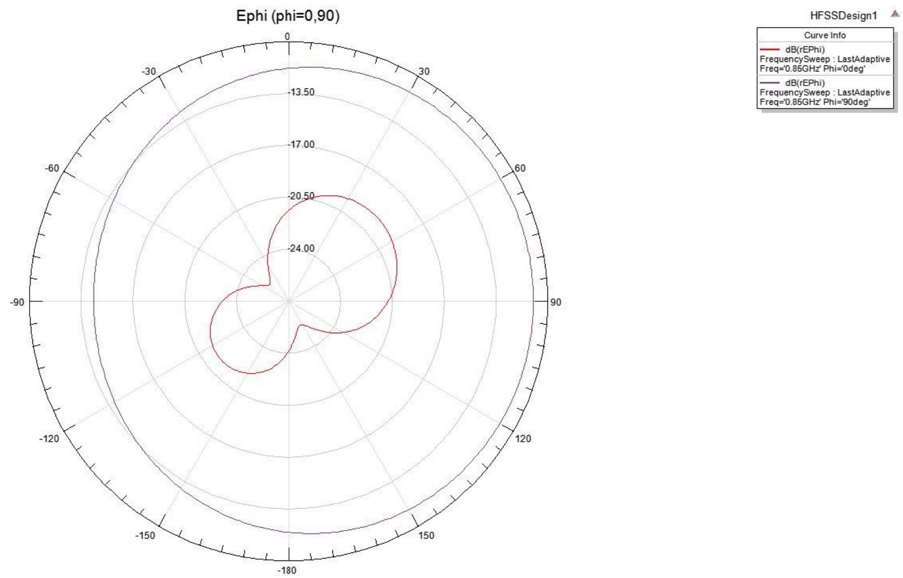

Figure 73. E_{Φ} radiation pattern as a function of ϑ for the original complex antenna model. Φ is given values of 0 and 90 degrees.

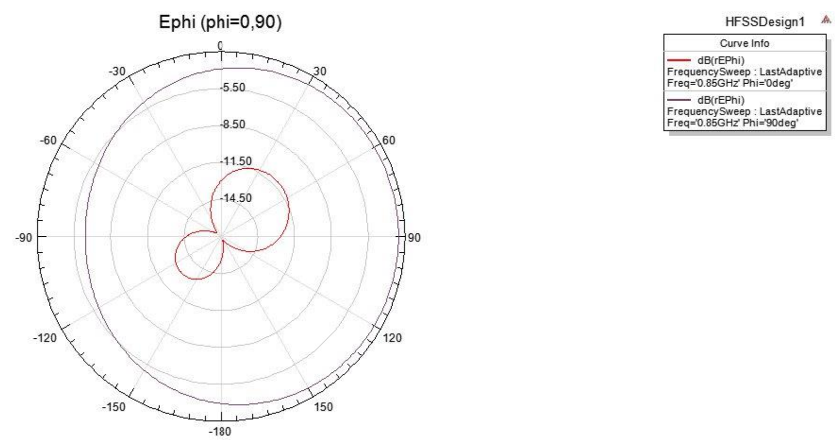

Figure 74. E_{Φ} radiation pattern as a function of ϑ for the optimized complex antenna model. Φ is given values of 0 and 90 degrees.

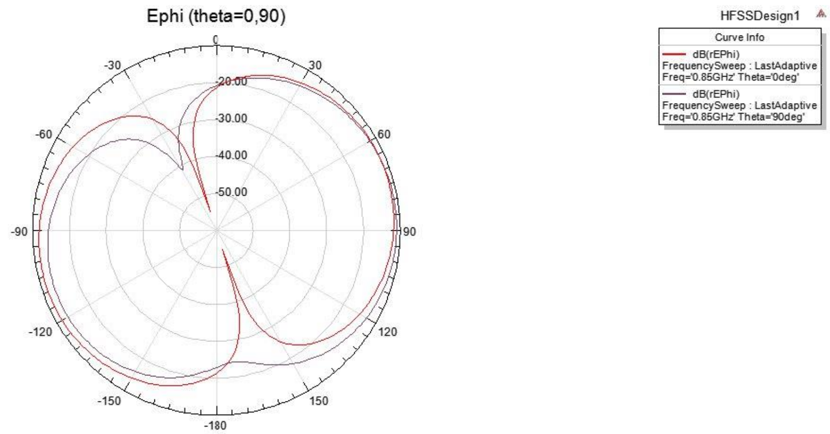

Figure 75. E_{Φ} radiation pattern as a function of Φ for the original complex antenna model. ϑ is given values of 0 and 90 degrees.

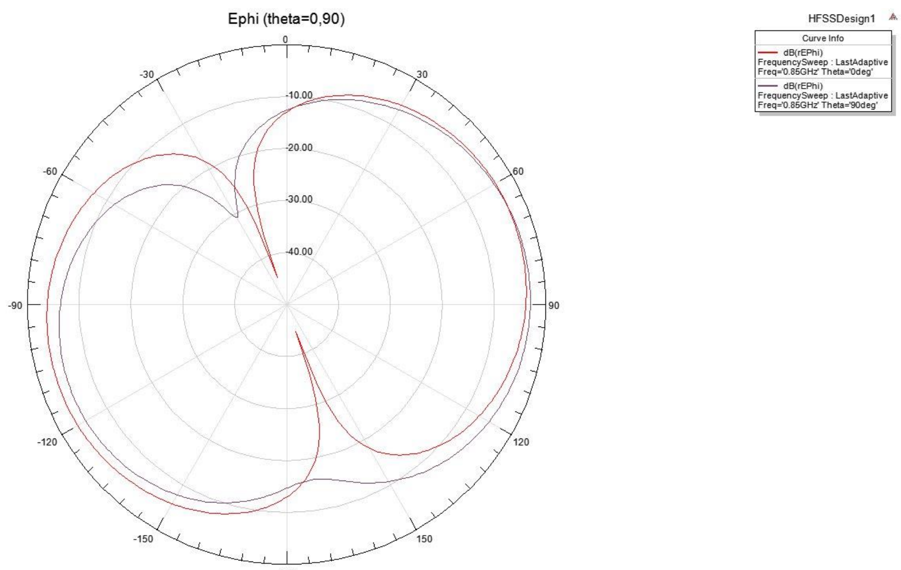

Figure 76. E_{Φ} radiation pattern as a function of Φ for the optimized complex antenna model. ϑ is given values of 0 and 90 degrees.

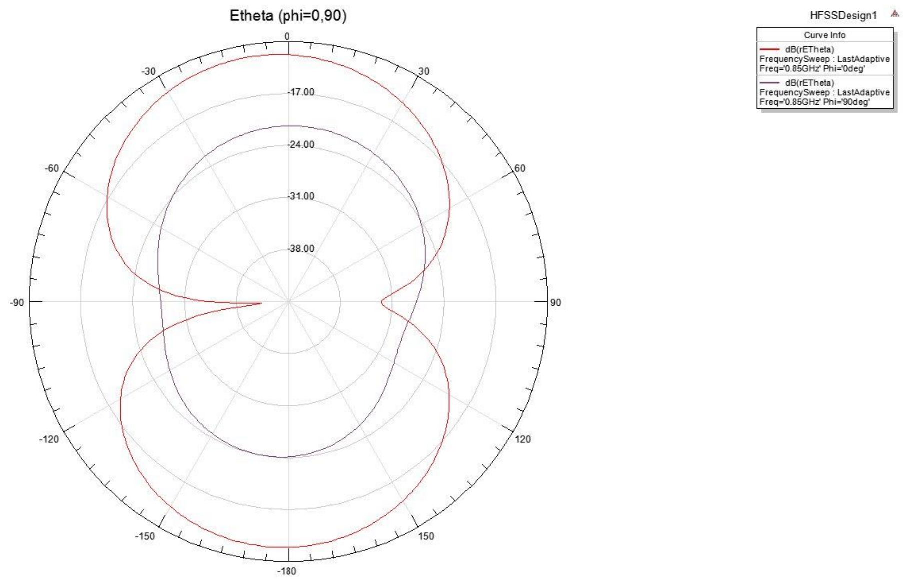

Figure 77. E_ϑ radiation pattern as a function of ϑ for the original complex antenna model. Φ is given values of 0 and 90 degrees.

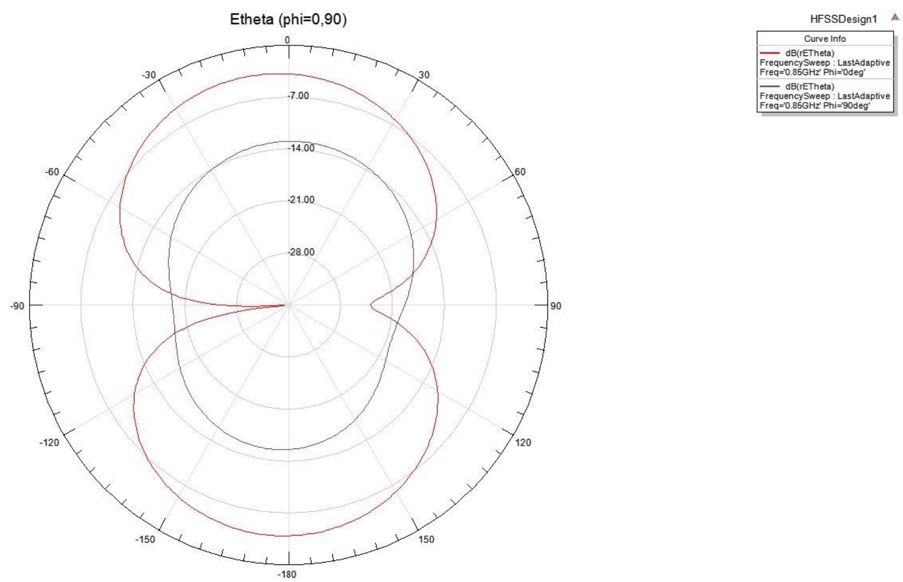

Figure 78. E_ϑ radiation pattern as a function of ϑ for the optimized complex antenna model. Φ is given values of 0 and 90 degrees.

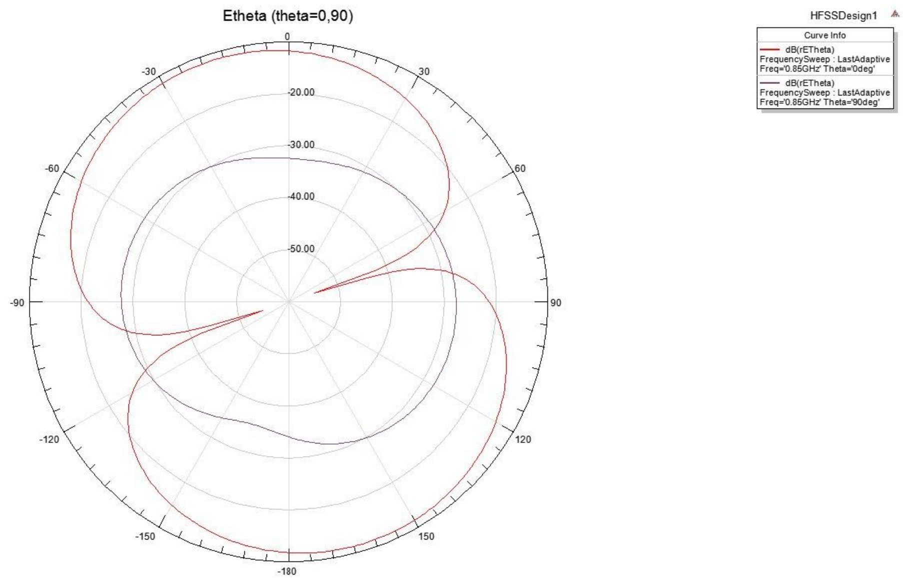

Figure 79. E_ϑ radiation pattern as a function of Φ for the original complex antenna model. ϑ is given values of 0 and 90 degrees.

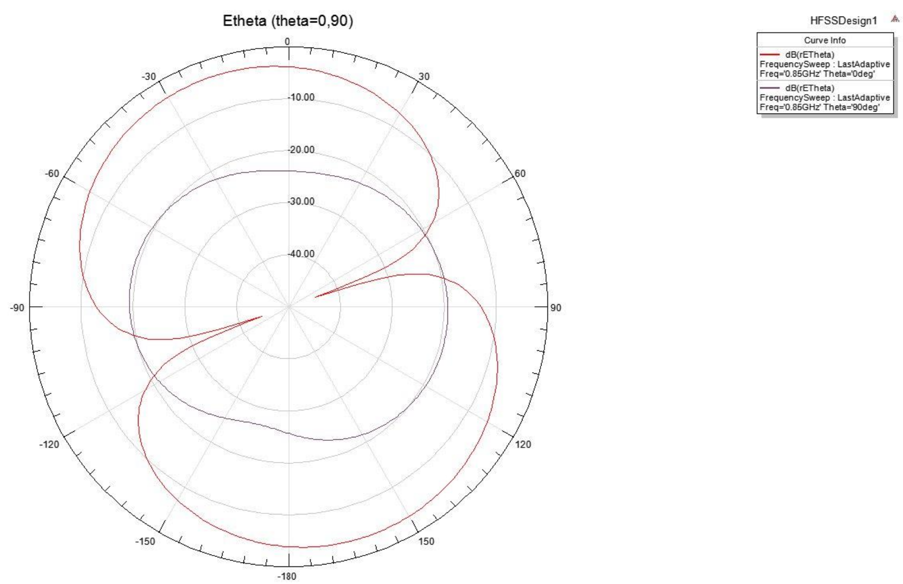

Figure 80. E_ϑ radiation pattern as a function of Φ for the optimized complex antenna model. ϑ is given values of 0 and 90 degrees.

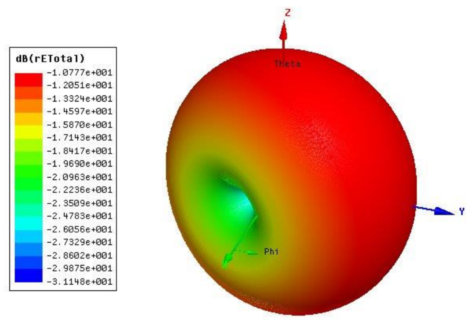

Figure 81. Three-dimensional radiation pattern for the original, un-optimized antenna model.

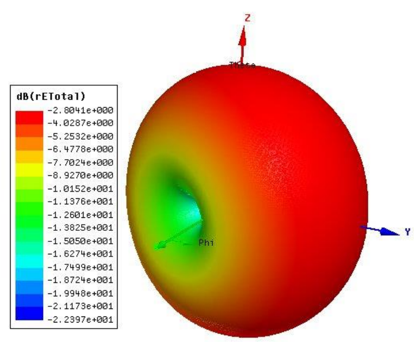

Figure 82. Three-dimensional radiation pattern for the optimized antenna model.

7.4. Additional Results

The following graphs show a more general view of the HFSS sweep results discussed in Section 4.1. Since the design focused on the 850 MHz band, the section discussed the behavior of the antenna at that frequency. By increasing the scope of the frequencies swept, the following graphs were developed that show how the antenna behaves at a range from 1 to 3GHz as well as at the lower frequency ranges.

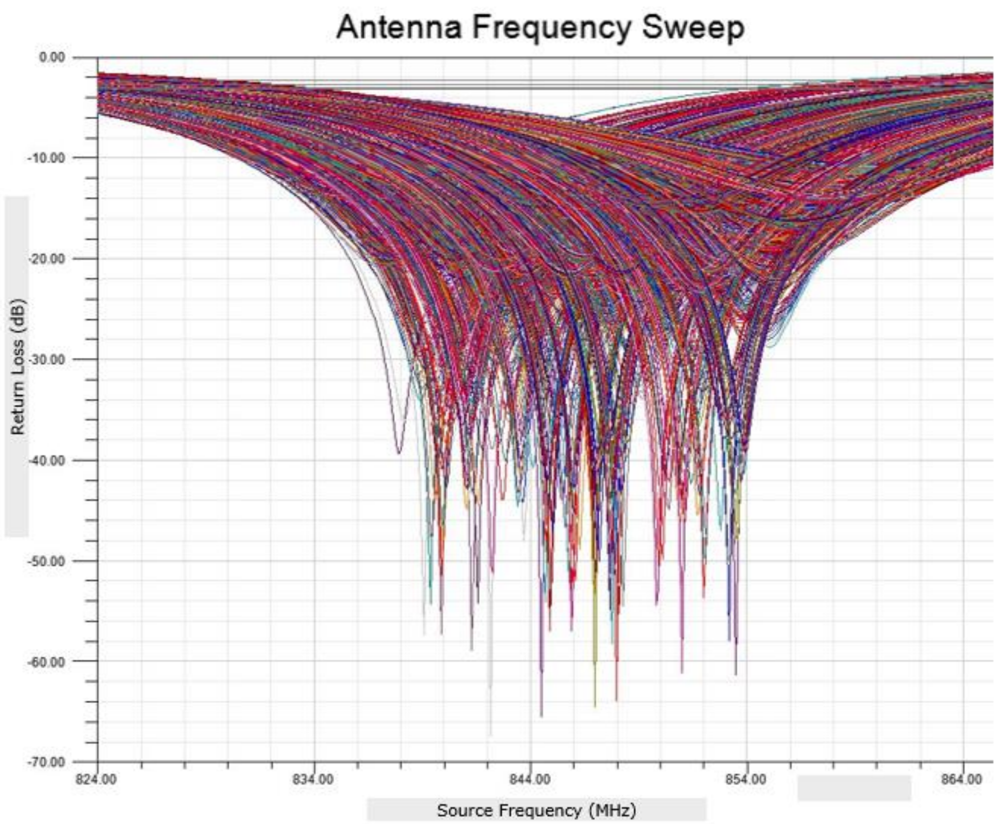

Figure 83. Image of the HFSS initial antenna S_{11} sweeps, as a function of tuner position, feed position, antenna length and tuning capacitance. Since each component was swept with 5 values, there are a total of 625 total frequency sweeps.

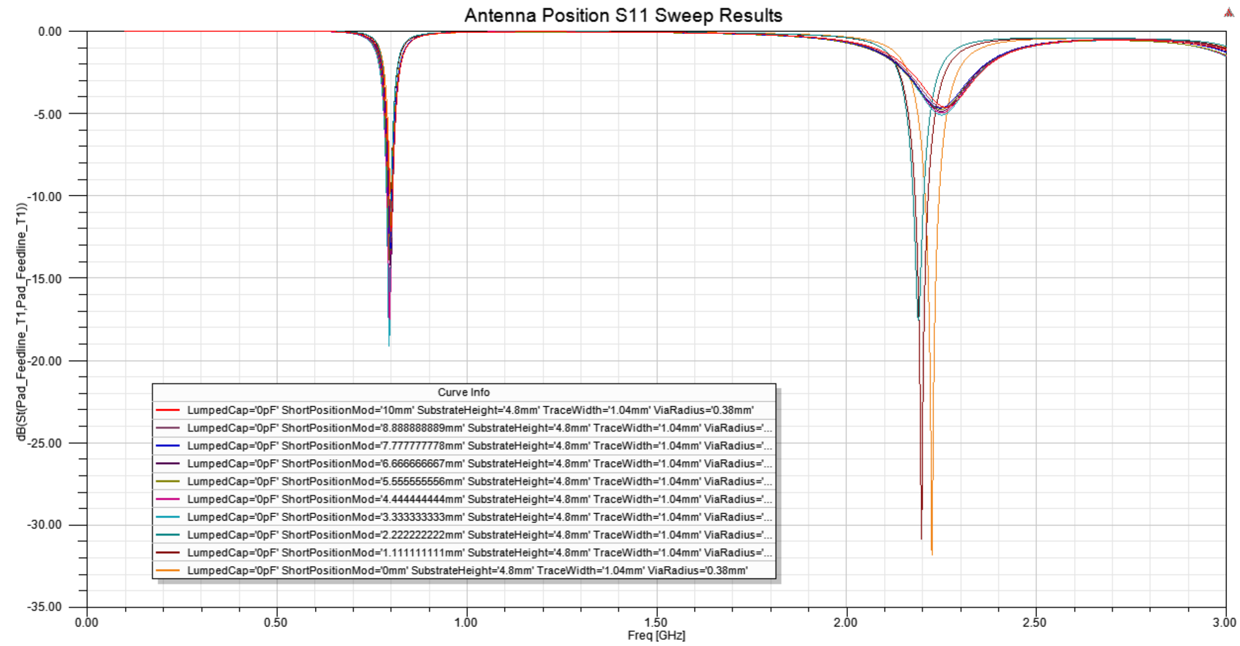

Figure 84. Image of the HFSS antenna position S_{11} sweeps, performed over a range from 0 to 3 GHz.

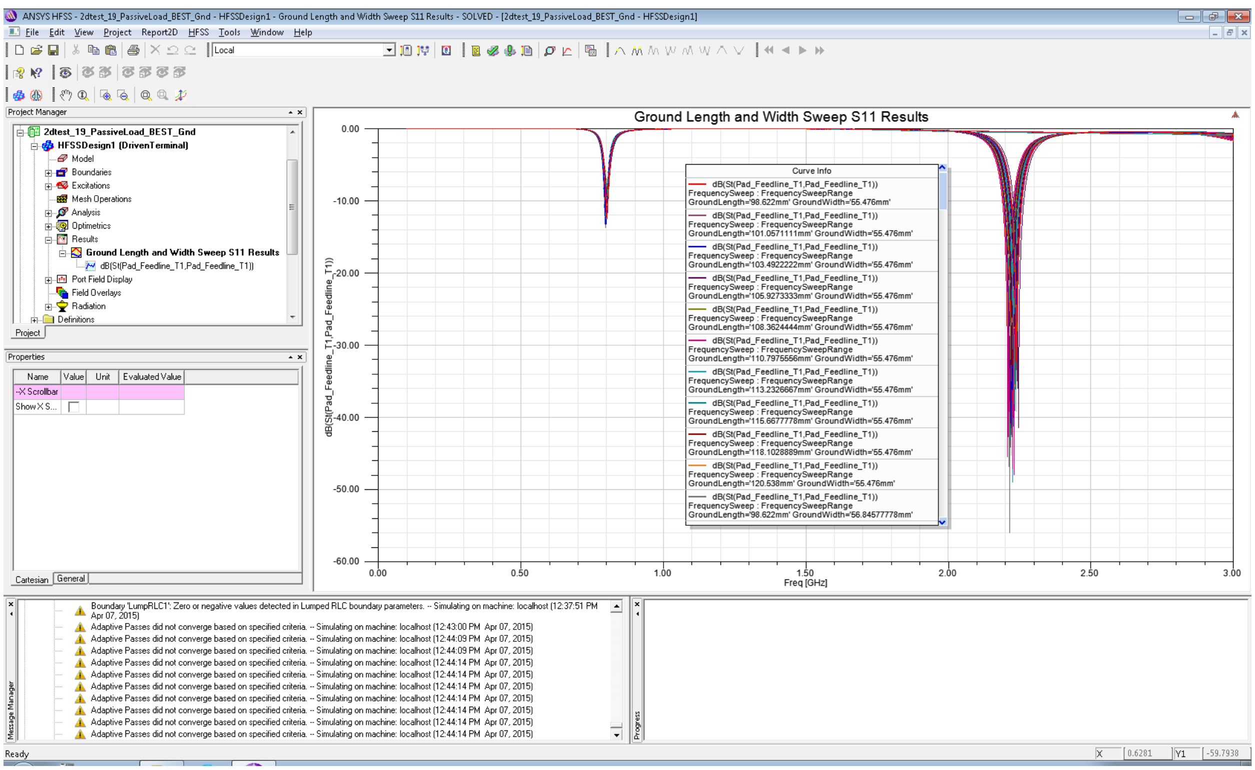

Figure 85. Image of the HFSS ground plane area S_{11} sweeps, performed over a range from 0 to 3 GHz.

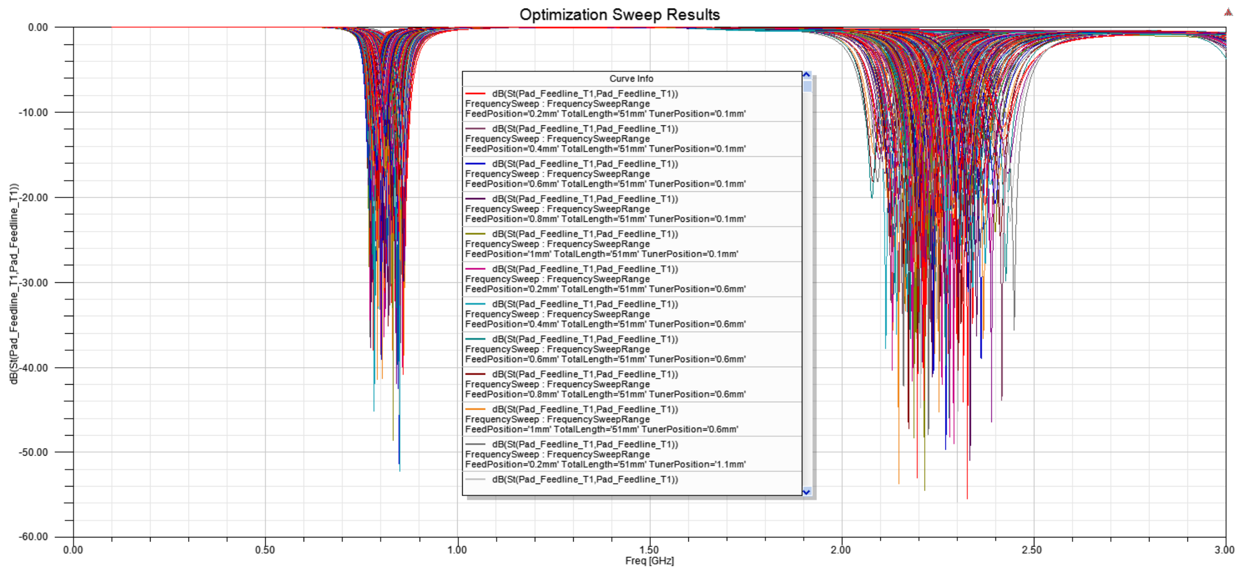

Figure 86. Image of the HFSS optimization S_{11} sweeps, performed over a range from 0 to 3 GHz.

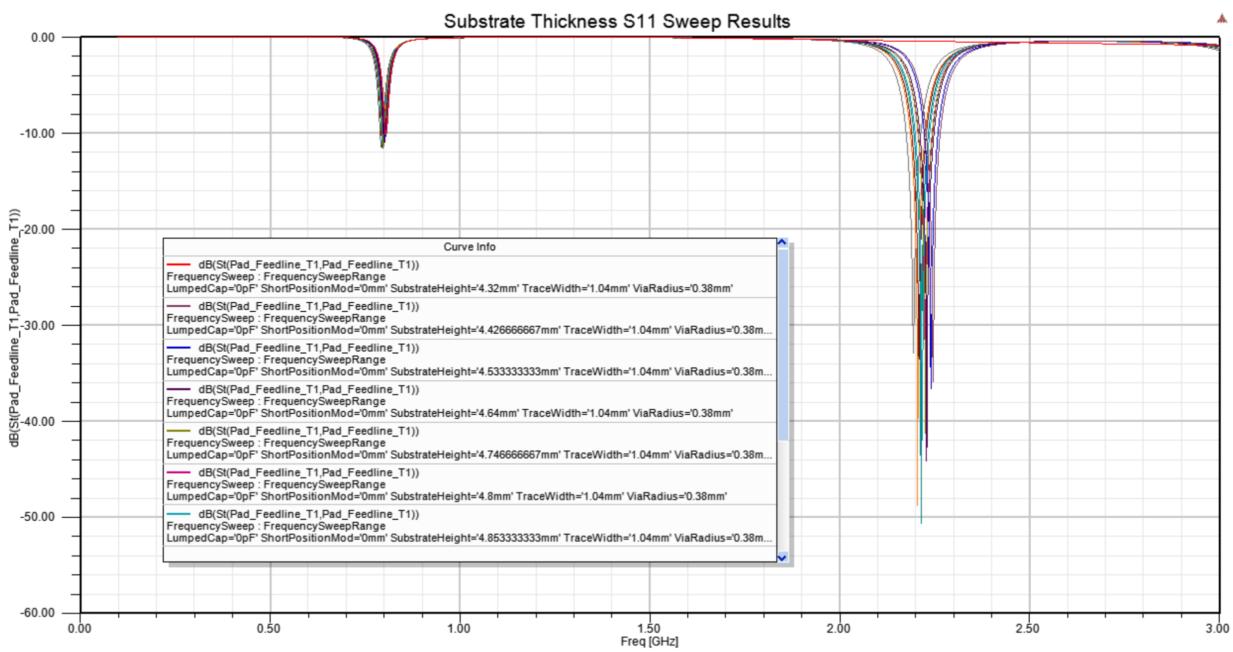

Figure 87. Image of the HFSS substrate thickness S_{11} sweeps, performed over a range from 0 to 3 GHz.

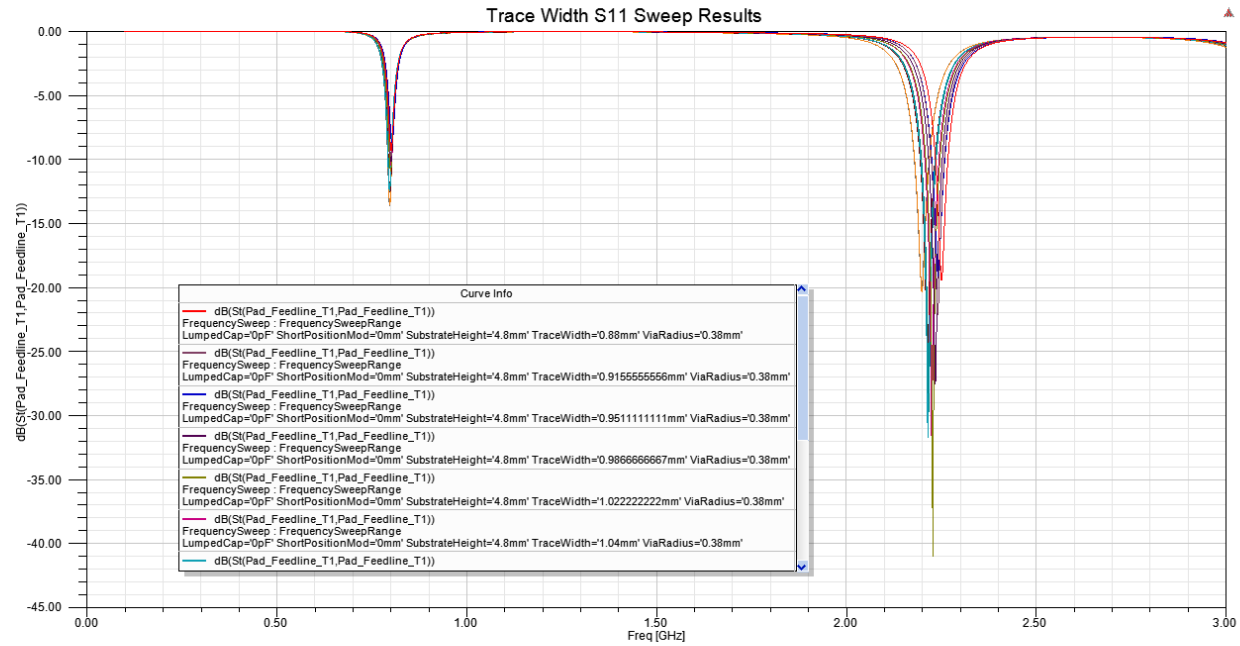

Figure 88. Image of the HFSS trace width S_{11} sweeps, performed over a range from 0 to 3 GHz.

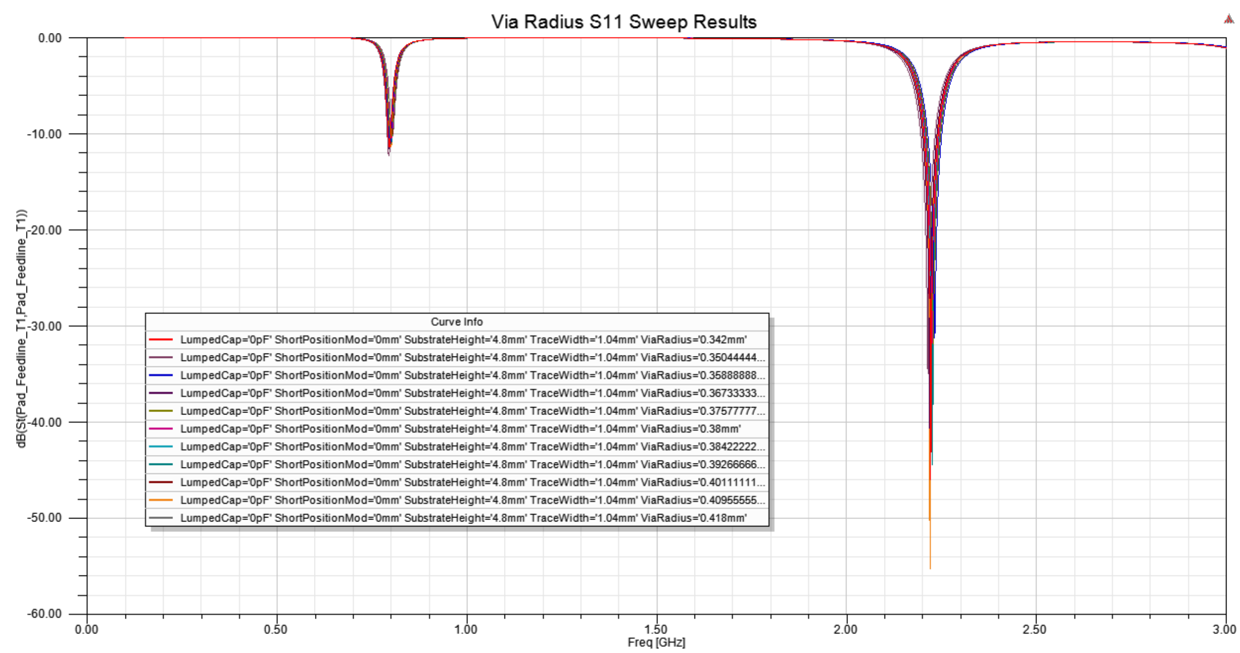

Figure 89. Image of the HFSS via radius S_{11} sweeps, performed over a range from 0 to 3 GHz.

7.5 MATLAB Code

Below is the example MATLAB Code used to import real and imaginary numbers of S_{11} parameter, and their respective frequencies taken from the network analyzer.

```
%Skyworks MQP 2014-2015
%Importing data from network analyzer
clc;
gamma = VarName2 + i*VarName3; %Impedance
%VarName2 presents Real numbers of S11
%VarName3 presents Imaginary numbers of S11

% plotting Reflection Coefficient
plot(VarName1, gamma);
%VarName1 is frequency values
grid on;
xlabel('Frequency [Hz]');
ylabel('S(1,1) [dB]')
title('S_1_1 Parameter with 0\Omega Resistor & No Matching Network ');
axis([0 3e9 -20 0]);
```

8. References

[1] H. J. Visser, O. Safari Books, and Books24x, *Antenna theory and applications*. Chichester, West Sussex, U.K: John Wiley & Sons, 2012.

[2] G. M. Khanal, "Design of a Compact PIFA for WLAN Wi-Fi wireless Applications."

[3] N. Trkulja, M. A. Morales, J. P. Michel, and L. T. Pham, *Tunable Filter Design for the RF Section of a Smartphone*. Worcester, MA: Worcester Polytechnic Institute, 2014.

[4] P. S. Hall, E. Lee, and C. T. P. Song, "Planar inverted-F antennas," *Printed Antennas for Wireless Communications,* 2007.

[5] M. Li, Q. Xue, and W. Che, "Wideband-integrated planar inverted-F antenna with meander line structures," *Microwave and optical technology letters,* vol. 51, pp. 384-387, 02/01 2009.

[6] C. Inho, L. Cheonhee, L. Yonghee, O. Jungkeun, J. Jinwoo, L. Hyeonjin*, et al.*, "A design of the multi-band chip antenna using meander line PIFA structure for mobile phone handset," pp. 1102-1105.

[7] K. W. Cozad, "FM RF Transmission Lines," ed, 2007, pp. 897-905.

[8] Federal Communications Commission. LG-D820 FCC Reports [Online]. Available: https://apps.fcc.gov/oetcf/eas/reports/ViewExhibitReport.cfm?mode=Exhibits&RequestTimeout=500&calledFromFrame=N&application_id=395625&fcc_id=ZNFD820

[9] L. V. Blake, M. W. Long, A. Knovel, amp, and C. Radar Technology Library - Academic, *Antennas: fundamentals, design, measurement*. Raleigh, NC: SciTech Pub, 2009.

[10] Z. Fuguo, Z. Chong, and X. Jiadong, "A simple and compact tri-band planar inverted-F antenna for personal communication handset applications," pp. 573-575.

[11] Z. N. Chen, *Antennas for portable devices*. Chichester: John Wiley, 2007.

[12] Ieee Iet Electronic Library Standards, *IEEE Standard Test Procedures for Antennas*, 1979.

[13] M. C. Huynh and W. Stutzman, "Ground plane effects on planar inverted-F antenna (PIFA) performance," *IEE Proceedings - Microwaves, Antennas and Propagation,* vol. 150, p. 209, 2003.

[14] 3rd Generation Partnership Project, "Evolved Universal Terrestrial Radio Access (E-UTRA); User Equipment (UE) radio transmission and reception," in *Operating bands and channel arrangement* vol. 3GPP TS 36.101, ed, 2014.

[15] D. Geen and D. Smith, "Compact anechoic chamber and antenna measurement system for microwave teaching and research applications," *MICROWAVE AND OPTICAL TECHNOLOGY LETTERS,* vol. 12, pp. 150-154, 1996.

[16] D. H. Schaubert, D. M. Pozar, and A. Adrian, "Effect of microstrip antenna substrate thickness and permittivity: comparison of theories with experiment," *IEEE Transactions on Antennas and Propagation,* vol. 37, pp. 677-682, 1989.

[17] IBIS. *Touchstone® File Format Specification*. Available: http://www.eda.org/ibis/

[18] I. Ruso. *PIFA_Planar_Inverted_F_Antenna*. Available: *http://www.qsl.net/va3iul/Antenna/PIFA/PIFA_Planar_Inverted_F_Antenna.pdf*

[19] E. Dahlman, S. Parkvall, and J. Skold, *4G: LTE/LTE-advanced for mobile broadband*: Academic Press, 2013.

[20] 3rd Generation Partnership Project 2, "Band Class Specification for cdma2000 Spread Spectrum Systems," in *Frequency bands and channel arrangement* vol. 3GPP2 C.S0057-E, ed, 2010.

[21] 3rd Generation Partnership Project, "User Equipment (UE) radio transmission and reception (FDD)," in *Frequency bands and channel arrangement* vol. 3GPP TS 25.101, ed, 2014.

[22] 3rd Generation Partnership Project, "Radio transmission and reception," in *Frequency bands and channel arrangement* vol. 3GPP TS 45.005, ed, 2014.